

U.S. DEPARTMENT OF COMMERCE
National Technical Information Service

AD-A025 393

A WINGTIP PHENOMENA

AIR FORCE INSTITUTE OF TECHNOLOGY

FEBRUARY 1975

167059

AD A025393

A WINGTIP PHENOMENA

by

JOHN ELI KEESEE

B.S., U. S. Air Force Academy

(1973)

SUBMITTED IN PARTIAL FULFILLMENT
OF THE REQUIREMENTS FOR THE
DEGREE OF MASTER OF SCIENCE

at the

MASSACHUSETTS INSTITUTE OF TECHNOLOGY

February, 1975

Signature of Author

John E. Keesee

Department of Aeronautics and Astronautics
January 22, 1975

Certified by

Thesis Supervisor

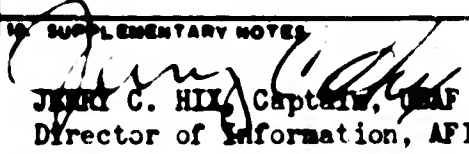
Accepted by

Chairman, Departmental Committee on Graduate Students



UNCLASSIFIED

SECURITY CLASSIFICATION OF THIS PAGE (When Data Entered)

| REPORT DOCUMENTATION PAGE | | READ INSTRUCTIONS BEFORE COMPLETING FORM |
|--|-----------------------|--|
| 1. REPORT NUMBER CI-76-13 ✓ | 2. GOVT ACCESSION NO. | 3. RECIPIENT'S CATALOG NUMBER |
| 4. TITLE (and Subtitle) A WINGTIP PHENOMENA ✓ | | 5. TYPE OF REPORT & PERIOD COVERED Master of Science Thesis ✓ |
| 7. AUTHOR(s) JOHN ELI KEESEE 2ND LT, USAF | | 6. PERFORMING ORG. REPORT NUMBER |
| 9. PERFORMING ORGANIZATION NAME AND ADDRESS AFIT student at the Massachusetts Institute of Technology, Cambridge MA ✓ | | 8. CONTRACT OR GRANT NUMBER(s) |
| 11. CONTROLLING OFFICE NAME AND ADDRESS Air Force Institute of Technology (CI) Wright-Patterson AFB OH 45433 | | 10. PROGRAM ELEMENT, PROJECT, TASK AREA & WORK UNIT NUMBERS |
| 14. MONITORING AGENCY NAME & ADDRESS (if different from Controlling Office) | | 12. REPORT DATE Feb 1975 |
| | | 13. NUMBER OF PAGES 110 112 |
| | | 15. SECURITY CLASS. (of this report) Unclassified |
| | | 16a. DECLASSIFICATION DOWNGRADING SCHEDULE |
| 18. DISTRIBUTION STATEMENT (of this Report) Approved for Public Release; distribution unlimited | | |
| 17. DISTRIBUTION STATEMENT (of the abstract entered in Block 20, if different from Report) | | |
| 19. SUPPLEMENTARY NOTES  JOHN C. HILL, Captain, USAF Director of Information, AFIT APPROVED FOR PUBLIC RELEASE AFR 19017. | | |
| 20. KEY WORDS (Continue on reverse side if necessary and identify by block number) | | |
| 20. ABSTRACT (Continue on reverse side if necessary and identify by block number) Attached | | |

A WINGTIP PHENOMENA.

by

JOHN ELI KEESEE

Submitted to the Department of Aeronautics and Astronautics on January 22, 1975, in partial fulfillment of the requirements for the degree of Master of Science.

ABSTRACT

An experimental investigation was conducted to study the vortex generated by a highly swept, sharp leading edge. The experiments were designed to uncover the interaction between a triangular planform wingtip having a sharp leading edge, and a rectangular wing with unswept, sharp leading edges. The structure of the leading edge vortex generated by the swept leading edge was studied by varying the span of the rectangular portion of the wing. The flow over the rectangular portion of the wing was studied as it was modified by the existence of the leading edge vortex. The flow very near the leading edge was investigated, to determine the applicability of boundary conditions used in current mathematical models.

The experiment was conducted in the five by seven foot, subsonic, wind tunnel at the Massachusetts Institute of Technology. The trapezoidal models differed only in the span of the rectangular center section, and varied in aspect ratio from 1.5 to 2.23. For comparison and study, the rectangular center sections were tested with round, parabolic, and ogive shaped fairings.

Forces on the models were obtained from a five wire strain gauge support system. The static pressure distribution over the triangular wingtip and the three fairings was obtained for all of the configurations of the model, and determined the location and strength of the vortices. The flow field surrounding the trapezoidal wings was observed and photographed by means of a hand held smoke generator in the flow.

The results show that the magnitude of the pressure peak due to the leading edge vortex on the triangular wingtip increased as the span of the rectangular center section increased. The position of the vortex relative to the leading edge remained essentially unchanged, indicating that the position of the vortex is governed by the vorticity generated by the leading edge, while the strength is determined by the lower surface

flow. The vortex was additionally influenced by the chordwise pressure gradient of the rectangular wing to induce vortex burst and complete stall of the wing with no vortex phenomena, at an angle of attack where lower aspect ratio wings would maintain attached flow. The vortex caused a smooth, unseparated flow over a portion of the rectangular center section, while the rest of that section was enveloped in a separation bubble from leading to trailing edge.

The pressures at the leading edge were not singular, as the Kutta condition suggests, but the exact angle of the flow at the leading edge could not be determined in this scale of analysis.

The rectangular wings showed less induced drag than is predicted for elliptic lift distributions, because of their small aspect ratio. The trapezoidal wings showed a greater drag, due to the increased loading near the wingtips. The rectangular wings with ogive and parabolically shaped fairings had less drag than the round fairing wings, because of their separation at the extreme extent of the tip.

Thesis Supervisor: Eugene E. Covert
 Title: Professor of Aeronautics and
 Astronautics

| | |
|---------------------------------------|--|
| ACQUISITION BY | |
| DTIC | WFO: Section <input checked="" type="checkbox"/> |
| DD | DD: Section <input type="checkbox"/> |
| DAIR: DTIC | <input type="checkbox"/> |
| ADVIS: DTIC | <input type="checkbox"/> |
| 7mm | Per 1473 |
| BY | |
| ACQUISITION, ASSOCIATION, DTIC | |
| WFO: Section <input type="checkbox"/> | |
| A | |

ACKNOWLEDGMENTS

The author would like to express his appreciation to all of those who helped in the preparation of this thesis, especially, however, to Professor Eugene Covert, whose continuing guidance and instruction were the foundation and cornerstones of the study.

Thanks are extended to Al Shaw and Fred Merlis for their aid in setting up the apparatus, and to Tom Hlatci, for his assistance in recording the data. Mrs. Anne Clee deserves the deepest appreciation for typing and editing the thesis

The author is indebted to the Fannie and John Hertz Foundation and the United States Air Force for their essential support.

The author would like to express his deepest appreciation to his wife, for her continued support, assistance, confidence and dedication, and to his God, for the help he gave.

THE UNIVERSITY OF CHICAGO

TABLE OF CONTENTS

| <u>Chapter No.</u> | | <u>Page No.</u> |
|--------------------|--------------------------|-----------------|
| 1 | Introduction | 11 |
| 2 | Description of Flow | 13 |
| 3 | Models of the Flow Field | 16 |
| 4 | Test Apparatus | 25 |
| 5 | Experimental Procedure | 28 |
| 6 | Discussion of Results | 34 |
| 7 | Conclusions | 49 |

Figures

| | | |
|----|---|----|
| 1 | Flow Around a Delta Wing | 52 |
| 2 | Trailing Vorticity Roll Up Distance | 53 |
| 3 | Edwards' Crossflow Plane | 54 |
| 4 | Coe's Delta Wing Model | 54 |
| 5 | Leading Edge Suction Analogy | 55 |
| 6 | Influence Coefficients for Pohlhausen's Lift Equation | 56 |
| 7 | Subsonic Wind Tunnel | 57 |
| 8 | Planform-Delta Wing | 58 |
| 9 | Planform-Three Inch Trapezoidal Wing | 59 |
| 10 | Planform-Six Inch Trapezoidal Wing | 60 |
| 11 | Planform-Twelve Inch Trapezoidal Wing | 61 |
| 12 | Wingtip Fairings | 62 |
| 13 | Force Measurement Model | 63 |

| <u>Figure</u> | | <u>Page No.</u> |
|---------------|--|-----------------|
| 14 | Pressure Distribution Measurement Model | 64 |
| 15 | Model Mounted in Tunnel - Sketch | 65 |
| 16 | Model Mounted in Tunnel - Photograph | 66 |
| 17 | Pressure Measurement Model Mounted in Tunnel | 66 |
| 18 | Cantilever Beam with Strain Gauges | 67 |
| 19 | Strain Gauge Bridge Circuit Schematic | 67 |
| 20 | Coefficient of Lift vs Angle of Attack: Delta Wing | 68 |
| 21 | Coefficient of Lift vs Angle of Attack: 3 Inch Trapezoid | 69 |
| 22 | Coefficient of Lift vs Angle of Attack: 6 Inch Trapezoid | 70 |
| 23 | Coefficient of Lift vs Angle of Attack: 12 Inch Trapezoid | 71 |
| 24 | Coefficient of Lift vs Angle of Attack: Delta and Trapezoidal Wings | 72 |
| 25 | Coefficient of Lift vs Coefficient of Drag: Delta Wing | 73 |
| 26 | Coefficient of Lift vs Coefficient of Drag: 3 Inch Trapezoid | 74 |
| 27 | Coefficient of Lift vs Coefficient of Drag: 6 Inch Trapezoid | 75 |
| 28 | Coefficient of Lift vs Coefficient of Drag: 12 Inch Trapezoid | 76 |
| 29 | Coefficient of Lift vs Coefficient of Drag: Delta and Trapezoidal Wings | 77 |
| 30 | Center of Pressure Location: Trapezoidal Wings | 78 |
| 31 | Pressure Distribution: Delta | 79 |

| <u>Figure</u> | | <u>Page No.</u> |
|---------------|---|-----------------|
| 32 | Pressure Distribution: Three Inch Trapezoidal | 80 |
| 33 | Pressure Distribution: Six Inch Trapezoidal | 81 |
| 34 | Pressure Distribution: Twelve Inch Trapezoidal | 82 |
| 35 | Smoke Flow around Delta Wing Near Edge of Vortex Flow | 83 |
| 36 | Smoke Flow around Delta Wing: Near Core of Vortex | 83 |
| 37 | Smoke Flow near Core: Front View | 84 |
| 38 | Smoke Flow near Core: Close Up | 84 |
| 39 | Smoke Flow around Twelve Inch Trapezoidal Wing | 85 |
| 40 | Sketch of Flow Near Leading Edge | 86 |
| 41 | Sketch of Flow over Delta Wing | 87 |
| 42 | Sketch of Flow over Three Inch Trapezoidal Wing | 88 |
| 43 | Sketch of Flow over Six Inch Trapezoidal Wing | 89 |
| 44 | Sketch of Flow over Twelve Inch Trapezoidal Wing | 90 |
| 45 | Coefficient of Lift vs Angle of Attack: Three Inch Rectangular Wing | 91 |
| 46 | Coefficient of Lift vs Angle of Attack: Six Inch Rectangular Wing | 92 |
| 47 | Coefficient of Lift vs Angle of Attack: Twelve Inch Rectangular Wing | 93 |
| 48 | Coefficient of Lift vs Coefficient of Drag: Three Inch Rectangular Wing | 94 |
| 49 | Coefficient of Lift vs Coefficient of Drag: Six Inch Rectangular Wing | 95 |

| <u>Figure</u> | | <u>Page No.</u> |
|-------------------|---|-----------------|
| 50 | Coefficient of Lift vs Coefficient of Drag: Twelve Inch Rectangular Wing | 96 |
| 51 | Center of Pressure Location: Three Inch Rectangular Wing | 97 |
| 52 | Center of Pressure Location: Six Inch Rectangular Wing | 98 |
| 53 | Center of Pressure Location: Twelve Inch Rectangular Wing | 99 |
| 54, 55, 56 | Pressure Distribution: Three Inch Rectangular Wing | 100-102 |
| 57, 58, 59 | Pressure Distribution: Six Inch Rectangular Wing | 103-105 |
| 60, 61, 62 | Pressure Distribution: Twelve Inch Rectangular Wing | 106-108 |
| 63 | Adjusted Drag Coefficient for All Models | 109 |
| <u>Tables</u> | | |
| 1 | | 110 |
| <u>References</u> | | 111 |

LIST OF SYMBOLS

| | |
|-----------|----------------------------------|
| A | aspect ratio |
| b | maximum span |
| C_{D_i} | coefficient of induced drag |
| C_{D_0} | coefficient of drag at zero lift |
| C_L | lift coefficient |
| C_{L_s} | section lift coefficient |
| C_p | pressure coefficient |
| C_s | suction coefficient |
| C_T | thrust coefficient |
| C | tunnel cross section |
| D_i | induced drag |
| d | vortex roll up distance |
| K_i | influence coefficient |
| K_p | influence coefficient |
| L | lift |
| L | local lift |
| m' | apparent mass |
| N | normal force |
| p | pressure |
| q | dynamic pressure |
| S | wing area |
| s | local span |
| T | thrust force |
| U | free stream velocity |

| | |
|-----------|-------------------|
| α | angle of attack |
| Γ | circulation |
| Λ | sweep angle |
| ρ | density |
| ϕ | surface potential |

Chapter I

INTRODUCTION

In almost all supersonic aircraft today, the wings are designed to have highly swept leading edges and very thin cross sections. These two characteristics lessen and delay the drag rise as the aircraft exceeds the speed of sound, but they also tend to induce leading edge vortex flows above the wing at all but the smallest angles of attack in subsonic flight. These vortices result in an increased lift for moderate to high angles of attack. This greatly increased lift is extremely important during the take-off and landing phases of supersonic aircraft, because it leads to shorter ground runs and lower stall speeds.

This type of flow effect has been studied for some time, but as yet there have been no good theoretical models for the flow. There is a great need for a more complete understanding of the flow field and its interaction with nearby wing sections and the fuselage. A greater understanding and an appropriate model of the flow field would allow prediction of the forces and moments, both static and dynamic, affecting the flight vehicle. Prediction of the behavior of the flow field would help the designer avoid pitfalls and develop the most efficient flight systems. A good model for vortex-type flow systems could, for example, predict the interaction of leading edge vortex flows with more rectangular wing planforms, like the interaction between a high wing and a fuselage, or the tip effect of swept tip helicopter blades.

The purpose of this report, then, is twofold. It is an examination of the effect of a leading edge vortex on the flow over several sharp

edged rectangular wings. Its purpose is to show the difference in the flow fields resulting from a leading edge vortex generated by a triangular plan-form wing tip, and round, parabolic, or ogive section fairings at the tip of the rectangular wings. The second purpose is to study, by inserting rectangular wings between the triangular wing tips, the effect of the aspect ratio increase on the leading edge vortex flow. Its purpose is to show some of the underlying structure of the leading edge vortex flow by separating the vortices, and perhaps determine the causes and characteristics of the flow. From this, the applicability of current mathematical models can be determined and the proper direction for further extensions of the model can be obtained.

DESCRIPTION OF FLOW

The flow of a fluid around a highly swept wing planform, for example, a delta wing, with a relatively sharp leading edge changes dramatically with angle of attack. At small angles of attack, the fluid flows smoothly over the wing surface, but at moderate angles of attack, the flow separates at the leading edge and spirals toward a vortex core above the wing. The vortex so created causes a reattachment of the flow inboard of the leading edge, creating two flow patterns, one inside the vortex "cone" and another outside, as shown in Figure 1. The inner flow consists of concentric spirals about the vortex core, the core flow, and the flow over the wing surface. The core flow is a viscous, highly rotational flow field, with a core velocity several times the free stream velocity along its axis. The inner flow next to the wing is initially toward the leading edge, but shortly after the fluid passes under the vortex core, the adverse pressure gradient causes the boundary layer flow to separate. The outer flow over the surface of the wing is nearly straight along the longitudinal axis of the wing.¹

The flow field of a slender delta wing was studied by Fink and Taylor, and Earnshaw and Lawford. These studies showed the position of the vortex, the total pressure above the wing, and flow patterns over the wing. Fink and Taylor noted the aspects of the flow mentioned before. They also noted that with increasing angle of attack, the main vortex cores moved away from the leading edge, the cores experienced a reduction in total pressure and the vortex sheets had an increased intensity. The flow over the center

portion of the wing was found to have a thinner boundary layer which was probably due to the effect of the increased strength of the vortices. The total pressure along rays through the vertex of the delta wing did not show that the velocity was constant, but over a middle region of the wing for moderate angles of attack, it might be considered conical,² i.e., that the velocity was constant along rays from the apex of the wing.

Earnshaw and Lawford (1966) further noted that the attachment and secondary separation lines were straight lines until they neared the trailing edge. This reinforces the conical flow assumption. Near the trailing edge, the secondary separation line curved toward the leading edge, and a reverse flow developed at higher angles of attack. This was apparently due to the vortex burst or laminar to turbulent boundary layer transition. They also showed that the stagnation line on the lower surface moves away from the leading edge with increased angle of attack, and the flow near the leading edge is in the span direction.³

The flow over a sharp edged rectangular wing without sweep also separates above rather small angles of attack. The separation on this type of wing has no regular pattern, like the vortex flow had. The streamlines passing over the leading edge are unable to follow the contour of the wing for moderate angles of attack, and, therefore, flow away from the wing and reattach to the wing surface at a chord position downstream. The flow under this stream surface is basically a recirculation type of flow and is not as structured as swept wings. As the angle of attack is increased, the point at which the streamlines reattach is moved further and further aft, until the flow no longer reattaches at all. At this point, the lift of the wing

is no longer determined by the Kutta condition at the trailing edge, and the wing is stalled. The creation of a separation bubble results in a loss of lift and an increase in drag.⁴

Vorticity enters the flow also at the trailing edge of the wing. The vorticity entering the flow at the trailing edge initially lies in a flat sheet behind the wing and is known to roll up into two vortex cores far downstream. The distance to where the vortices are considered rolled up is proportional to the aspect ratio and span, and inversely proportional to the coefficient of lift. For low aspect ratio wings, the vortex sheet is rolled up very near the trailing edge, usually within a chord length. These distances are shown in Figure 2.⁵ Fink and Taylor also noted that the vorticity of the trailing edge rolls up independently of the leading edge vortex, and the two vortices appear to wrap around one another in a helix pattern.²

MODELS OF THE FLOW FIELD

Several models for leading edge vortex flows have been proposed and solved with varying success. The flat plate delta wing is usually chosen for consideration because of its simplicity.

The earliest and simplest model of the flow field is given by slender body theory. By assuming that the wing is slender, i.e., that dimensions perpendicular to the flow direction are smaller than dimensions along the flow direction, they were able to approximate the equations of motion of the fluid by considering the fluid to be at rest and the flow situation to be that of a widening plate having a vertical velocity of $U\alpha$ where U is the free stream velocity and α the angle of attack. The local lift force is then given by

$$l = U \alpha \frac{dm'}{dt} = U^2 \alpha \frac{dm}{dx} \quad (3.1)$$

where m' is the apparent mass of a flat plate. Two dimensional flow theory gives

$$m' = \pi s^2 \rho$$

Then

$$\frac{dm'}{dx} = 2\pi s \rho \frac{ds}{dx} \quad (3.2)$$

and

$$l = 4\pi\alpha \frac{1}{2}\rho U^2 s \frac{ds}{dx} \quad (3.3)$$

$$C_L = 2\pi\alpha \frac{ds}{dx} \quad (3.4)$$

The surface potential, ϕ , is given by

$$\phi = \pm U\alpha \sqrt{s^2 - y^2} \quad (3.5)$$

so that

$$\Delta p = 2\rho \frac{\partial \phi}{\partial t} \quad (3.6)$$

$$\Delta p = 2\rho U \frac{\partial \phi}{\partial s} \frac{\partial s}{\partial x} \quad (3.7)$$

$$\Delta p = 2\rho U^2 \alpha \frac{s}{\sqrt{s^2 - y^2}} \frac{ds}{dx} \quad (3.8)$$

The pressure has an infinite peak where $y = s$, i.e., at the edge of the wing. These results have several interesting points. A portion of a wing where the span does not change with x will contribute nothing to the lift, as will all portions of the wing behind the maximum span, because all cross sections behind the maximum span of the wing will lie in the wake of the wing, and can develop no pressure difference. Further, the center of pressure for triangular wings is the center of area, and the pressure

distribution along lines through the vertex of the triangular wing is uniform, because s and y are linear functions of x on those lines.

Integration of (3.6) gives

$$\int \Delta p dx = 2\rho U \phi \quad (3.9)$$

so, therefore,

$$\frac{dL}{dy} = \int \Delta p dx = 2\rho U^2 \alpha \sqrt{\left(\frac{b_{max}}{2}\right)^2 - y^2} \quad (3.10)$$

so that the spanwise distribution of lift is elliptical. With elliptical spanwise lift, the induced drag is known to be minimum and given by

$$D_i = \frac{L^2}{\pi q b^2} \quad (3.11)$$

Integrating the lift distribution across the span

$$L = \frac{\pi}{4} \rho U^2 \alpha b^2 \quad (3.12)$$

$$C_L = \frac{\pi}{2} R \alpha \quad R = \frac{b^2}{S} \quad (3.13)$$

$$C_{Di} = \frac{C_L^2}{\pi R} = C_L \frac{\alpha}{2} \quad (3.14)$$

where R is the aspect ratio of the wing.⁶

This theory assumes attached flow for the wing and is, therefore,

an inaccurate description of the flow. It predicts an infinite pressure at the leading edge and a finite pressure difference distribution on the trailing edge, which should be zero. The results generated by the theory are fairly good for very small aspect ratios.

A better flow model was created by Edwards, who tried to incorporate the vortex phenomena of the flow. He assumed that the flow about a delta wing could again be considered slender, as Jones and Cohen had defined it, and further that the flow was conical. He modeled the vortex sheet that is generated by the leading edge as a concentrated vortex, and then introduced a branch cut to connect the vortex to the leading edge, to represent the vortex feeding sheet. To find the strength and position of the concentrated vortices he required that there be no forces on the vortex, and that there be no net force on the feeding sheet. The final condition on the flow is the Kutta condition, i.e., that the velocities and pressures remain finite at the leading edge. A cross section of his flow picture is shown in Figure 3. The final result of his work is that

$$C_L = \frac{\pi}{2} AR\alpha + \pi(R)^{1/2}\alpha^{5/2} \quad (3.15)$$

This result overestimates the lift of the wing and has several inadequacies. First, the actual vortex sheet contains vorticity that effects the flow near the leading edge to a great degree. Secondly, because the vorticity wraps around the vortex core, there is an induced axial velocity that is unaccounted for in this analysis. Note, however, that the first term matches the slender body theory result.⁷

Mangler and Smith applied a theoretical treatment to the flow over a delta wing by simulating the vortex layer by a vortex sheet in spiral form, wrapping into the vortex core found in the flow. Using slender body theory, they reduced the situation again to a two-dimensional problem, and treated the core of the spiral separately from the outer extent that springs from the leading edge. They required that the sheet lie in a stream surface of the flow and not have a pressure difference across it. By assuming that the flow is conical, and that slender body theory applies, the solution for the velocity potential was found to be the sum of a harmonic function in the cross flow plane and a function of the streamwise coordinate alone, where the second function dropped out for wings with zero thickness. The boundary conditions employed were that the vortex sheet and core had no forces on them and that the vortex sheet, the vortex core and wing surface were stream surfaces of the flow. A Kutta condition was applied at the leading edge, so that the velocities and pressures would be finite there.

Their paper shows the form of the boundary conditions in the transverse plane, and the solution near the core. The vortex sheet is represented by a circular arc in the transformed plane with a given distribution of vorticity. After the boundary conditions are matched at a few points on the arc, the strength and shape of the vortex sheet are then found.⁸

The results of this theory are better than before, but still not particularly good. There is some error in the location of the vortex that seems to affect the accuracy of the predicted forces. The predicted core positions are generally farther outboard and lower than the experimental positions obtained by Fink and Taylor.⁸

Later, Coe introduced a factor to account for the vortex entrainment that causes high axial velocities in the core. He modeled the flow as a vortex core, a distribution of sinks, and an axial velocity, all on two rays from the apex of the wing, as shown in Figure 4. He required flow to be tangent to the plate, smooth outflow at the plate edges, and a stationary vortex core. He assumes that the body is slender and that the flow is conical, but he must rely on experimental data to determine the core locations.⁹

The results are somewhat better than those previously found. He does not account for any vortex sheet in his analysis, and even though the form of his solution is apparently correct, it has little applicability since it requires experimental data.

By far the most accurate method of determining forces on a delta wing was proposed by Pohlhausen. He described the flow as a combination of potential lift and vortex lift. The potential lift was determined by finding the distribution of bound vorticity in the wing that satisfies the boundary condition that the induced velocity of this system equal $U \sin \alpha$ at certain points on the wing. The normal force is then determined as

$$N = \rho \Gamma b U \cos \alpha \quad (3.16)$$

and the lift as

$$L = N \cos \alpha \quad (3.17)$$

He defines the circulation as

$$\Gamma = K_p \frac{SU}{2b} \sin \alpha \quad (3.18)$$

and K_p is determined numerically by lifting surface theory. This gives

$$C_{Lp} = K_p' \sin \alpha \cos^2 \alpha \quad (3.19)$$

where K_p depends only on the planform of the wing.

The vortex lift of the wing is determined by an analogy to leading edge suction. The flow ahead of the stagnation point on the underside of a wing, if attached to the surface, is accelerated around the leading edge, as shown in Figure 5. This develops a low pressure which acts as a thrust on the wing. The leading edge suction force remains essentially constant as the radius of the leading edge is varied, because, as the radius decreases, the pressure increases, but acts on a smaller area. The flow around a sharp edge separates and flows into a spiral vortex and the exterior flow is caused to reattach itself to the upper surface. Pohlhausen contends that the forces required to reattach the outer streamlines to the surface are equal to the forces required to maintain the attached flow of a round leading edge. With the sharp leading edge, there is separation at the leading edge, and the lift force developed by the potential flow must be normal to the surface.

The leading edge suction force is perpendicular to the leading edge, and so a thrust coefficient may be defined as

$$C_T = C_S \cos \Lambda \quad (3.20)$$

The normal force is equal to the suction force so that

$$C_L = C_T \frac{\cos \alpha}{\cos \Lambda} \quad (3.21)$$

The thrust of the leading edge is determined from the velocities normal to the leading edge and the circulation by

$$T = \rho \Gamma b (U \sin \alpha - w_i) \quad (3.22)$$

where w is the induced velocity of the trailing vortex system. The total effective circulation, Γ , has already been determined for the potential lift, so that

$$C_T = \left(1 - \frac{w_i}{U \sin \alpha}\right) K_p \sin^2 \alpha \quad (3.23)$$

Pohlhausen lets

$$\frac{w_i}{U \sin \alpha} = K_p K_i \quad (3.24)$$

where

$$K_i = \frac{\partial C_{D_i}}{\partial C_L^2} \quad (3.25)$$

and, since it is a function only of planform, it is determined by lifting

surface theory. We have

$$C_T = (K_p - K_p^2 K_i) \sin \alpha \quad (3.26)$$

$$C_{L_v} = (K_p - K_p^2 K_i) \sin^2 \alpha \frac{\cos \alpha}{\cos \Lambda} \quad (3.27)$$

The total lift of the wing is then determined as sum of the potential and vortex lift.

$$C_L = K_p \sin \alpha \cos^2 \alpha + (K_p - K_p^2 K_i) \cos \alpha \frac{\sin^2 \alpha}{\cos \Lambda} \quad (3.28)$$

The constants K_p and K_i for delta wings are shown in Figure 6.¹⁰

The agreement of his theory with experiment is quite good for the prediction of lift and induced drag. The errors that effect his calculation are principally due to a breakdown in the assumptions of attached flow. When the vortex bursts over the wing, there is an associated loss of pressure and decrease in lift. Also, in very slender wings, the two vortices generated by the leading edge may interact and form an asymmetrical and, sometimes, unsteady pattern above the wing. The principle problem with the theory is its foundation on the equivalence of the suction force and the vortex force, which is only intuitive. The principle advantage of the theory is its unprecedented accuracy. Pohlhamus has extended his theory to non-delta wings, and supersonic flow conditions.¹¹

Chapter IV

TEST APPARATUS

The experiment was conducted in the five by seven foot anechoic wind tunnel at the Massachusetts Institute of Technology. The tunnel is a continuous circuit wind tunnel with an open test section, as shown in Figure 7. The controls for the tunnel are outside the testing room, but the testing room is large enough that most of the force measurement apparatus could be kept inside, and the model was always in view while force measurements were being taken. In addition, the hand held smoke probe could be placed anywhere in the flow field, and observations could be made from any angle.

The models used are shown in Figures 8 through 14. The triangular wing tips have a root chord of twelve inches, and a span of 4.5 inches each, resulting in a sweep of 69.44 degrees at the leading edge. The three rectangular center sections had spans of three, six and twelve inches. All were 0.75 inches thick, giving a thickness ratio of 6.25 percent, and were tapered on the top and bottom within three inches of the leading and trailing edges. The triangular tips were tapered for three inches at the trailing edge, and 1.1 inches at the leading edge, to match the rectangular center section. The triangular wing tips were constructed of wood with aluminum leading and trailing edges, so that sharp edges could be obtained all around the model. The rectangular center sections were similarly constructed, with sharp aluminum leading and trailing edges. Round, ogive, and parabolic fairings, shown in Figure 12, could be attached to the rectangular sections. These were equipped with four static pressure ports at 48 percent

chord to determine the pressure distribution near the tip. A special triangular wing tip, constructed entirely of mahogany, but still with sharp edges, was equipped with eight static pressure ports to determine the pressure distribution normal to the leading edge across the delta wing tip. These pressure ports are positioned at about 45 percent chord. The pressure tubes from the ports led to the trailing edge, where they were joined to the tubing that led to the manometer. The angle of attack and alignment of the model were maintained by an aluminum bar that extended behind the model.

The model hung in the tunnel supported by wires attached to a rack mounted above the flow. The crossmembers of the rack supported five small cantilevered beams which were fitted with strain gauges. The model setup is shown in Figures 15, 16 and 17. The model hung from the cantilevered beams on .018 inch music wire, so that the stress in the cantilevered beams was directly proportional to the tension in the wires.

The wires were attached to the model at three points. At exactly mid-chord, two small rings were attached to the model near the wing tip. Each of these rings was attached directly to a strain gauge that measured the vertical forces at that point. Each ring had an additional wire that was attached to another ring directly upstream. This ring hung from a strain gauge, and was also connected to a fixed point on the floor of the tunnel by another wire that formed a 135° angle to each of the other two. The tension in the vertical wire was, therefore, exactly the tension in the horizontal wire, and the forward two strain gauges determined the drag of the model. From the sting on the rear of the model, one wire was

attached to a strain gauge one foot behind the two lift strain gauges, giving center of pressure data. Finally, one wire was attached to a weight, out of the airflow, that loaded the entire system.

The cantilever beam with its strain gauges are shown in Figure 18. The strain gauges mounted on the cantilever beam form a bridge circuit as shown in the simplified diagram of Figure 19. The balance simply adjusts the current flow to zero. As the beam undergoes a bending stress, the resistance of the top gauges is increased and the lower decreased, giving a net voltage to be measured, directly proportional to the force exerted. This voltage was then read on a digital voltmeter inside the tunnel.

The pressure distribution data was simply measured on a manometer, outside the tunnel. The pressure ports in the model were connected to tubing at the trailing edge. This tubing continued horizontally behind the model to where it was supported, and then to the floor where it connected to larger diameter tubing, and finally the manometer. The manometer used Meriam fluid, with a specific gravity of 0.824, and was inclined at an angle of 16.5 degrees from the horizontal. None of the pressure measurement equipment was attached to the model during the force measurement runs.

Flow visualization was accomplished by the use of vaporized oil. The oil vapor was injected into the airstream at the end of a four foot hand held wand. The wand was heated along its length to create the oil vapor. The smoke generally dispersed slowly, and appeared white, which was particularly visible in this situation. Photographs of the flow visualization were taken with a Polaroid camera, mounted in the test section.

Chapter V

EXPERIMENTAL PROCEDURE

Before the forces on the wings were determined, the strain gauges were calibrated and a check was made to insure that the readout was indeed linear to the force applied. This was done by loading them with known weights and recording the response.

The forces on the wing were found using the calibration of the voltage readout. Three readings were taken, one before the wind tunnel was started, one while the wind tunnel was running, and one after, for each of the strain gauges. For all of the force and pressure distribution measurements, the tunnel was run at 88 feet per second.

The angle of attack was changed by replacing the wire between the sting and fifth strain gauge. The angle of attack was measured with a level mounted on a variable scale. The angles of attack tested for each model were about 0, 5, 10, 15 and 20 degrees, with some variation between models.

The model configuration was changed by attaching the triangular tips, or the tip fairings to either the three, six, or twelve inch wide rectangles. The triangular wing tips were tested in the delta wing configuration, as well as with the various center sections. In each configuration, the five angles of attack were tested.

Two separate runs were needed to determine the tare drag of the model, because the model was held from lateral sway by two strings in the tests on the rectangular wings. A round bar of diameter 0.218 inches and 12 inches long was supported by the wires in the tunnel, and the drag forces were measured. The coefficient of drag of the rod was known to be 1.1%,

based on frontal area,¹² so that a drag was calculated and subtracted from the measured force. The remainder, the drag of the wires, was then subtracted from the test data.

Test results were obtained that showed that the deflection of the cantilevered beams was 0.006 inches per pound tension applied. For the twelve inch trapezoidal wing, the lift force on each cantilever beam was 6.095 pounds and the force reduction on the fifth cantilever beam was 1.803 pounds. This resulted in an increase in the angle of attack of 0.23 degrees. This is the maximum increase in angle of attack and it has been added to the data results.

Wall effects were calculated to determine their effect on the angle of attack of the model. The change due to the tunnel walls was found to be 0.281 degrees for the largest model from

$$\Delta\alpha_i = \frac{S/c}{8} C_L \quad (5.1)$$

where c is the tunnel cross section area. This adjustment was negligible for the smaller models at lower angles of attack.¹³

The data was reduced to lift and drag coefficients and center of pressure location for the model. The drag was obtained from the sum of the forces on the front two strain gauges, minus the tare. The lift was obtained from the sum of the forces on the other three strain gauges. The center of pressure was determined by first assuming the models had no moment at zero lift. Then the center of pressure was determined by the equation

$$x_{cp} = - \frac{F_5}{L} \quad (5.2)$$

where x_{cp} is the distance forward of the mid chord, and F_5 is the force on the fifth cantilever beam. Force coefficients and center of pressure locations were then plotted in Figures 20 through 30 and 45 through 53. Table 1 shows the areas and aspect ratios for the various configurations of the model.

The coefficient of lift vs coefficient of drag curves were reduced by adjusting C_D for aspect ratio. The coefficient of drag of a wing, assuming elliptic lift distribution is given by

$$C_D = C_{D_0} + \frac{C_L^2}{\pi AR} \quad (5.3)$$

Let two wings of different aspect ratio with equal C_{D_0} be given by

$$C_{D_1} = C_{D_0} + \frac{C_{L_1}^2}{\pi AR} \quad (5.4)$$

and

$$C_{D_2} = C_{D_0} + \frac{C_{L_2}^2}{\pi AR} \quad (5.5)$$

The equivalent drag coefficient adjusted for aspect ratio at the same lift coefficient is given by¹⁴

$$C_{D_2} = C_{D_1} + \frac{C_{L_1}^2}{\pi} \left(\frac{1}{AR_2} - \frac{1}{AR_1} \right) \quad (5.6)$$

The results of this adjustment are shown in Figure 63.

The pressure distribution data was taken on the manometer board with the tunnel running at 88 feet per second. The various configurations were tested at the same five angles of attack that were used for the force measurements. The model was tested in all of the possible configurations that were used in the force measurements.

The heights of fluid from the manometer were used directly to calculate the coefficients of pressure over the tips. The change in pressure could be determined from

$$\Delta p = \frac{\Delta h}{12} (\gamma) \rho_w \sin 16.5^\circ \quad (5.7)$$

where p is pressure in pounds per square foot, Δh is the height of the fluid in inches, γ is the specific gravity, and ρ_w is the weight density of water, with a manometer angle of 16.5 degrees. The coefficient of pressure is

$$C_p = \frac{p - p_\infty}{\frac{1}{2} \rho U^2} \quad (5.8)$$

The numerator of this equation is just the difference in the heights of the fluid between the point in question and the static pressure of the undisturbed flow, multiplied by $\frac{\rho_w (\gamma)}{12} \sin 16.5^\circ$. The denominator is the difference in the heights of fluid between the static pressure probe and the total pressure probe of the undisturbed flow, multiplied by the same coefficient. That coefficient, therefore, is cancelled out of the equation and

the coefficient of pressure becomes simply the ratio of the differences in the heights of the fluid. The coefficients of pressure are shown in Figures 31 through 34, and 54 through 62. The pressure coefficients have been plotted against the linear dimension of the wing tip. This method of display was chosen so that the pressure distributions might be more easily compared between the configurations of the wing tip and between changes in the aspect ratio of the basic wing.

The flow visualization tests were run at a speed of 44 feet per second. Using the lift data from the earlier experiments and assuming that the lift was due entirely to the bound vortex system, the models were all run at the same total circulation, given by

$$C_L = \frac{\Gamma}{U_s} \quad (5.9)$$

By varying the angle of attack, a proper coefficient of lift could be chosen for each wing area to match the circulation of the delta wing at 20 degrees. The other angles of attack were 12.2 degrees for the trapezoidal model with three inch center section, 8.8 degrees with the six inch center section and 4.6 degrees with the twelve inch center section. Later, the twelve inch trapezoidal model was observed at an angle of attack of 15 degrees. Photographs were taken along the leading edge of the delta wing. The camera was mounted upstream in such a position so as not to disrupt the flow over the wing, and yet provide as much detail of the flow as possible. Pictures were also taken from the side, and sketches were made of the flow situation when they were more suitable. These pictures and sketches are shown in Figures

35 through 44.

The experiments were conducted at negative angles of attack, in the usual sense, so that the lift would pull down on the wires, and any chance of lifting the model to the point where the wires would be slack was eliminated. From this point on in this report, the wing will be discussed as if it were at positive angles of attack, with the vortex system above the wing rather than below it, so that the discussions may be described in the way most readers are familiar with.

Chapter VI

DISCUSSION OF RESULTS

The uncertainty of the force measurement was recorded for a portion of the force measurement data. The forces became quite oscillatory for the higher angles of attack, and lateral oscillations of the slender rectangular models required the two additional wires be added to stop the sway. Still, a low frequency variation in the lift was experienced on several models, especially the six inch span rectangular wings with ogive and parabolic edges. The variations in recorded forces were less than two percent in the worst cases of oscillation. The effect of zero wander during the run was considerably less than this amount.

The angle of attack was measured by a variable angle level placed on the model, and this reading was accurate to within a quarter of a degree. The value of uncertainty in angle of attack is obtained from the variation in the change in angle of attack between models, since the lengths of the fifth wires that determined the angle of attack were the same for all models.

The manometer was connected to the model by a rather long set of pressure tubes. The effect of these tubes was to damp out fluctuations in the pressure, with its long response time. The manometer could be read to an accuracy of 0.05 inches, which was an error of 0.0064 in the coefficient of pressure.

The effect of the pressure tubes attachment to the trailing edge was evaluated in a test on the delta wing, where its effect should have been greatest. The delta wing was run with two sets of pressure tubes, one on each half-wing. The change in pressure distribution is shown in Figure 31.

The error induced appears to be less than two percent of the coefficient of pressure. The general trends of the pressure distribution are preserved exactly.

From the calibration data, the transducers had an error of, at most, 0.013 pounds or an error in coefficient of 0.0044. This is considerably less than the uncertainty in the measurement due to oscillations.

The results of the force measurements on the delta wing and the rectangular wings with delta wing tips are shown in Figures 20 through 30. In Figure 20, the coefficient of lift is compared to that predicted by Pohlhamus, and to that predicted by slender body theory. The results of Pohlhamus' theory agree very well, and the linear slender body theory appears to represent the coefficient of lift curve adequately up to angles of attack around 14 degrees. The initial lift curve slope is much less than the linear theory prediction, probably because the real flow does not develop a vortex for small angles of attack. The trapezoidal wings are remarkably well represented by slender body theory in the angles of attack shown. From Figure 24, it is seen that the lift curves for the delta wing, and the three and six inch trapezoidal wings are quite similar, while the twelve inch trapezoidal wing is quite different from the others. Measuring C_{L_α} at $\alpha = 0$ gives varied values of initial lift curve slope, as seen in Table 1, but the general result of the lift curve slope is about the same for the models other than the twelve inch rectangular wing. The very marked similarity between the first three models and the fourth seems to show a change in the flow situation between the groups. The twelve inch rectangular wing shows a stall condition that the other wings do not, in

the range of angles of attack tested. The aspect ratio increase is the greatest in the change from six to twelve inch centerspan, however.

The coefficient of drag curves in Figures 25 through 29 show the same effect. As Figure 29 shows the delta wing and the three and six inch trapezoidal wings have almost identical C_L vs C_D curves, while the twelve inch with delta wing tip is markedly different. The beginning of stall may be seen on the six inch rectangular wing, but there is no effect as great as the reduction in drag for a given coefficient of lift in the twelve inch rectangular wing. Its flow structure is apparently different from that of the other three models.

The induced drag of the trapezoidal wings is, in general, greater than that predicted by Equation (5.3). The increased drag is due to the non-elliptic lift distribution of the wings, and the rapid roll up of the trailing vortices, due to the increased vorticity in the flow.

The center of pressure was determined by assuming that there was no moment at zero lift, i.e., no camber in the wings, and that the wings did not induce flow curvature in the wind tunnel. Figure 30 shows the center of pressure data for the delta and wings with delta wing tips. The value for the higher angles of attack are the more reliable figures, because when the coefficient of lift is near zero, if there is any moment, the distance to the center of pressure will approach infinity.

The location of the center of pressure for the delta wing is at the 60 percent chord location. Slender body theory predicts that the center of pressure will be at the two thirds chord location, but the loss of lift at the trailing edge is responsible for the more forward location.⁶ This

value corresponds with other experimental results.²

The center of pressure moves forward with aspect ratio changes in the trapezoidal models. The three inch trapezoidal wing has a center of pressure at the 47 percent chord location, and the six inch wing has a location at about 38 percent chord. The twelve inch model has a center of pressure that appears to move with angle of attack. This is due to the change in flow conditions with angle of attack from smooth flow to short bubble separation and eventually to long bubble separation and complete stall. This changes the pressure distribution, while the other models do not exhibit the same flow characteristics.

The forward location of the center of pressure may have caused the vortex on the twelve inch trapezoidal wing to burst, when the smaller models did not. The higher adverse pressure gradient and a more forward center of pressure of the twelve inch trapezoidal wing may have induced the vortex to burst because of its chordwise pressure distribution in the center portion of the wing.

The spanwise pressure distribution results are shown in Figures 31 through 34. The pressure distribution for the delta wing, Figure 31, is not unlike results obtained previously.^{2,3} The double peak found at the highest angle of attack is due to the secondary separation of the boundary layer. The pressure peak moves inboard with increasing angles of attack, as noted in earlier tests.² The three centermost pressure stations reveal the flow outside of the spiral induced by the vortex is nearly directly along the axis, as mentioned earlier, and is apparently constant across the span in this region. It is also noticed that the pressure very near the

leading edge does not have a singularity, but instead appears to approach some finite value, although this value varies with angle of attack. Also, the unevenness of the pressure distribution between the fourth and fifth pressure ports as due to the shape of the wing. The slope of the wing changed midway between those two points, and the flow under the vortex crossed that ridge at a large angle.

In the case of the three inch trapezoidal wing, the coefficients of pressure near the peaks are increased by around twenty percent for the two highest angles of attack. Additionally, the vortices appear to have moved toward the centerline of the wing, especially for the higher angles of attack. For the two highest angles of attack, the velocities near the centerline are not constant in the span direction, as they were for the delta wing, but the lower three angles of attack are quite similar to the curves for the delta. This seems to indicate that, at least at the higher angles of attack, there is a change in the nature of the vortex. Noted are its change in position, the change in strength, and the change of lateral extent of its interaction with the flow over the rectangular portion.

For the six inch trapezoidal wing, the vortex seems to be located at the same position as it was for the three inch wing. Again, the strength of the vortex is increased, this time at about 10 and 15 degrees, and the effects of separation are seen in the highest angle of attack. The separation in the center section has reduced the peak pressure in the distribution and widened the influence of the vortex, so that the pressure is becoming more evenly distributed with span. This apparently is due to the interaction of the vortex flow with the separated region of the wing. Again, for

the lowest three angles of attack, the velocity is constant over the section of the delta wing tip outside of the vortex region, but the higher two angles of attack show the previously mentioned interaction with the interior flow situation. The curves near the center section are almost identical to those of the three inch rectangular model until this interaction begins.

The twelve inch trapezoidal wing shows the beginning of the same interaction at 16.0 degrees angle of attack and is completely stalled at 20.9 degrees. The highest two angles of attack were run twice because of the uncharacteristic profile of the 20.9 degree stall. There is no vortex in the flow at this angle. The pressure is constant in a completely separated form of the flow. The pressure distribution at 16 degrees is similar to the beginning stall condition of the six inch wing at 20 degrees. There is a considerable interaction between the delta wing flow and the sharp edged rectangle flow that is not found in the lower angles of attack. Again, the lower angles of attack show a very similar profile outside of the vortex flow. The pressure peak is located nearly the same place as it was for the three and six inch models, indicating that the effect of the rectangular section of the wing on the vortex is primarily an increase in strength. There is no change in the interaction with the upper surface of the wing at the lower angles of attack. This indicates that the strength of the vortex is determined by the flow under the wing, rather than the edge conditions. Its strength is determined by a separation condition, rather than the vorticity generated by the leading edge. Since the high pressure on the underside of a wing induces spanwise flow there, it is reasonable to assume that this spanwise flow increases the pressure difference in the

vortex required to attach the flow to the upper surface of the wing. The spanwise flow is increased with aspect ratio for the aspect ratios we are considering.

The vortices seem to have little effect on each other on the trapezoidal wings, because the extent of the vortex is not changed with increasing aspect ratio. The delta wing, however, does show some interaction because the location of the vortices is changed, even though there is a portion of the wing with straight flow between the vortices.

A description of the flow visualized by smoke is shown in Figures 35 through 44, outlining the various regions of the flow. The delta wing is shown in Figures 35 through 38, at an angle of attack of 20 degrees. Smoke released from the underside of the wing flows past the leading edge and then either into the core of the vortex or around the outer flow. A sketch of the flow that enters the core at about one third of the chord is shown in Figure 40. It is very difficult to determine exactly what happens at the leading edge. The flow there makes the turn around the leading edge very quickly, and it is very difficult to study the exact flow situation. No conclusion can be made, therefore, concerning the angle of flow that leaves the surface of the wing.

It was noticed, however, that smoke could not be injected to the vortex flow from the other side of the wing if the smoke probe was too close to the surface near the leading edge. If it was located too close, the smoke would remain on that side of the wing, condense, and run along the leading edge. This seems to indicate, with this model of delta wing at least, that the flow in the boundary layer does not flow toward the

leading edge, when it is very near it, but changes direction in the boundary layer, as in separation. This effect was not noticed previously, but most earlier models were either flat or had a smaller angle of bevel at the leading edge. The effect may simply be due to a separation phenomena, or a result of the condensation of oil in the boundary layer, but it may also indicate that the flow does not leave the leading edge parallel to the surface. More study is needed in this location.

The separation of the boundary layer flow beneath the vortex was clearly seen in all runs with smoke visualization, because the oil condensation formed a ridge on the surface of the wing. This ridge line was in exactly the same position for all of the models tested. This is because the peak pressure was in the same location for each of the models at the angles of attack they were tested, although the peak location was a function of angle of attack.

The flow in the delta wing vortex was studied to a little closer detail using the oil smoke visualization, and at an angle of attack of fifteen degrees. The vortex layer nearest the core was found to originate near the apex of the delta. The flow picture may be seen in Figures 37, 38 and 40. The smoke released from a point went directly to that layer, and remained approximately that distance from the center of the core as it passed over the wing and down the tunnel, except for its diffusion. The core position was stationary and apparently stable. No burst was detected, and the same ring of smoke initially formed extended far down the tunnel. The smoke may have been kept out of the core by centrifugal acceleration, because the center of the vortex may be seen to be nearly free of smoke in

Figures 37 and 38. However, the layers of the vortex may not all enter the core if the rate at which the vortex sheet approaches the center is similar to the rate of increase of scale in the conical flow. There is some interaction between the vortex and the rolling up trailing edge vorticity seen in Figures 37 and 38 as kinks in the vortex axis.

Moving the smoke probe further from the wing at the same chord position resulted in flow that is farther from the core, but part of the flow that is still inside the vortex region and around the core, as seen in Figure 35. Part of this flow continues to encircle the core, while a portion of the smoke remains in the flat portion of the wake created at the center of the wing, between the two stagnation lines.

No smoke could be introduced into the core region. This may have been due to the centrifugal effect of the flow, the high axial velocities and diffusion rates, or the probe's effect on the stability of the vortex flow. The position required was extremely critical, and, perhaps, may not have been reached.

The three inch trapezoidal wing was observed at 12.2 degrees. It was noticed that the outer streamline of the vortex region was not straight but, instead, curved toward the centerline of the wing. This appears to be the result of the centerward shift of the vortex core that was observed in the pressure distribution curves. The interaction between the two vortices in the delta wing may prevent this effect. This result may also be due to the fact that the strength of the vortex, associated with the spanwise flow on the undersurface of the wing, is no longer linear. However, the separation line under the vortex remained a straight line.

The six inch trapezoidal wing showed a similar result in Figure 43, but the effect was not nearly so pronounced. This is due to the fact that the angle of attack was only 8.8 degrees. The separation line was exactly as before, but a new flow regime was created. In this model, a separated flow bubble was observed from the leading edge to the trailing edge of the rectangular section. This separation bubble is the expected flow situation for sharp edged unswept wings at moderate angles of attack. Smoke introduced into the bubble remained, for the most part, inside the bubble. The separated region formed the center of the wing, while between it and the vortex region, there was an area of flow where the flow was unseparated and nearly straight. This flow is caused by the vortex influence on the flow, causing it to remain close to the wing. It is similar to the flow sometimes found at the centerline of a delta wing.

For the same total circulation, the twelve inch trapezoidal wing had smooth flow throughout with no observable vortex, so the angle of attack for the test was increased to 15 degrees. At this point, the section was beginning to show the first effects of stall in the measured force and pressure distribution curves. At fifteen degrees, the flow was very similar to the previous model. The vortex, the separated bubble, and unseparated flow between them were observed, as shown in Figure 44. The deflection of the streamlines in the unseparated region toward the center on the last half of the wing were considerably greater than on the previous model and are, therefore, presumed to be a function of the angle of attack.

The ability of the vortex to induce unseparated flow away from the vortex region is limited, therefore. As seen in Figures 43 and 44, this

region is not very large and stall eventually may destroy the vortex entirely, at angles of attack when the vortex would normally continue to exist on the delta wing. The vortex appeared to begin a short distance inboard of the intersection of the unswept and swept portions of the leading edge. The extent of this interaction was small, but apparently necessary for the attachment of the unseparated flow that continued aft of it in the region between the vortex and separated regions.

There is a great disparity in aspect ratio between delta wings and rectangular wings that appear to be of similar size. A delta wing has twice the aspect ratio of a rectangular wing of the same span and root chord. For this reason, the smallest aspect ratio of the wings with delta tips is 1.50, while the largest rectangular wing has an aspect ratio of only 1.157 and the smallest has a value of only 0.329. This causes a wide variation in the results for wings that appear to be similar, yet have widely varying aspect ratios. For example, there is an increase in aspect ratio from 0.329 for the three inch rectangular wing with round fairings to 1.60 for the three inch rectangle with triangular tips.

The results of the force measurements on rectangular wings are shown in Figures 45 through 53. A comparison of the lift curves is shown in Figures 45 through 47. For the three inch rectangular wing, the remarkable similarity between the curves for the ogive and parabolic fairings, and their difference from the wing with round fairings implies that there is a considerable difference in the flow situation at the tips. It is known that the flow around the tip tends to flow from the lower surface to the upper, because of the pressure difference and the vorticity shed from the wing. The sharp ogive, and the parabolic section fairing are apparently "sharp"

enough that they generate more vorticity in the flow near the tip forming a vortex above the wing, resulting in greater lift on those wings for a given angle of attack. At this Reynolds number, the ogive and parabolic faired wings are approximately the same flow situation.

The six inch rectangle is different, however, because the difference between the ogive and parabolic faired wings, and the round fairing wing, is less distinct. The twelve inch rectangles are completely different from the three inch wing, because now the three curves are very nearly the same. This seems to imply that the undersurface of the wing, as before with the highly swept wings, seems to determine the strength of the upper surface vortex, at these somewhat larger aspect ratios. The increased outflow near the wing tip as aspect ratio is increased may be the cause of the fact that the three curves for the rectangle become the same as aspect ratio is increased.

It is also noticed, as shown in Table I, that there is an aspect ratio change between the round fairing, and the parabolic and ogive fairings. This adds to the difference in lift, and is responsible for a portion of the difference.

Figures 48 through 50 show the C_L vs C_D curves for the rectangular wings. Figure 48 shows that the wing with round fairings has considerably higher drag for a given lift coefficient in the three inch rectangle wings. This effect is less pronounced in the six inch rectangle wings, and almost non-existent in the twelve inch rectangle wings.

The probable reason for this phenomena is that the round fairings allow the tip vortices to be much closer than the ogive and parabolic

fairings, due to the relative sharpness of their edges. The sharp edged wings, therefore, have a higher effective aspect ratio. This would cause the wake to roll up sooner resulting in a greater induced velocity and higher induced drag for the round fairings.

This explanation is upheld by the pressure coefficient data, seen in Figures 54 through 62. In every case, for the parabolic and ogive fairings, a pressure peak is seen on the fairing and it moves toward the centerline with angle of attack. The curves for these two are quite similar, which explains why the lift and drag characteristics are similar. The tip region is stalled for the twelve inch rectangles, indicated by the even pressure distribution, but the lift curves do not imply that the whole wing had been stalled. The pressure distribution on the round fairings does not show very much about the situation of the flow there, partially because of the small percentage of span explored. It does show that the general trend of increased velocity around the tip with angle of attack, due to the increased circulation of the wing and stall may be observed from the increase in pressure coefficient at an angle of attack of 20 degrees on the twelve inch wing.

The reduction of the C_L vs C_D curves using Prandtl's relation, Equation (5.6), is shown in Figure 63. The curves for all of the trapezoidal wings, and the delta wing are fairly close together, and the twelve inch rectangular wings are also very similar. The drag of all of the wings of aspect ratio less than one is considerably less, under this adjustment scale, than the group of higher aspect ratio wings. The six inch rectangular wings are grouped together and the three inch rectangular wings show a reverse

curve into negative drag. This indicates that Equation (5.6) overestimates the adjustment, and, therefore, its estimate of the induced drag is in error. The amount of induced drag appears to be proportional to the coefficient of lift squared, because wings of the same aspect ratio fall on the same line. The difference in the nature of the curves for aspect ratios less than one indicates that the induced drag is not proportional to the inverse of aspect ratio for these wings. The induced drag is much less than Equation (5.3) predicts.

Comparing Figures 29, 48, 49 and 50, the six and twelve inch rectangular wings have C_L vs C_D curves that are similar to the trapezoidal wings, and the delta wing, despite wide aspect ratio differences. The three inch rectangular wing, however, has a much higher drag for a given lift. The most likely reason for this is that the trapezoidal wings have a very high concentration of vorticity near the tips for their aspect ratio. The rectangular wings have a more evenly distributed lift, not concentrated near the tips as in the trapezoidal wings, with leading edge vortices. The concentration of vorticity near the tips causes the trailing vortex sheet to roll up more quickly and produce a greater induced drag.

The center of pressure location is shown in Figures 51, 52 and 53. The center of pressure is considerably ahead of the center of area predicted by slender body theory⁶, but this is to be expected since the theory should not apply to unswept wings. The pressure peak due to the sharp leading edge would tend to move the center of pressure forward as aspect ratio increased.

The center of pressure location is, in general, farthest forward for the six inch rectangular wings. Because some of the curves tend to

diverge as α approaches zero, a moment must exist for zero angle of attack. There is no possible method of determining this using the five wire support for the model, so that the information concerning center of pressure should be questioned. The effect of the zero lift moment on the center of pressure decreases with angle of attack. The zero lift moment is apparently caused by a defect in the model resulting in an effective camber.

CONCLUSIONS

In general, the results of the experiments show that the trapezoidal wings have more induced drag than elliptically loaded wings of the same aspect ratio, because of the increased concentration of vorticity near the wing tip from the highly swept leading edge. The strength of the leading edge vortex increased with increasing aspect ratio in such a way that the three and six inch trapezoidal wings exhibited lift and drag curves that were nearly identical to those of the delta wing. The increase in strength of the leading edge vortices was necessary for attachment of the flow to the upper surface of the wing because of the increased spanwise flow on the undersurface associated with the rectangular portion of the wing. The vorticity generated by the swept leading edge apparently determines the location of the vortex, because the vortex was found to be in the same location for all of the trapezoidal wings. The delta wing, however, has some interaction between the two leading edge vortices, because they were displaced a small amount toward the leading edge.

The rectangular portion of the wing exhibited a separation bubble over a portion of the upper surface in the six and twelve inch trapezoidal wings. Next to this bubble, an unseparated flow was induced by the vortex. The extent of this interaction was small, but apparently increased with angle of attack. The stall of the wing destroyed the vortex, and angles of attack just below stall had the effect of spreading the pressure peak due to the vortex. The adverse pressure gradient on the rectangular portion of the wing may have caused the vortex to burst at these angles. At lower

angles of attack, the interaction of the vortex and rectangular wing flow was limited to the induced unseparated flow region.

The pressure distribution near the tip of the rectangular wings exhibited a pressure peak indicating that a small vortex had been generated by the vorticity at the wing tip. At the test Reynolds number, the ogive and parabolic fairings apparently are sharp enough to create a separated flow there. The curves for these two fairings were remarkably similar, and exhibited a lower drag for a given lift than the round fairings. This effect was partially due to the somewhat reduced aspect ratio of the wing with round fairings, but, additionally, the flow did not appear to separate at the extreme tip, resulting in a lower effective aspect ratio as well. The six and twelve inch rectangular wings were all very similar curves indicating that the separation was also governed by the spanwise flow near the tip.

The experimental lift and drag curves show that slender body theory gives an approximate value of the lift, but begins to have significant error at high angles of attack, and when aspect ratio becomes too large. Pohlhausen's theory predicts the lift curve very well for the tested delta wing. The induced drag predicted for an elliptic lift distribution underestimates the drag on the trapezoidal and delta wings, and overestimates the drag on the low aspect ratio wings. This is not unexpected, however, because lifting line theory fails at low aspect ratio.

Further study is required to determine what angle the flow leaving the leading edge creates with the leading edge, and whether separation occurs on the underside of the wing. The Kutta condition, requiring finite

velocities and pressures at the leading edge, is satisfied, but the exact details of the flow situation there requires further examination. Additional study of the effect of sweep on the strength of the leading edge vortices of trapezoidal wings is required, as well as further study of the structure of the vortex itself, for a complete and thorough knowledge of the flow. There may be additional usefulness in a more complete study of the unseparated flow region of trapezoidal wings, to determine if chordwise fences or moderate sweep might increase the size of this region, and, hence, improve the overall characteristics of the total wing.

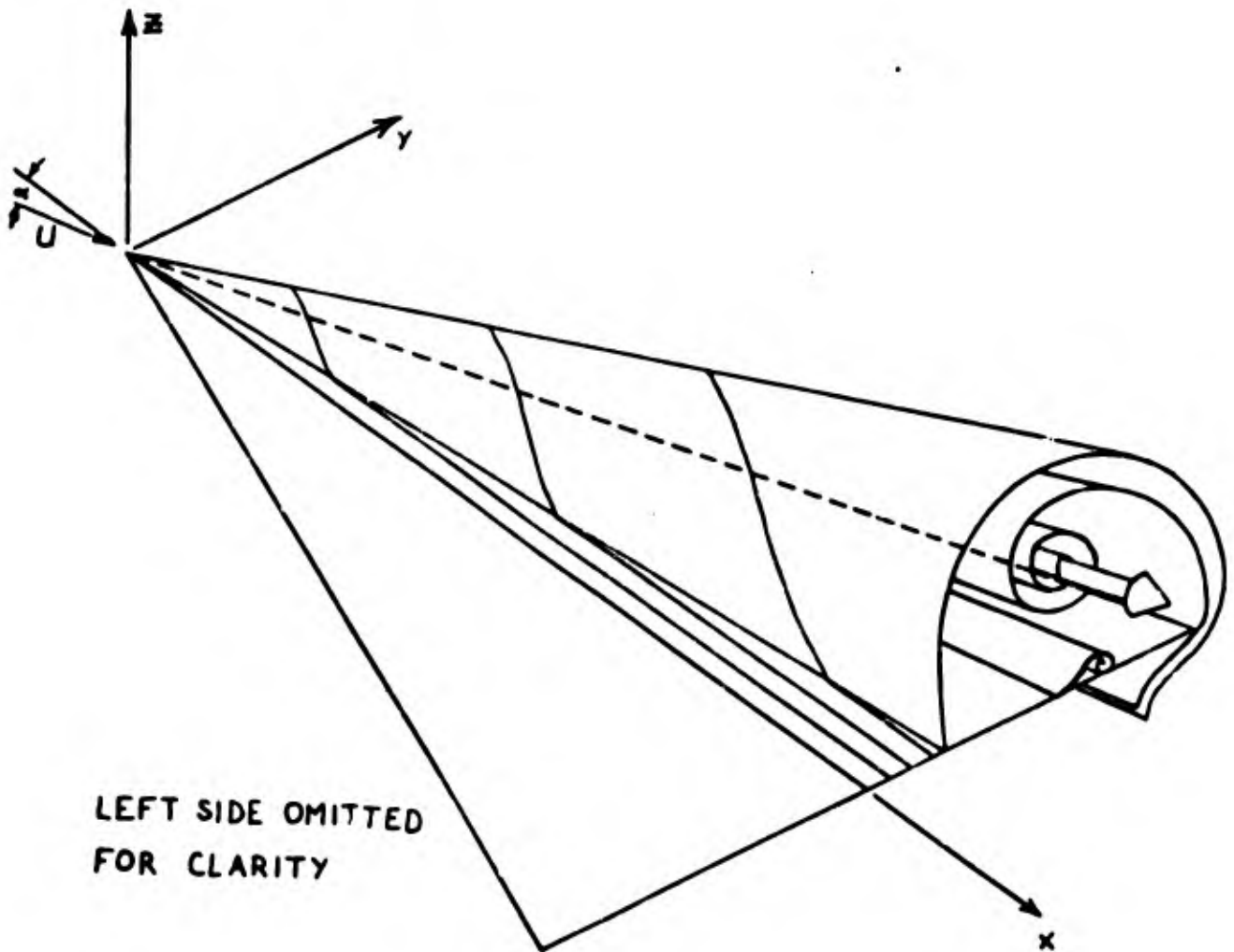


FIGURE 1 FLOW AROUND A DELTA WING

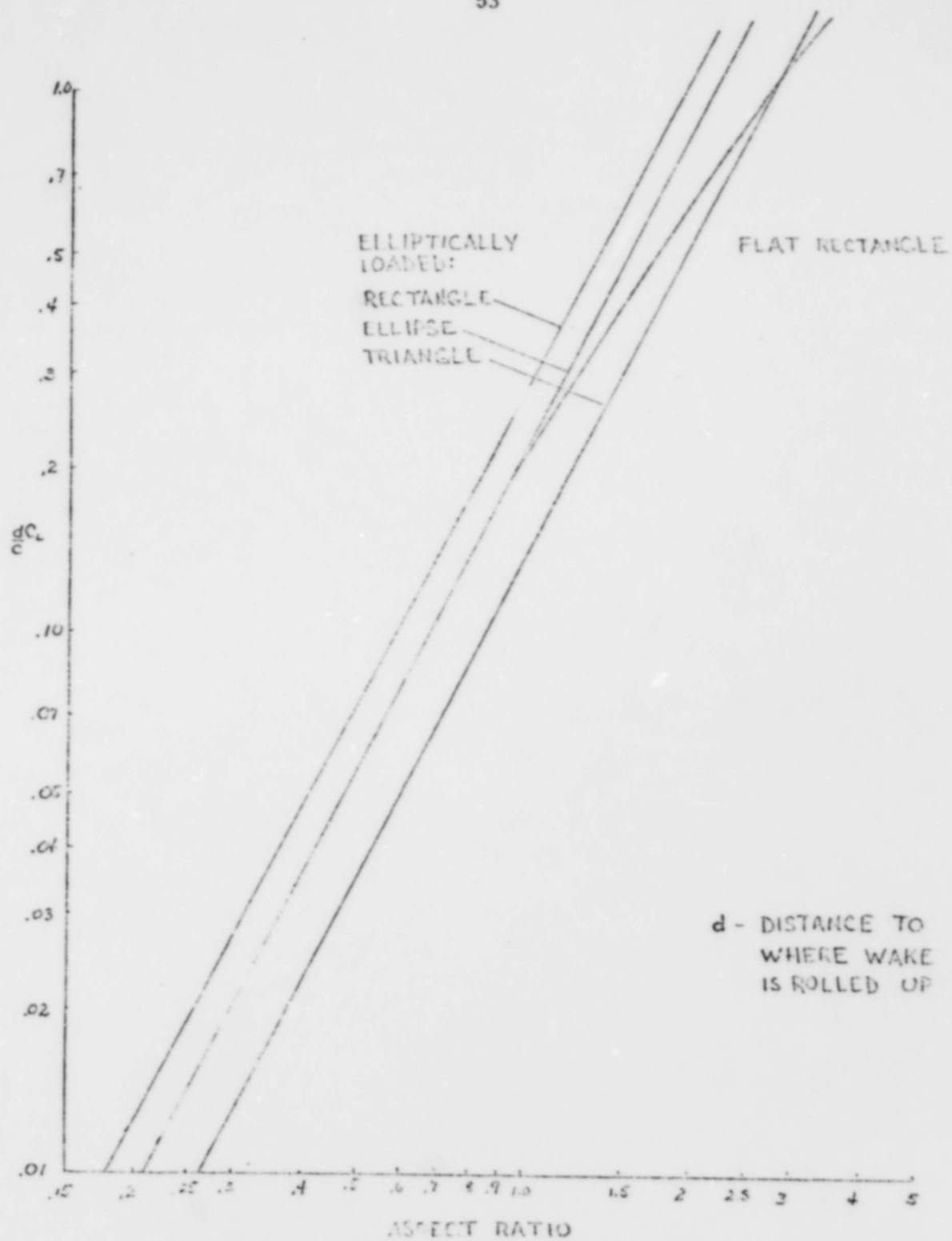


FIGURE 2 - TRAILING VORTICITY ROLL UP DISTANCE

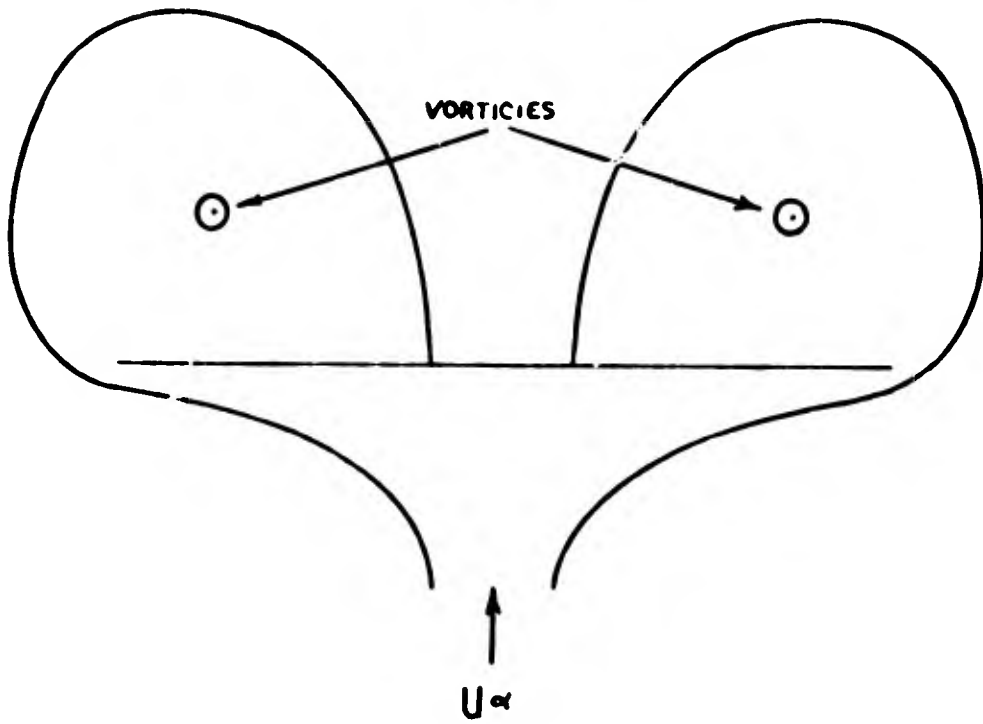


FIGURE 3

EDWARDS' CROSSFLOW PLANE

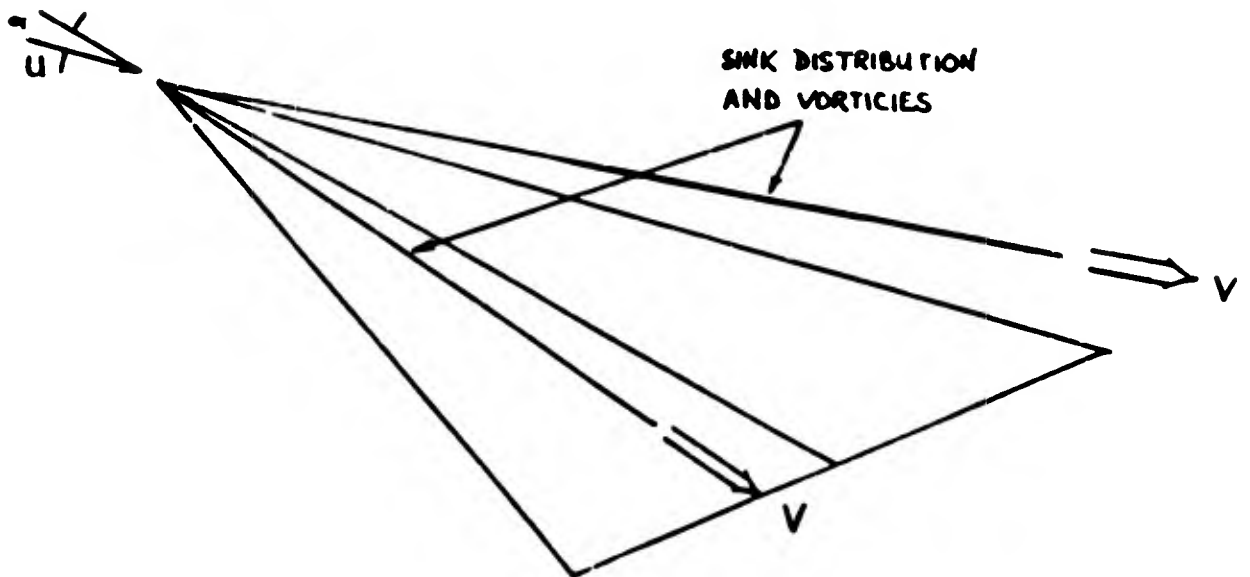


FIGURE 4

COE'S DELTA WING MODEL

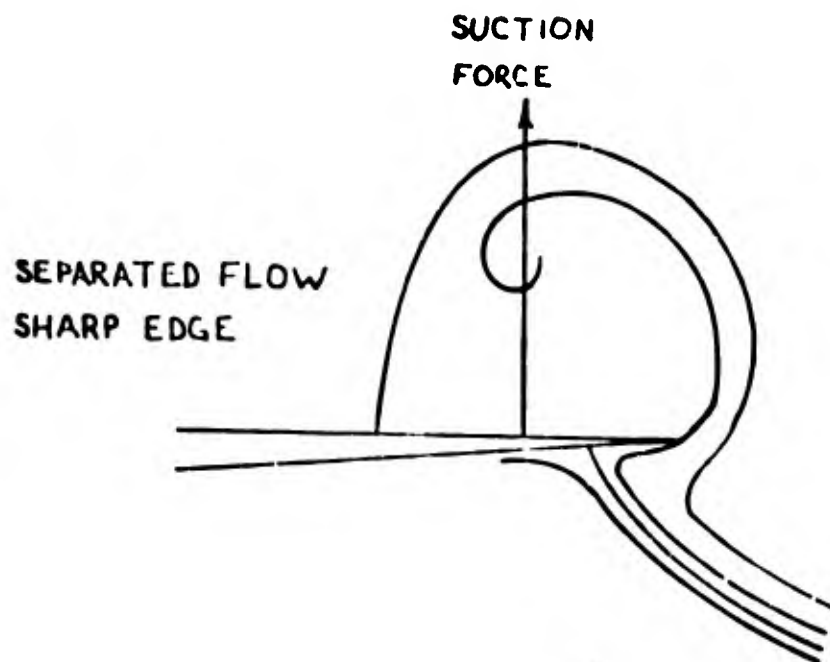
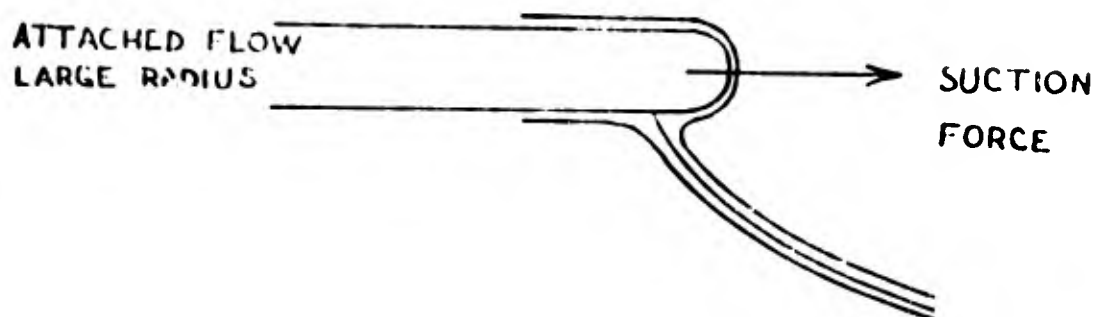


FIGURE 5
LEADING EDGE SUCTION ANALOGY

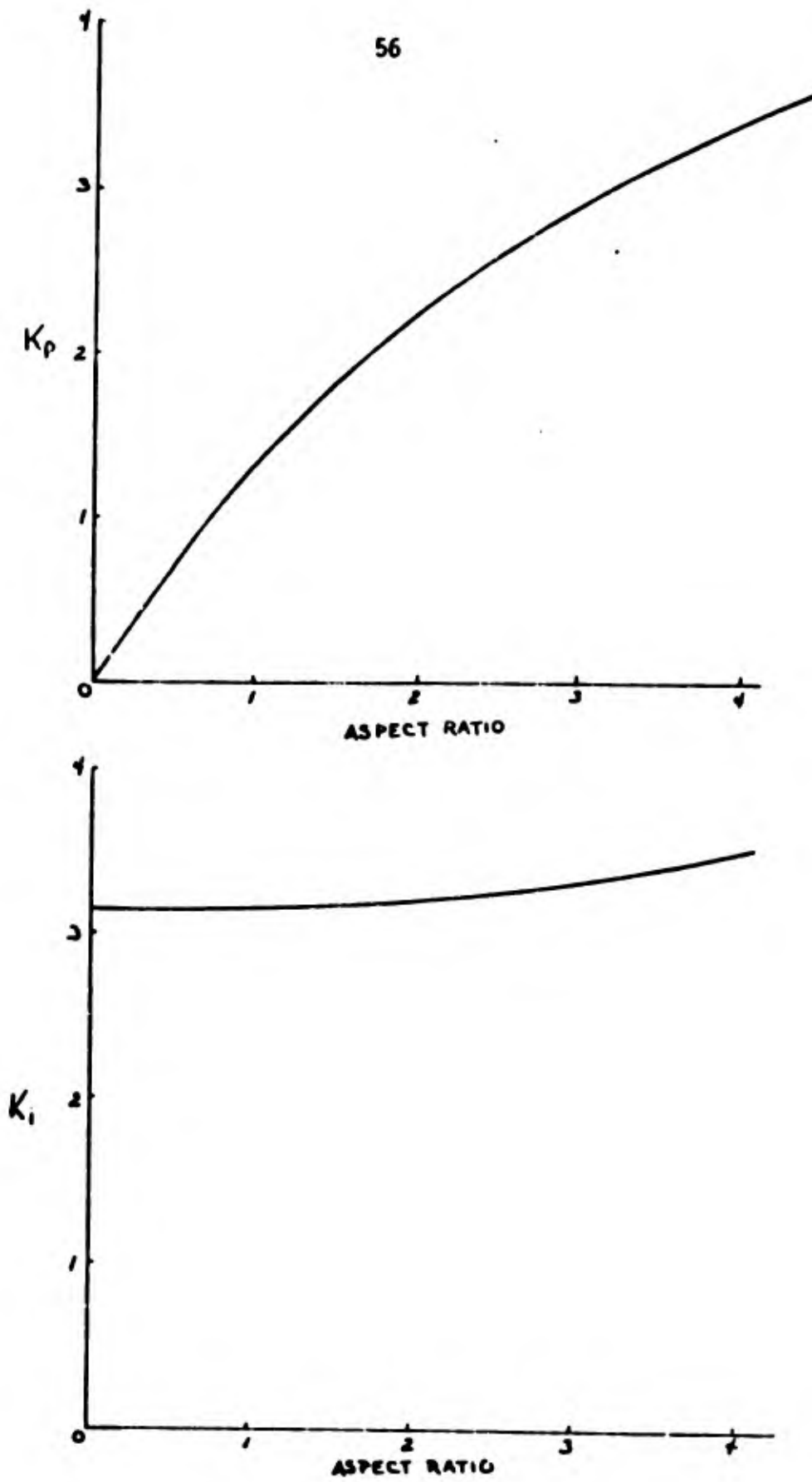


Figure 6 INFLUENCE COEFFICIENTS FOR POHLHAMUS' LIFT EQUATION

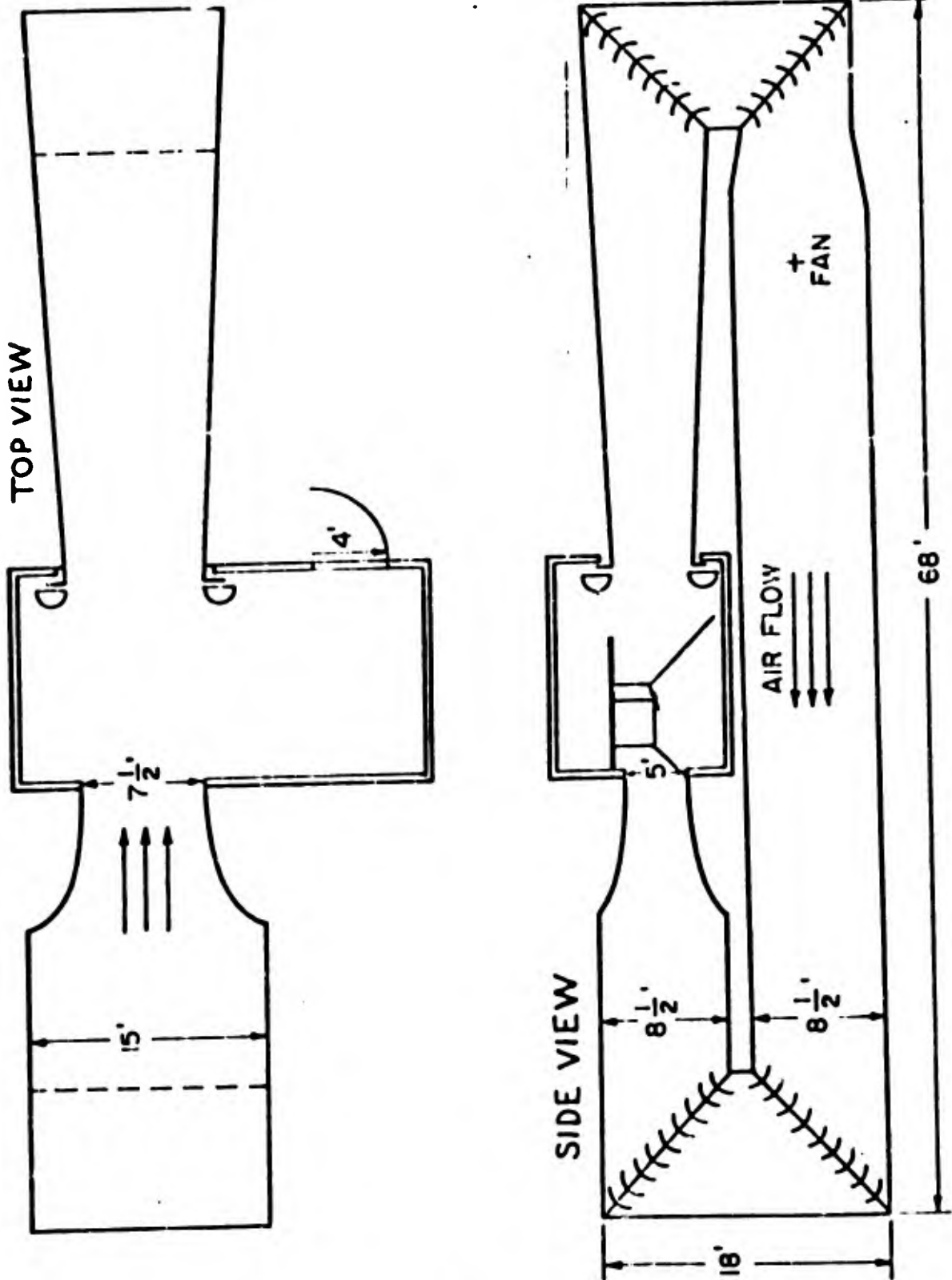
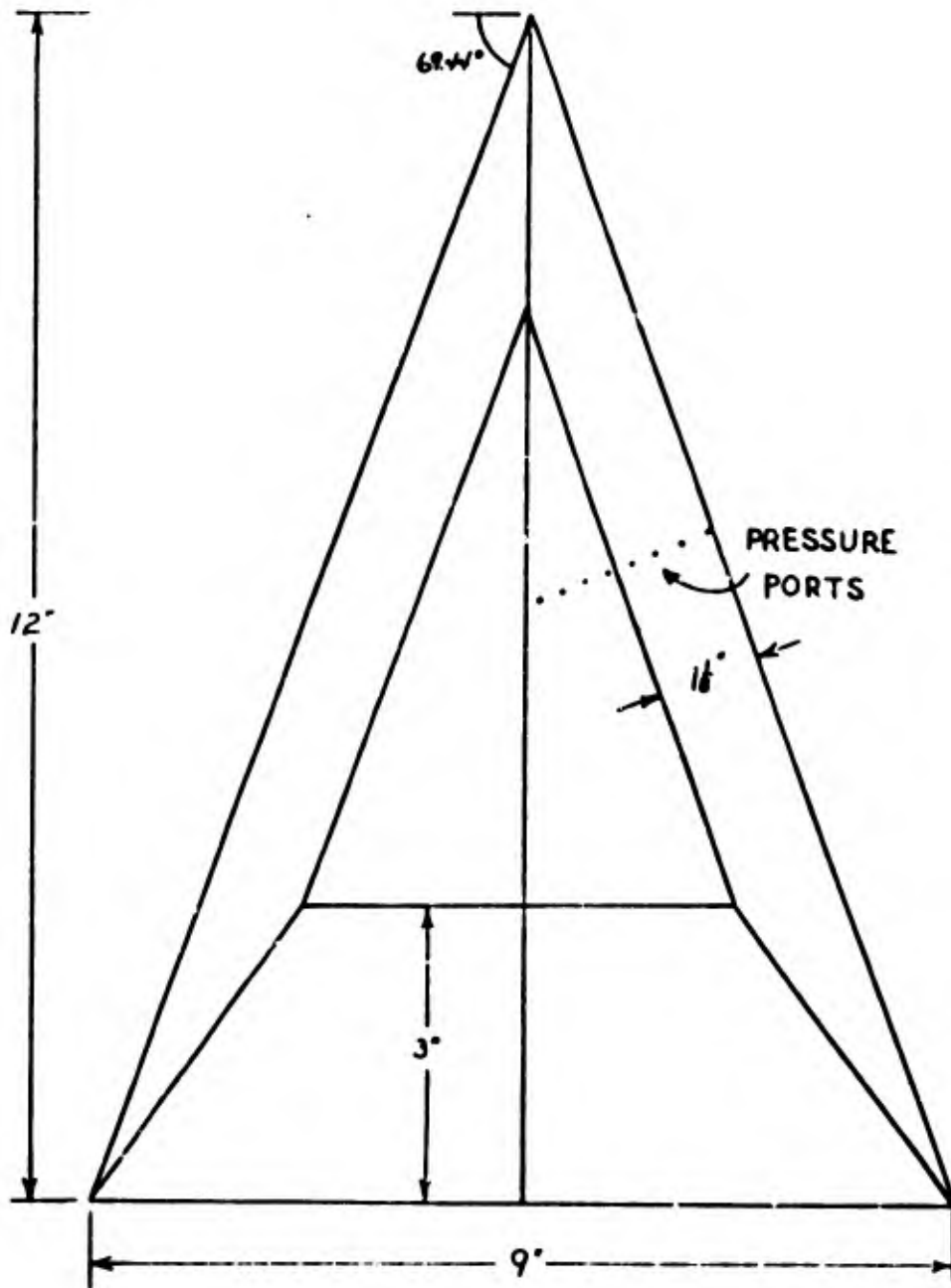


FIGURE 7
SUBSONIC WIND TUNNEL



$\frac{1}{2}$ SCALE
DIMENSIONS IN INCHES

FIGURE 8
PLANFORM-DELTA WING

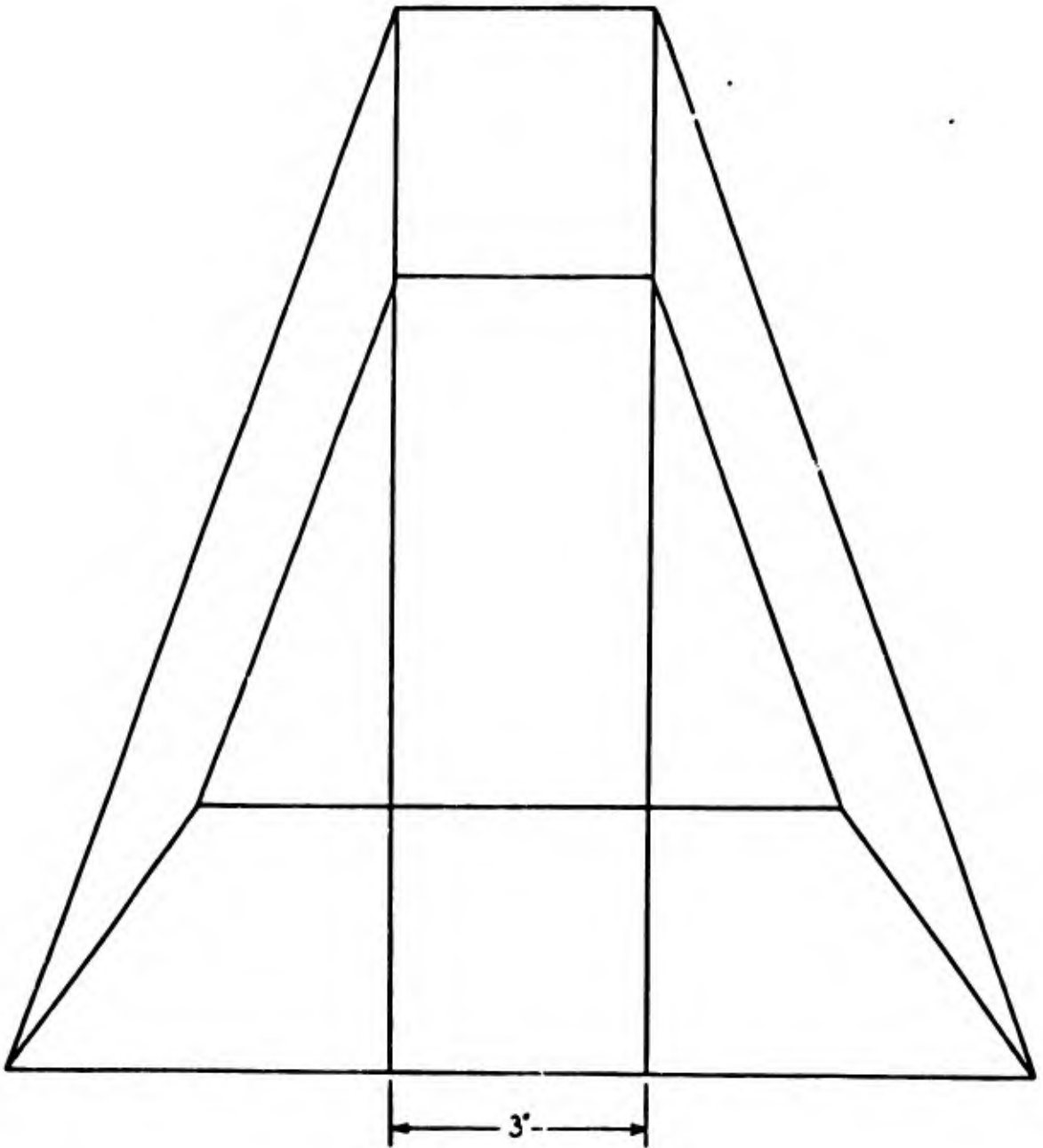


FIGURE 9
PLANFORM-THREE INCH TRAPEZOIDAL WING

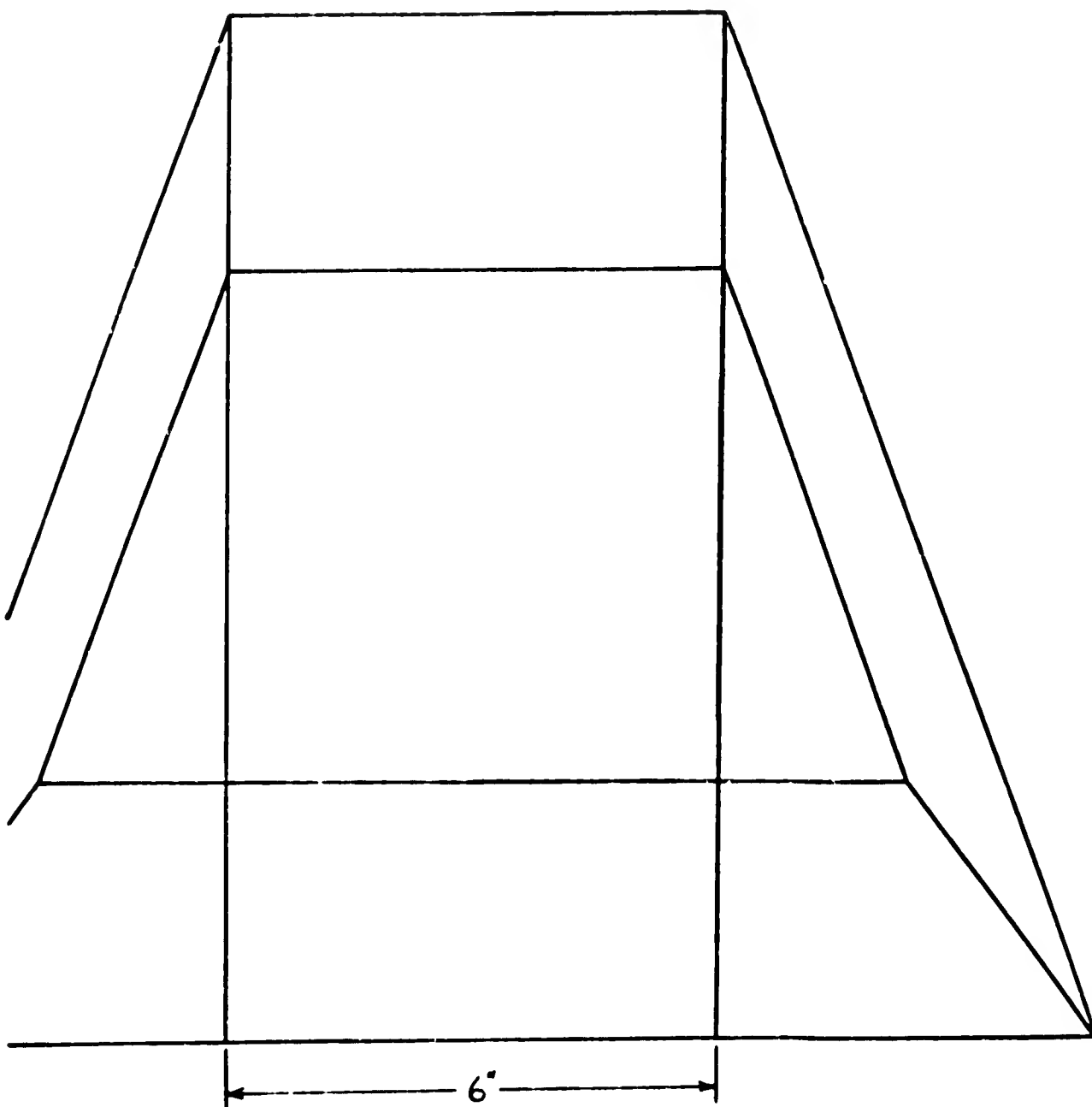


FIGURE 10

PLANFORM-SIX INCH TRAPEZOIDAL WING

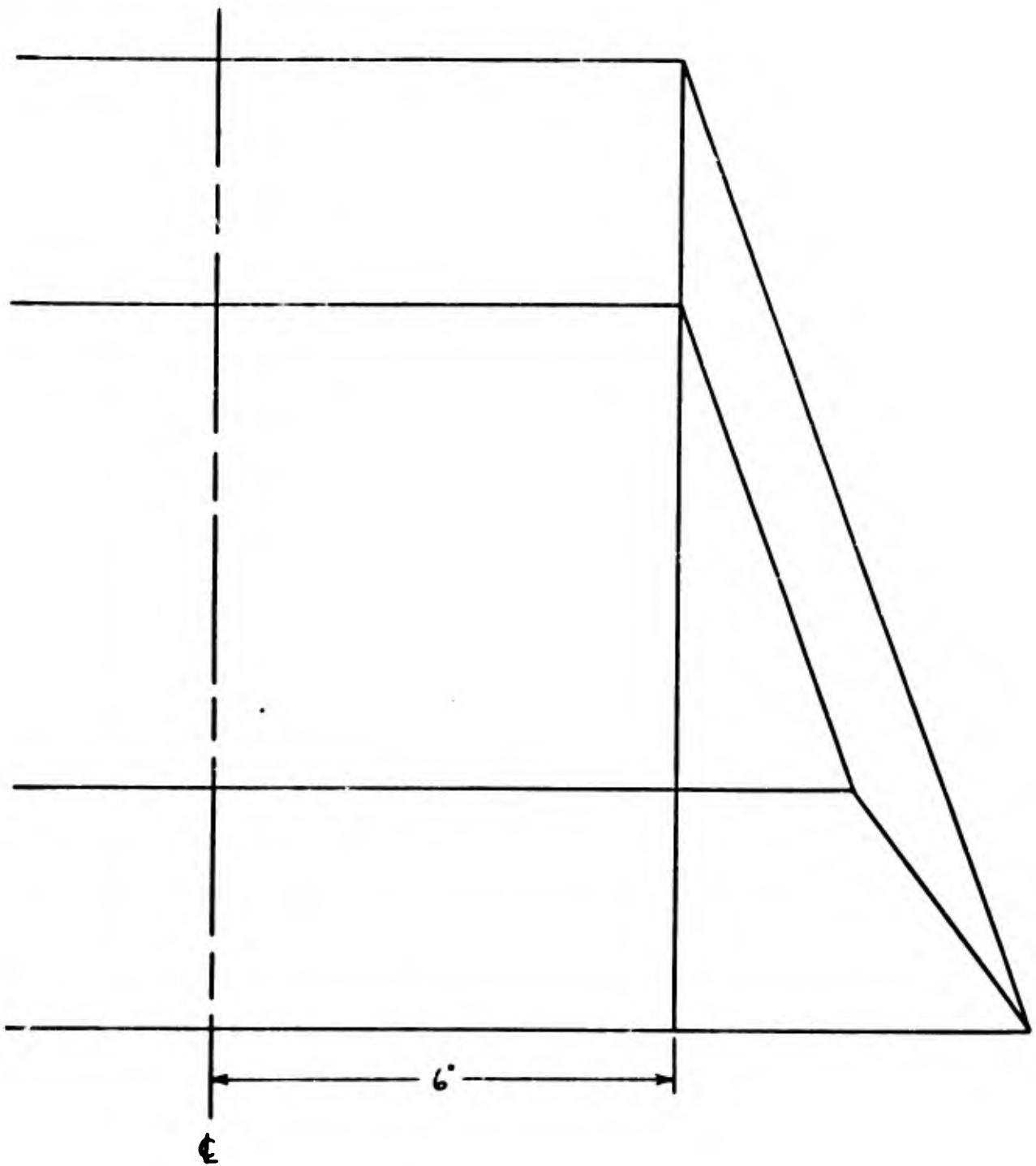


FIGURE 11
PLANFORM-TWELVE INCH TRAPEZOIDAL WING

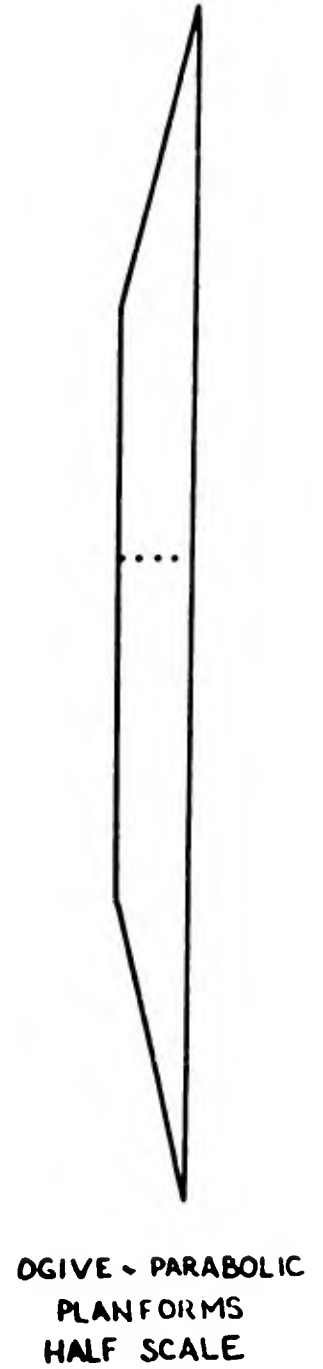
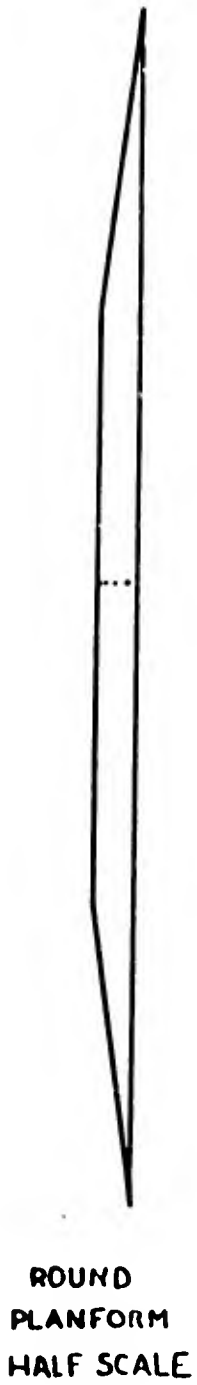


FIGURE 12
WINGTIP FAIRINGS

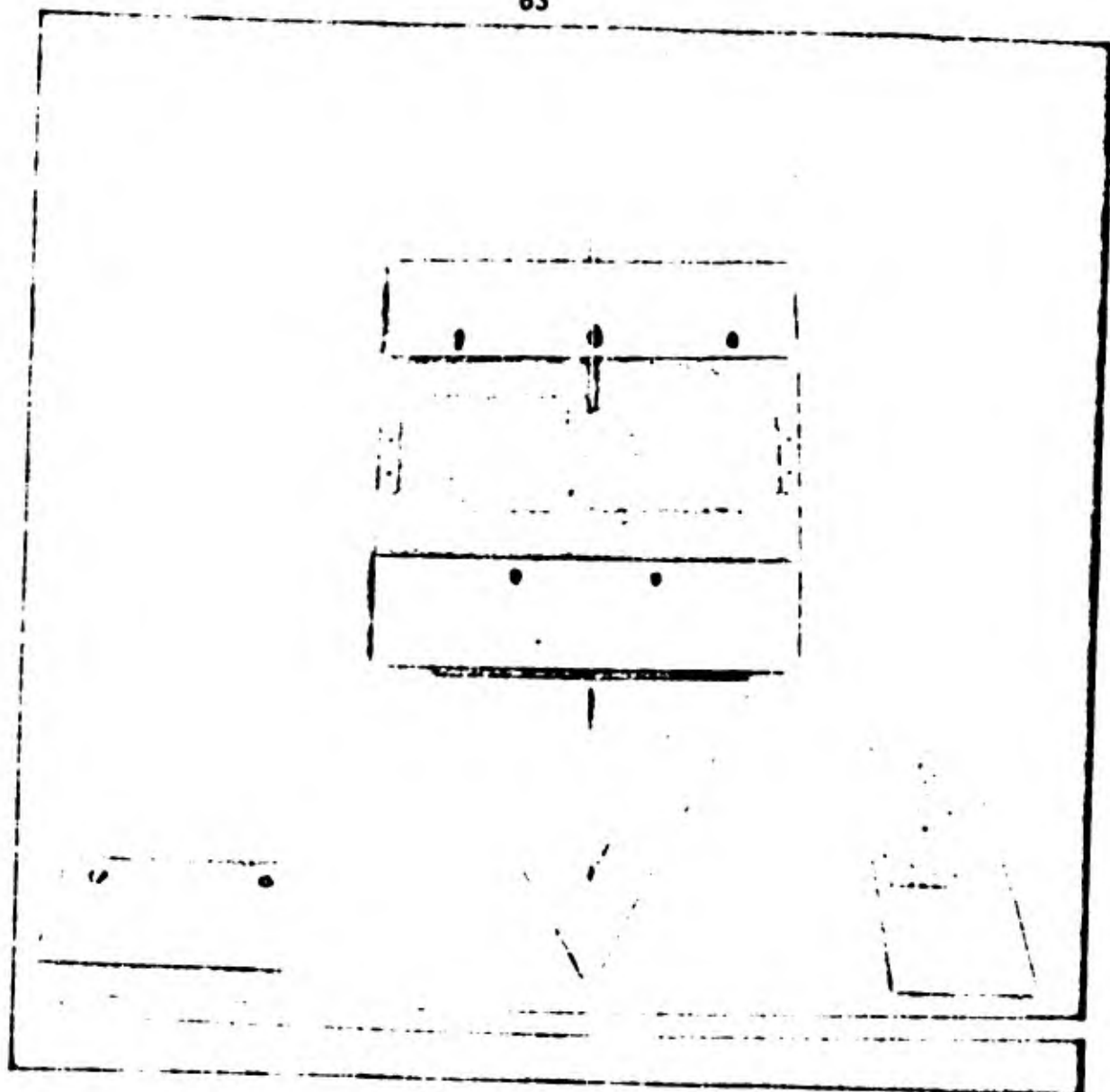


FIGURE 13
FORCE MEASUREMENT MODEL

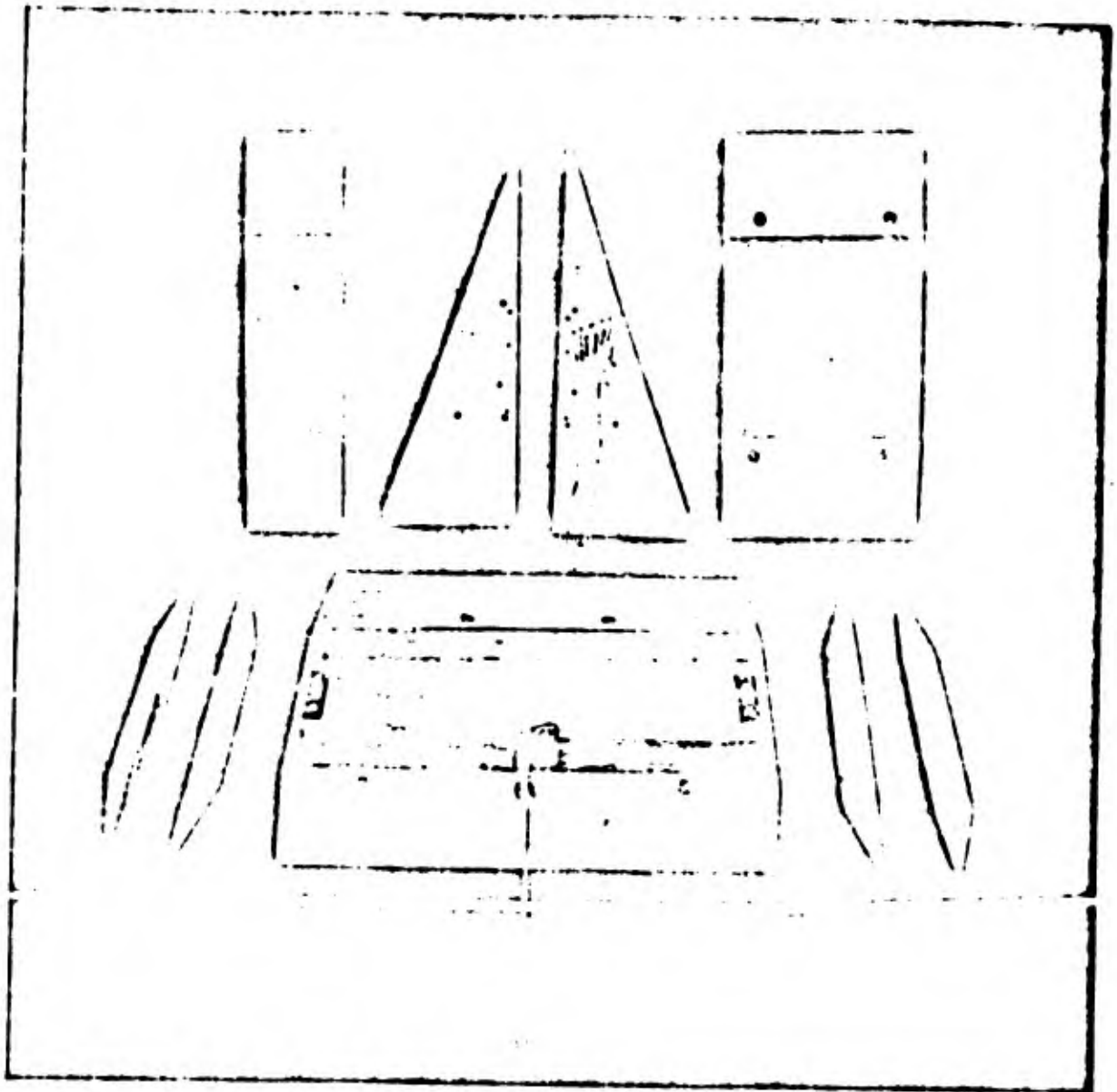


FIGURE 14
PRESSURE DISTRIBUTION MEASUREMENT MODEL

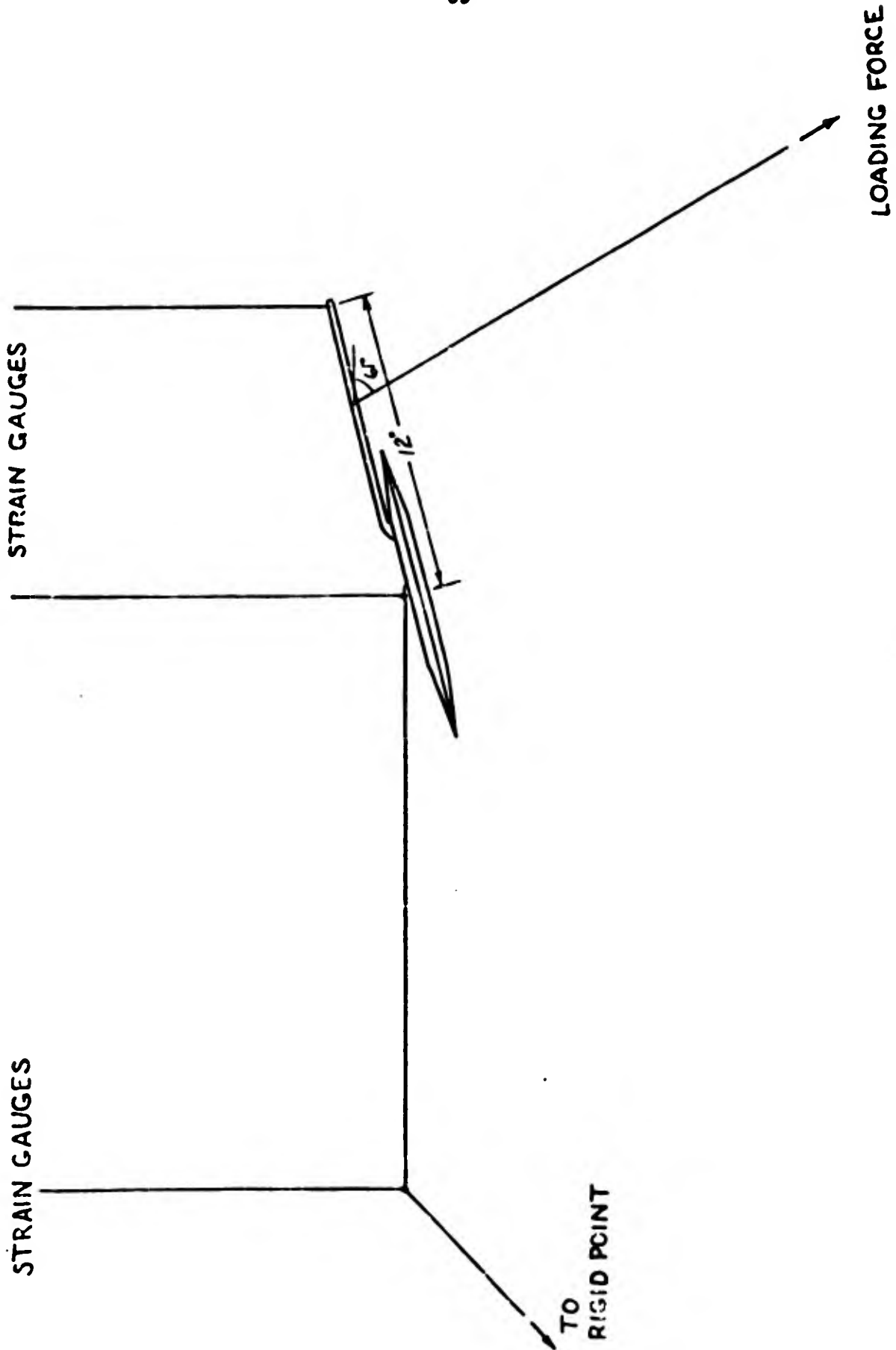


FIGURE 15
MODEL MOUNTED IN TUNNEL - SKETCH



FIGURE 16

MODEL MOUNTED IN TUNNEL - PHOTOGRAPH



FIGURE 17

PRESSURE MEASUREMENT MODEL MOUNTED IN TUNNEL

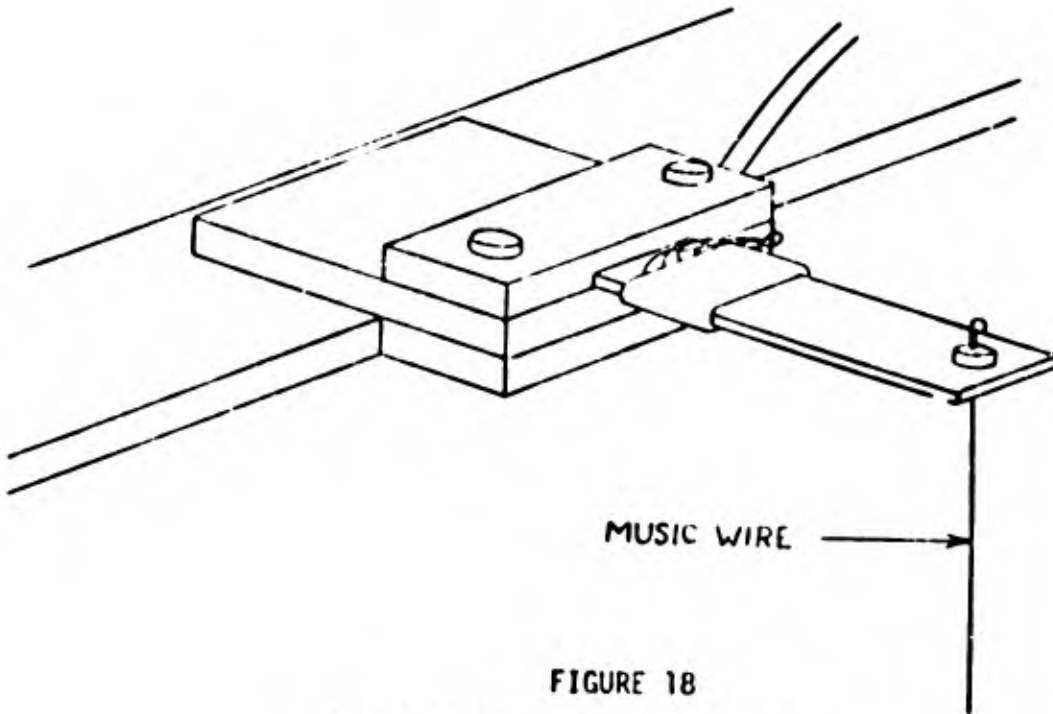


FIGURE 18

CANTILEVER BEAM WITH STRAIN GAUGES

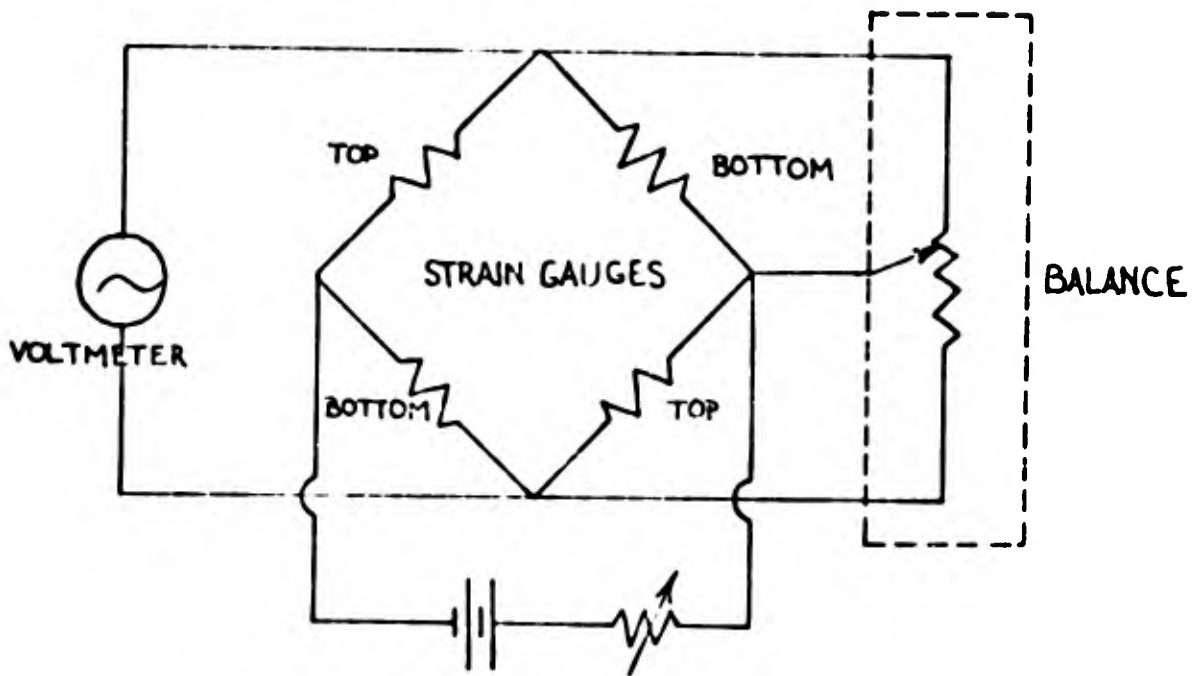


FIGURE 19

STRAIN GAUGE BRIDGE CIRCUIT SCHEMATIC

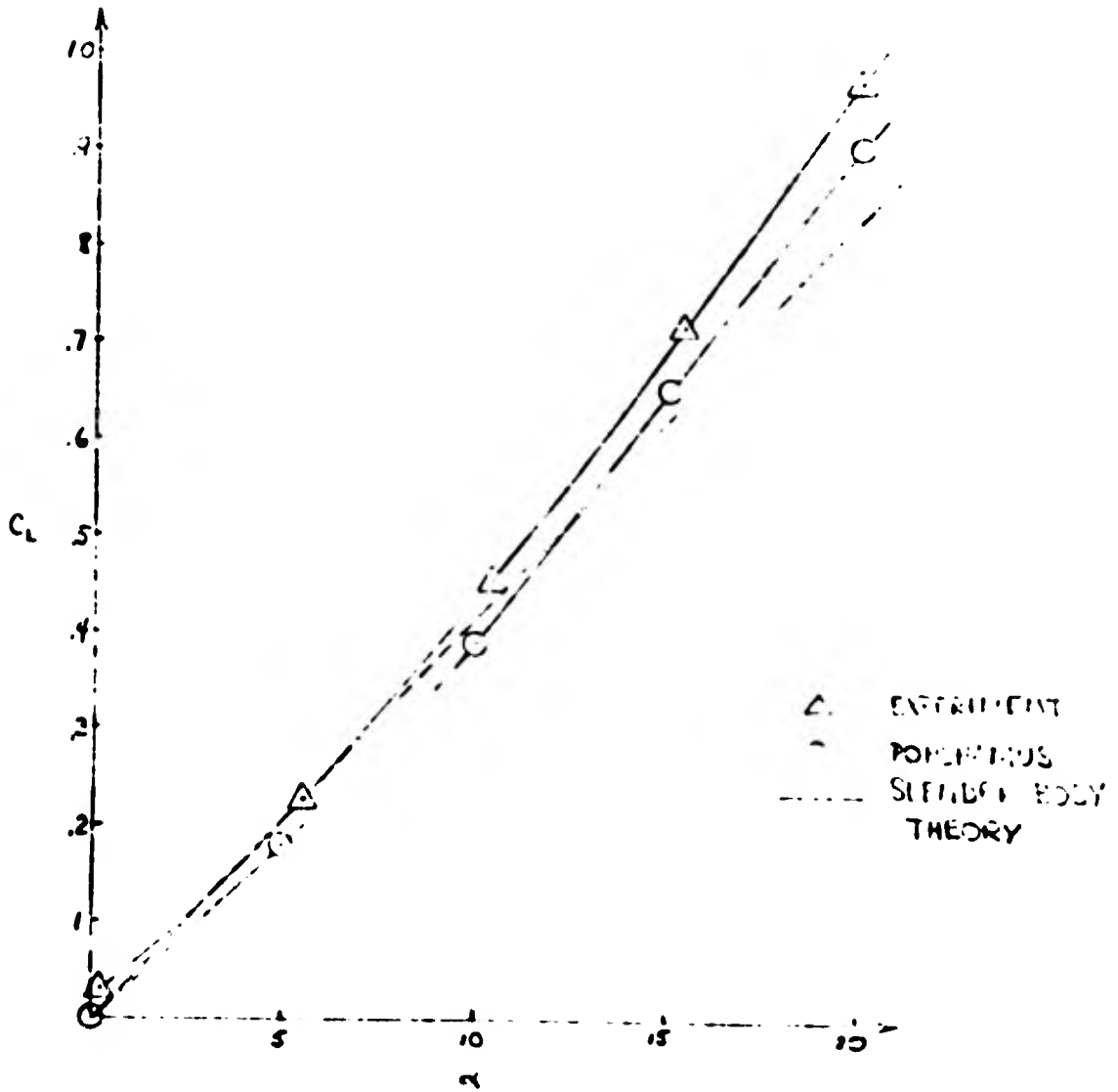


FIGURE 20

COEFFICIENT OF LIFT VS ANGLE OF ATTACK: DELTA WING

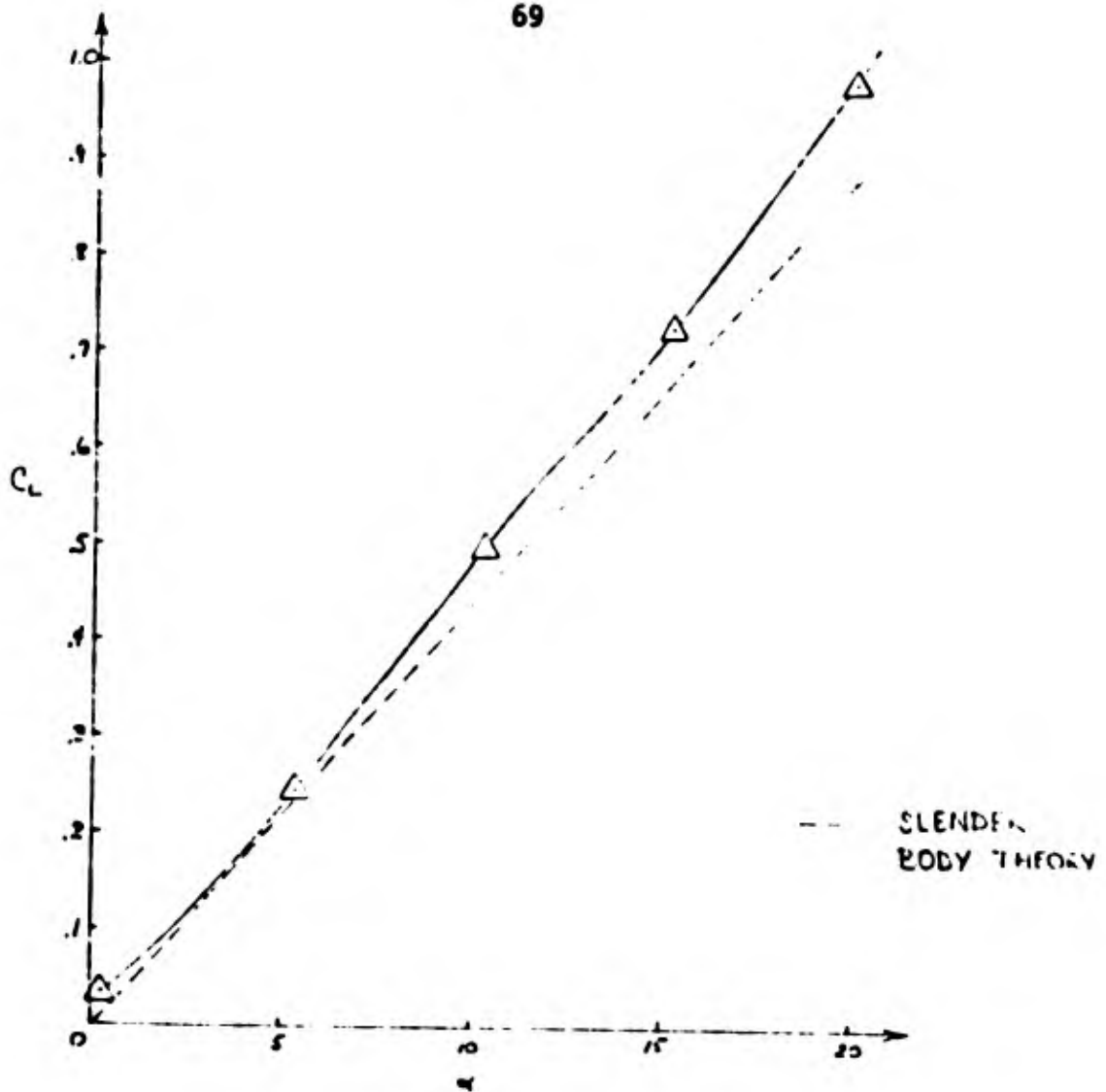


FIGURE 21
COEFFICIENT OF LIFT VS ANGLE OF ATTACK: 3 INCH TRAPEZOID

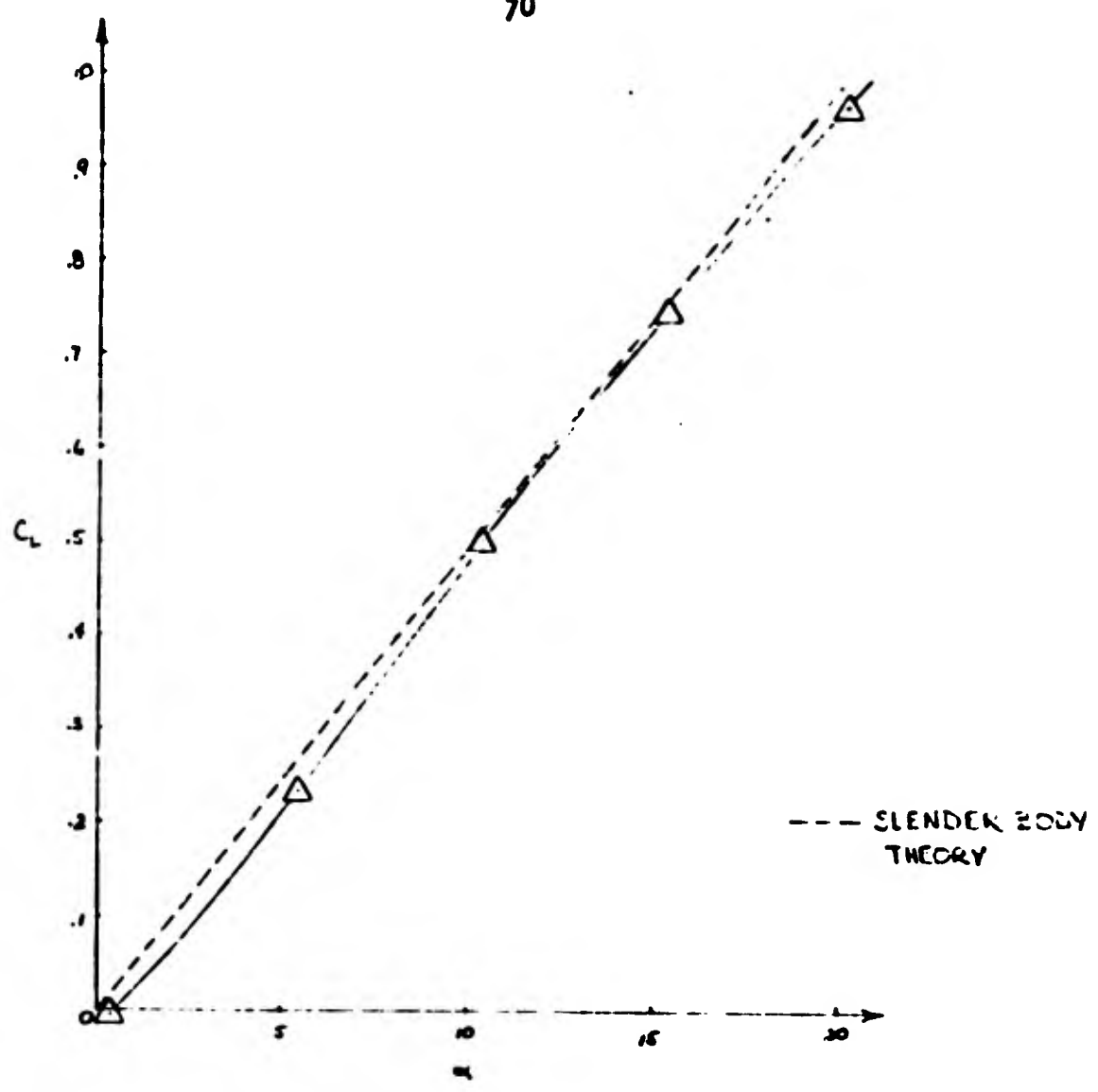


FIGURE 22
COEFFICIENT OF LIFT VS ANGLE OF ATTACK: 6 INCH TRAPEZOID

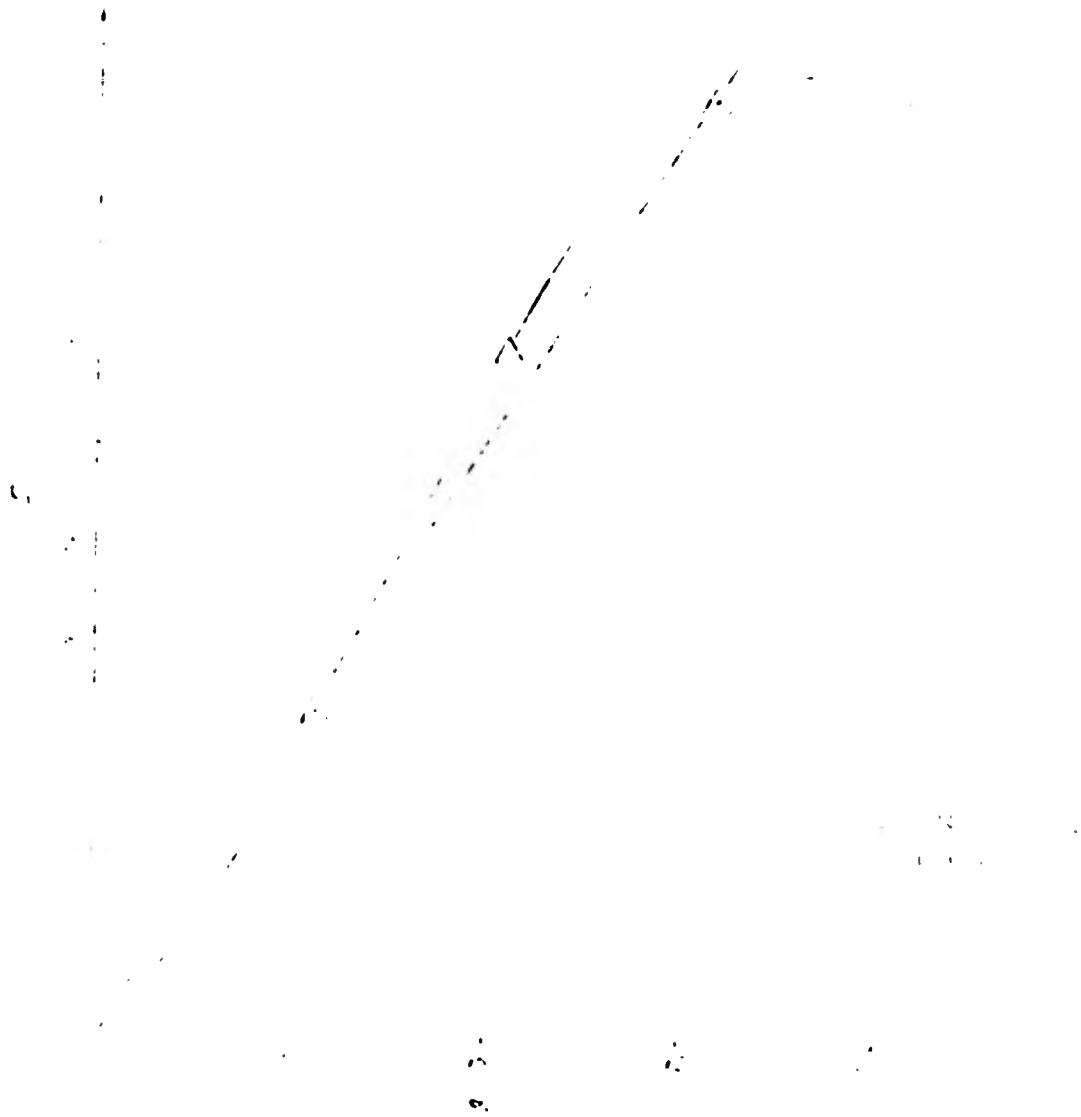


FIGURE 23

CONCENTRATION OF AQUEOUS SOLUTION OF ATP^{3-} IN H_2O AT 25°C

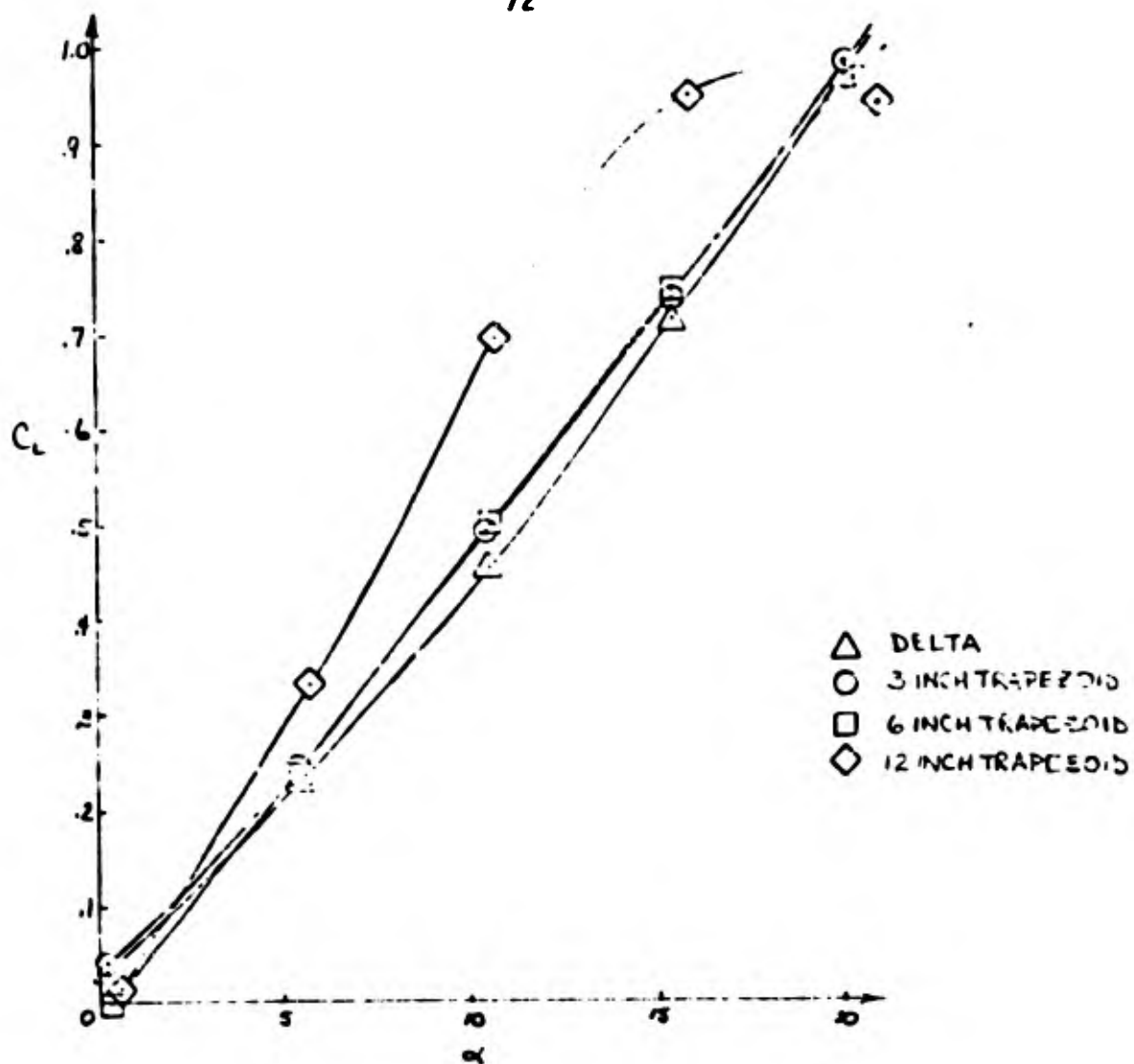


FIGURE 24

COEFFICIENT OF LIFT VS ANGLE OF ATTACK: DELTA AND TRAPEZOIDAL WINGS

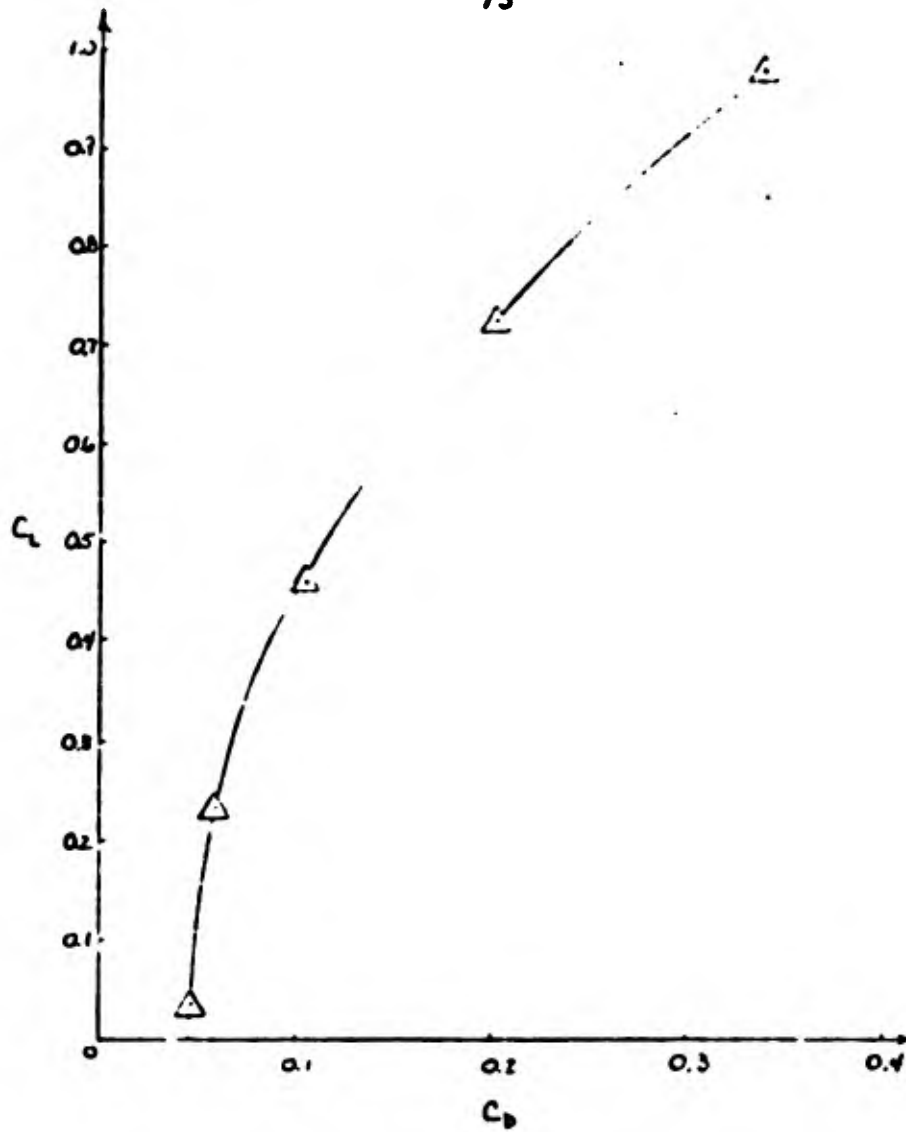


FIGURE 25

COEFFICIENT OF LIFT VS COEFFICIENT OF DRAG: DELTA WING

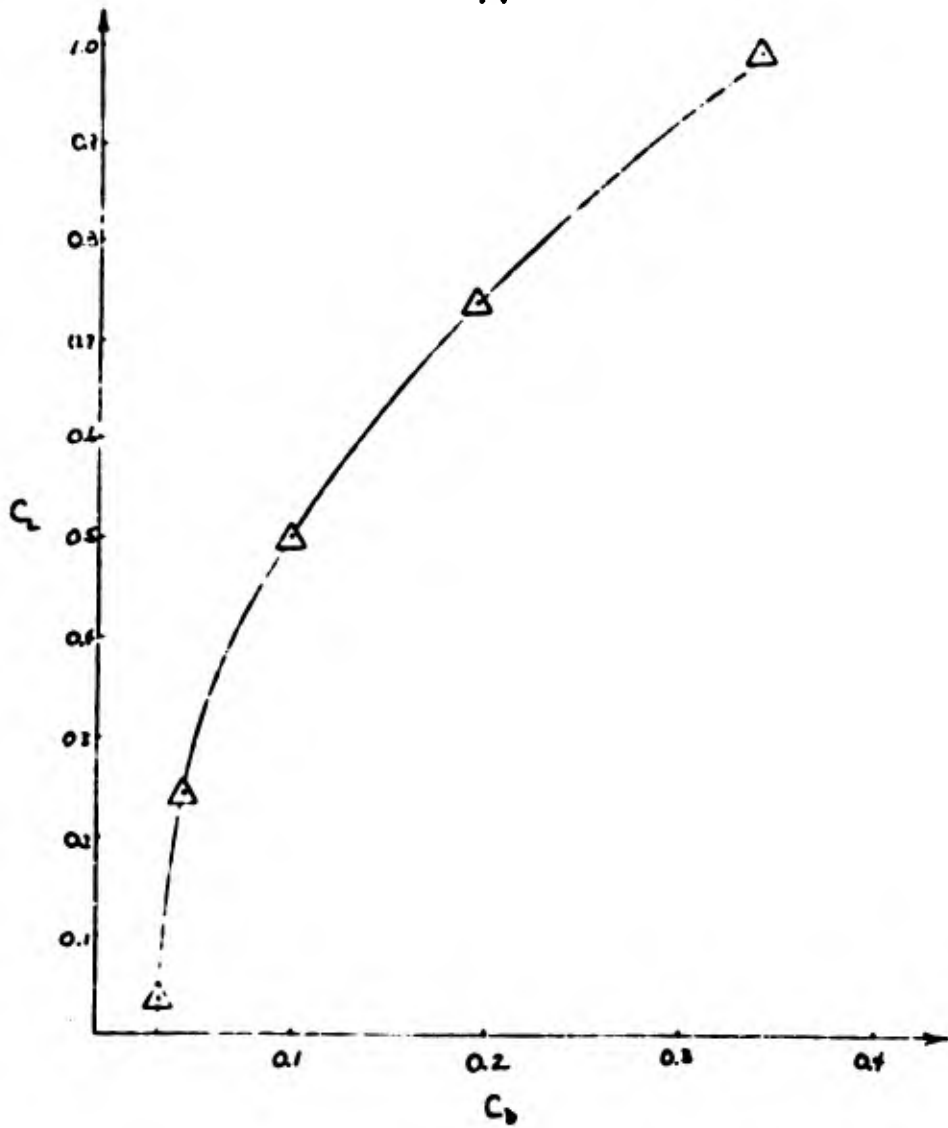


FIGURE 26

COEFFICIENT OF LIFT VS COEFFICIENT OF DRAG: 3 INCH TRAPEZOID

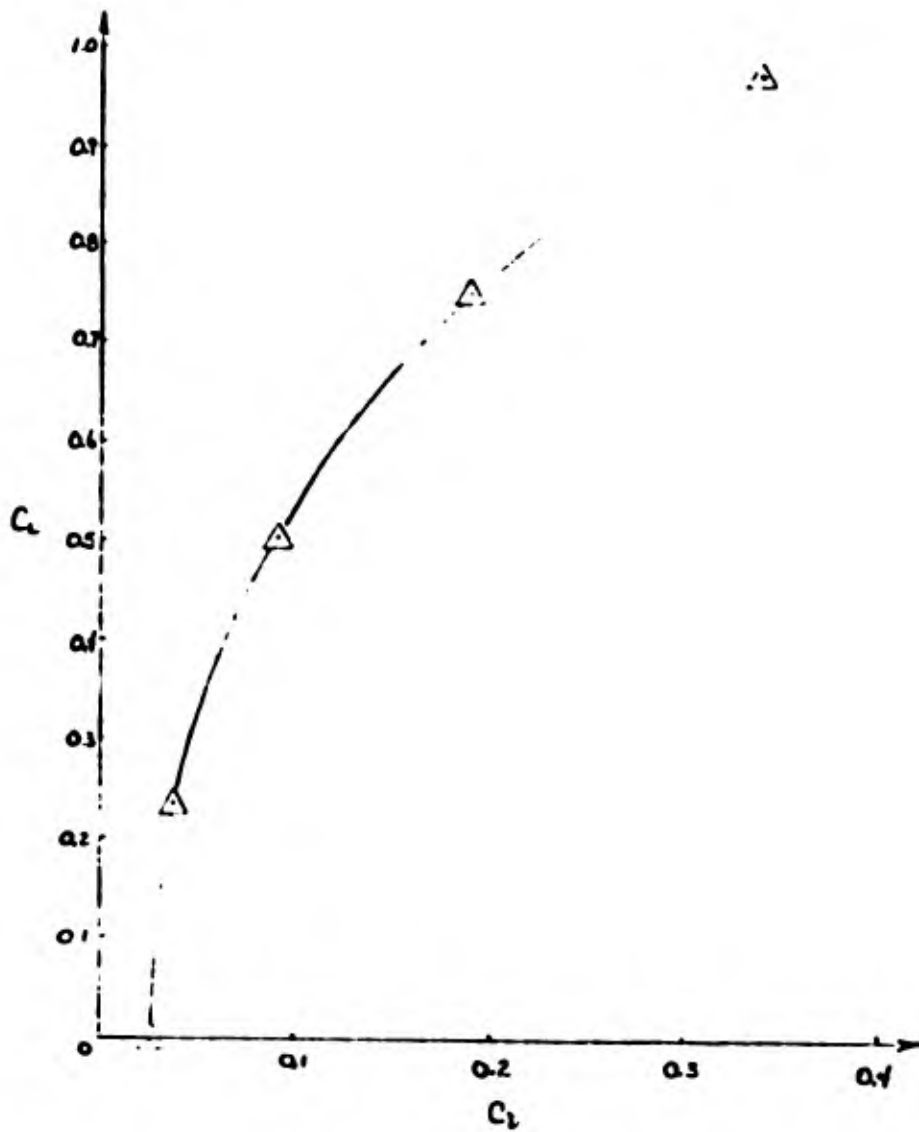


FIGURE 27

COEFFICIENT OF LIFT VS COEFFICIENT OF DRAG: 6 INCH TRAPEZOID

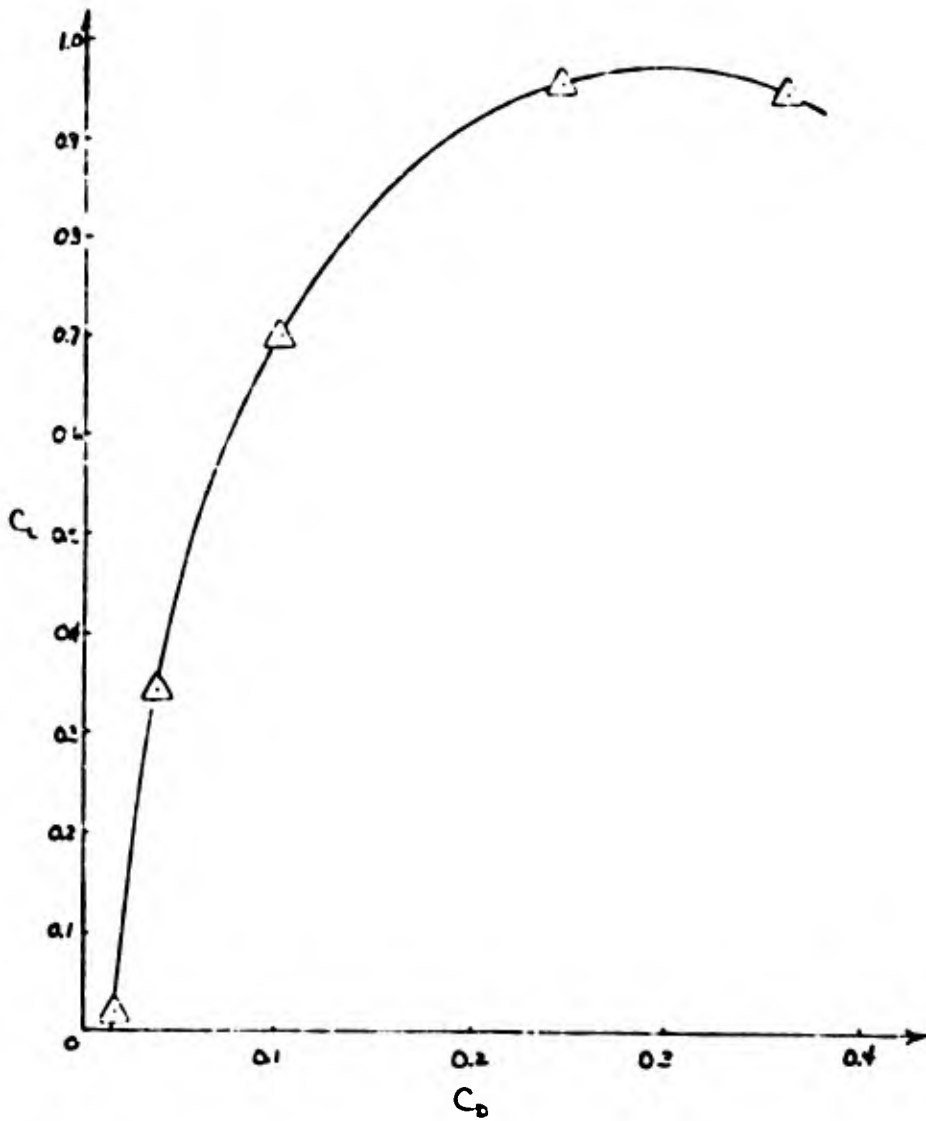


FIGURE 28

COEFFICIENT OF LIFT VS COEFFICIENT OF DRAG: 12 INCH TRAPEZOID

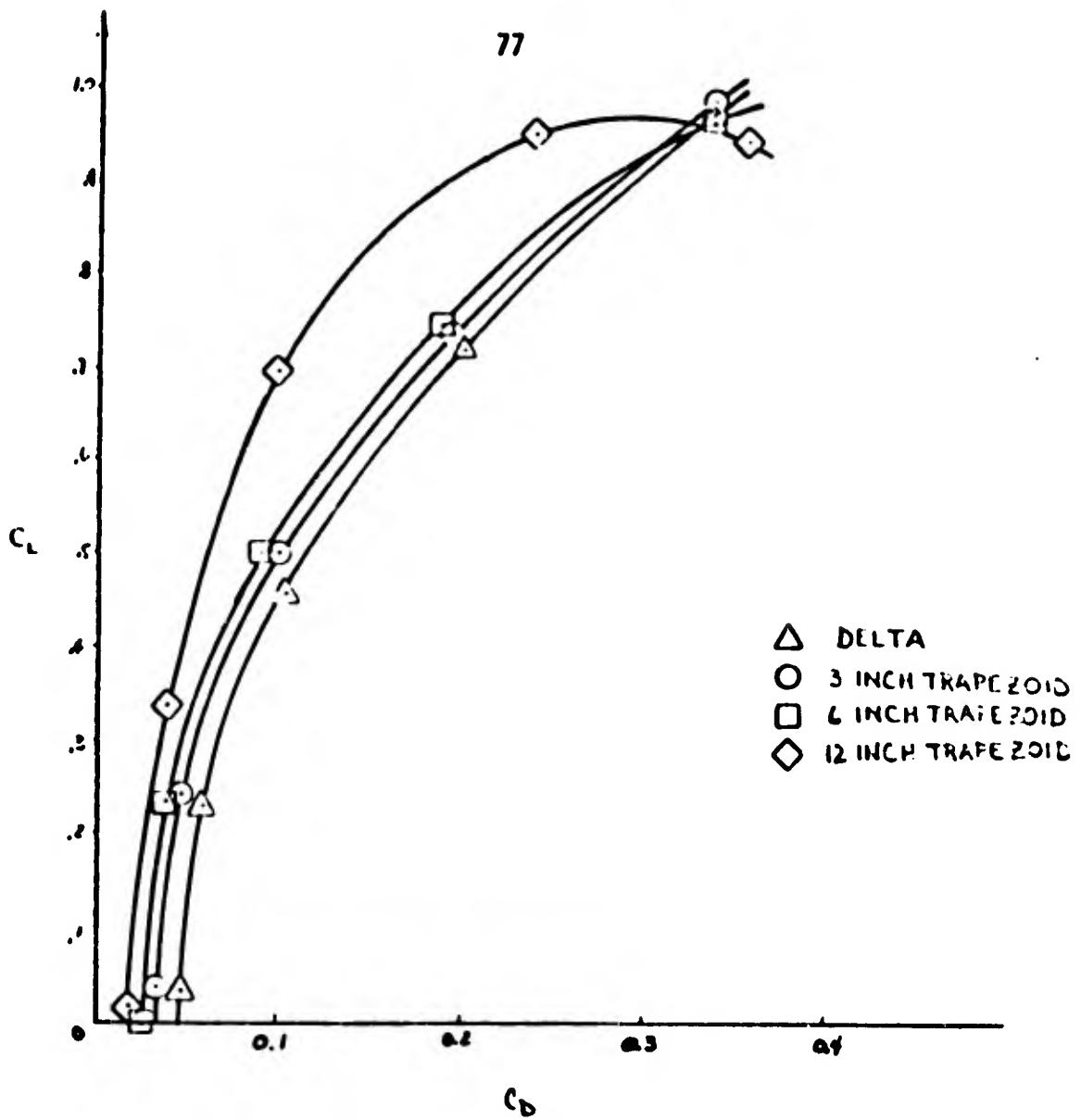


FIGURE 29

COEFFICIENT OF LIFT VS COEFFICIENT OF DRAG: DELTA AND TRAPEZOIDAL WINGS

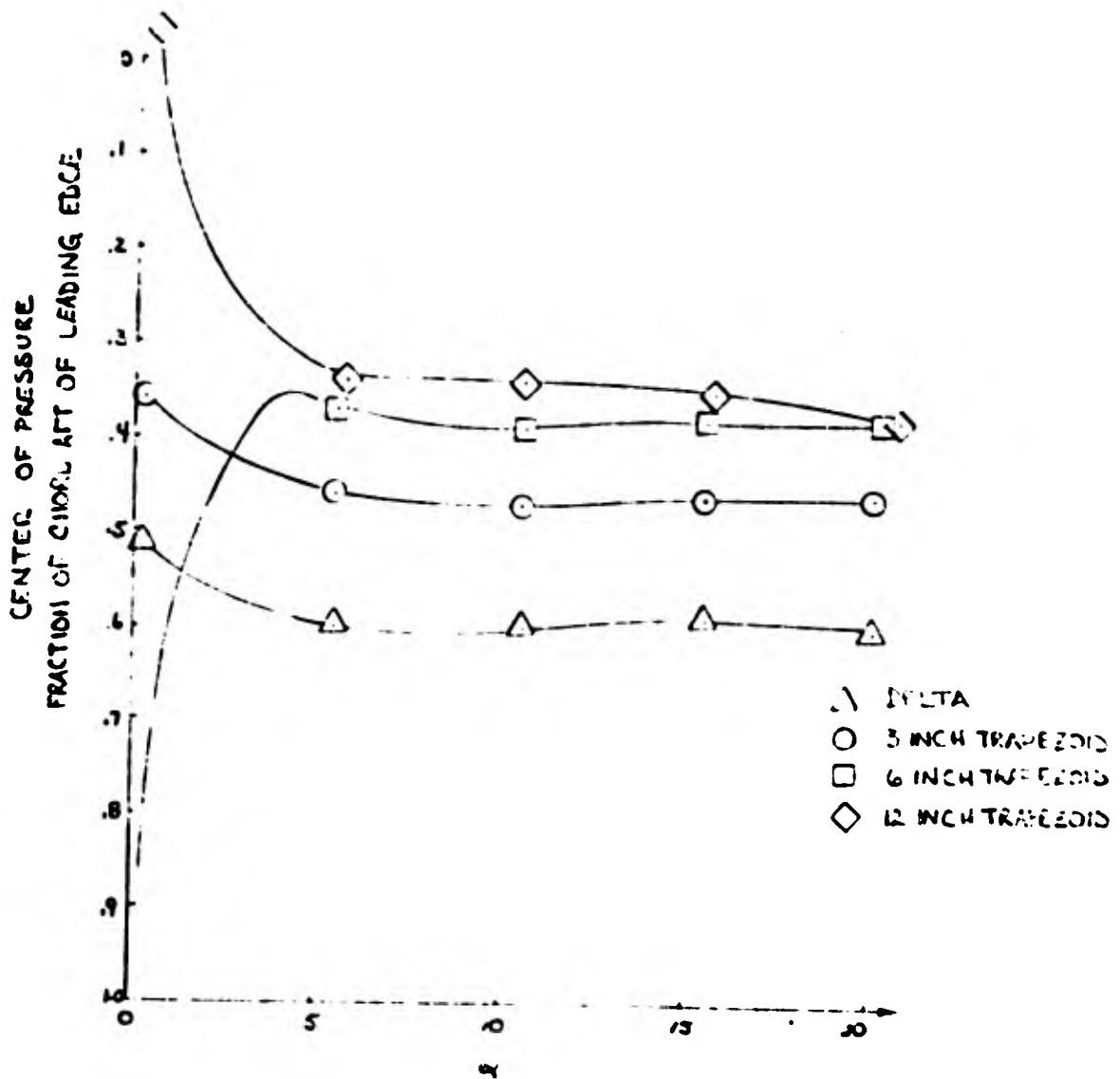


FIGURE 30
CENTER OF PRESSURE LOCATION: TRAPEZOIDAL WINGS

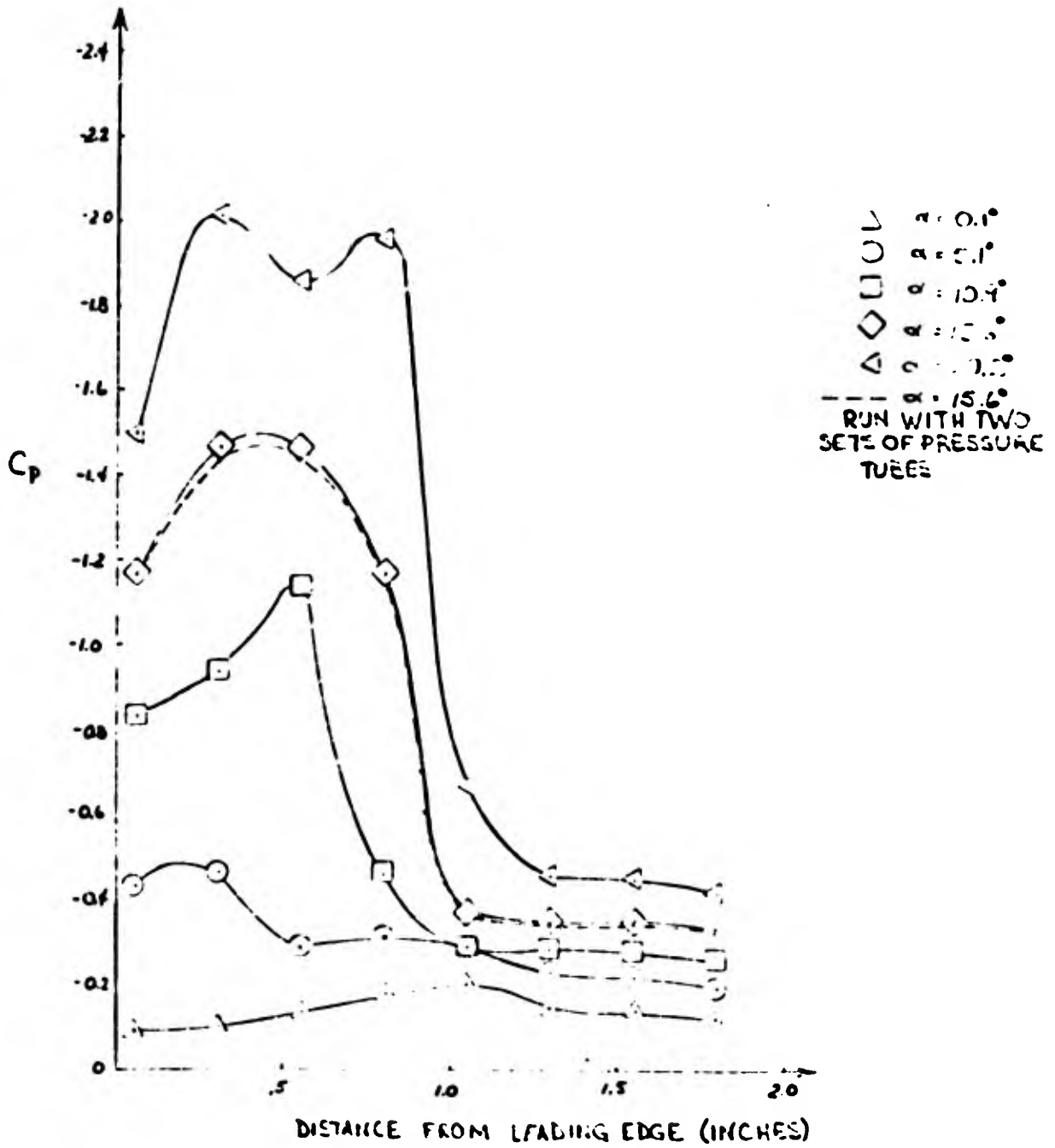


FIGURE 31
PRESSURE DISTRIBUTION: DELTA

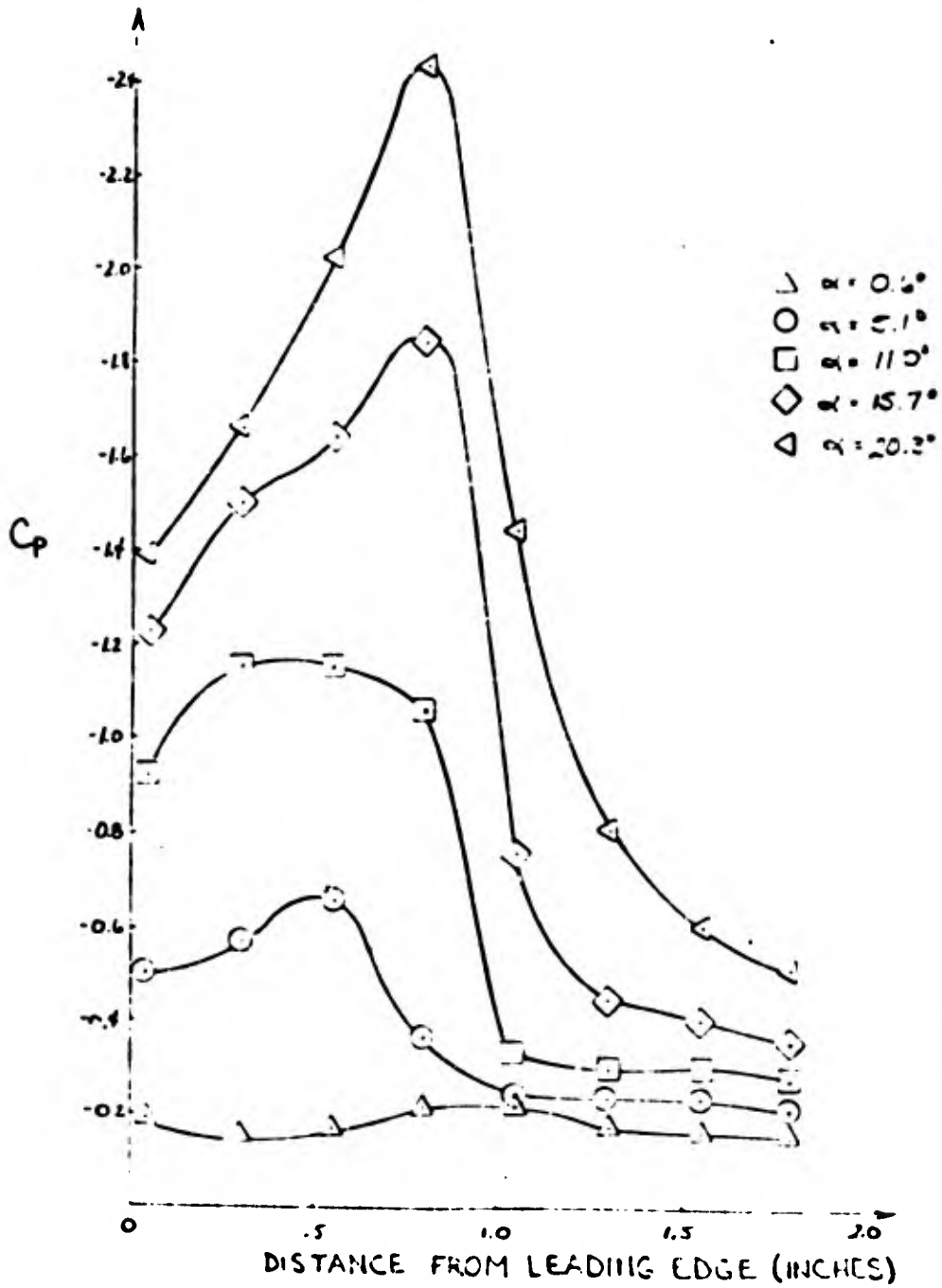


FIGURE 32
PRESSURE DISTRIBUTION. THREE INCH TRAPEZOIDAL

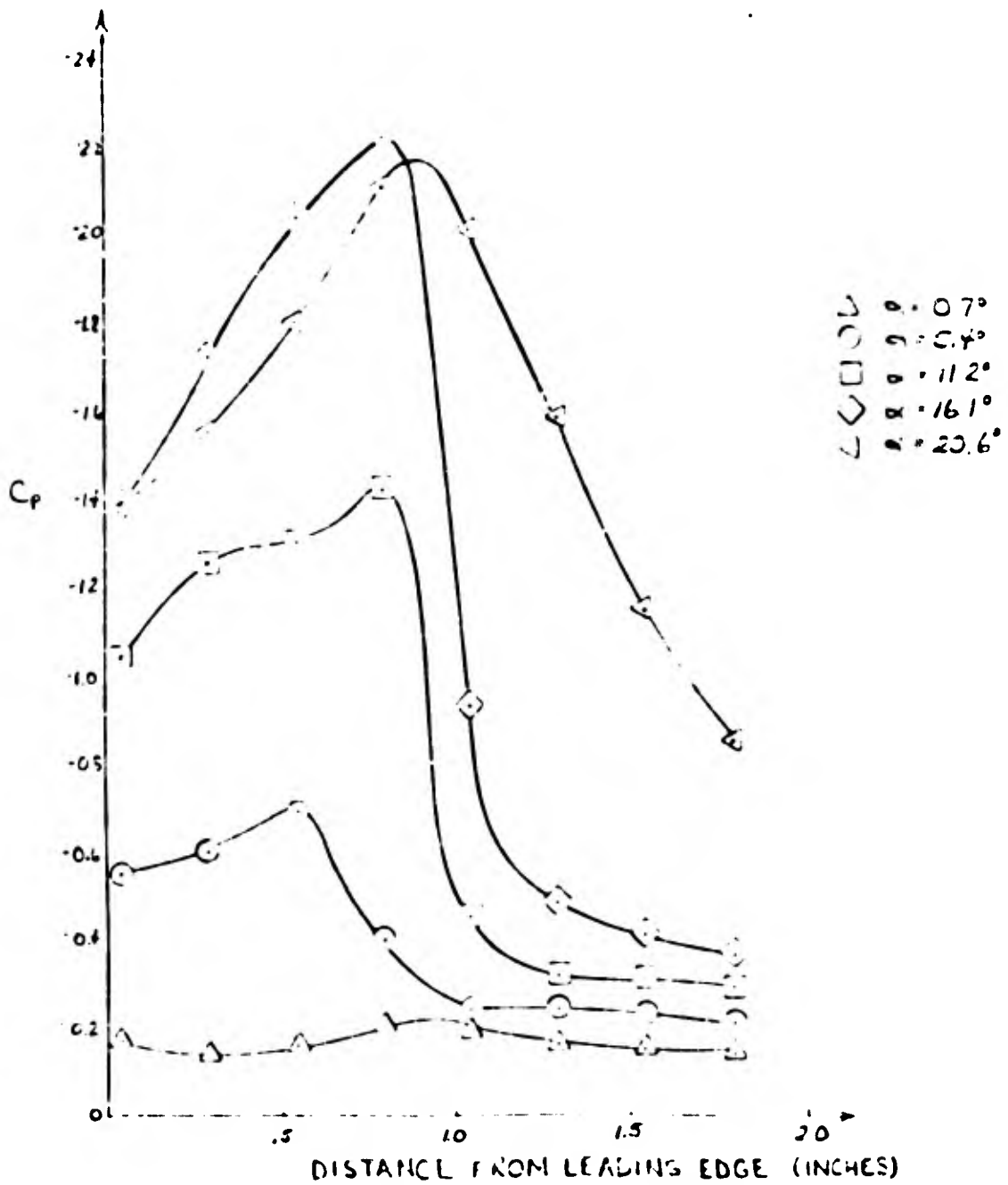


FIGURE 33

PRESSURE DISTRIBUTION: SIX INCH TRAPEZOIDAL

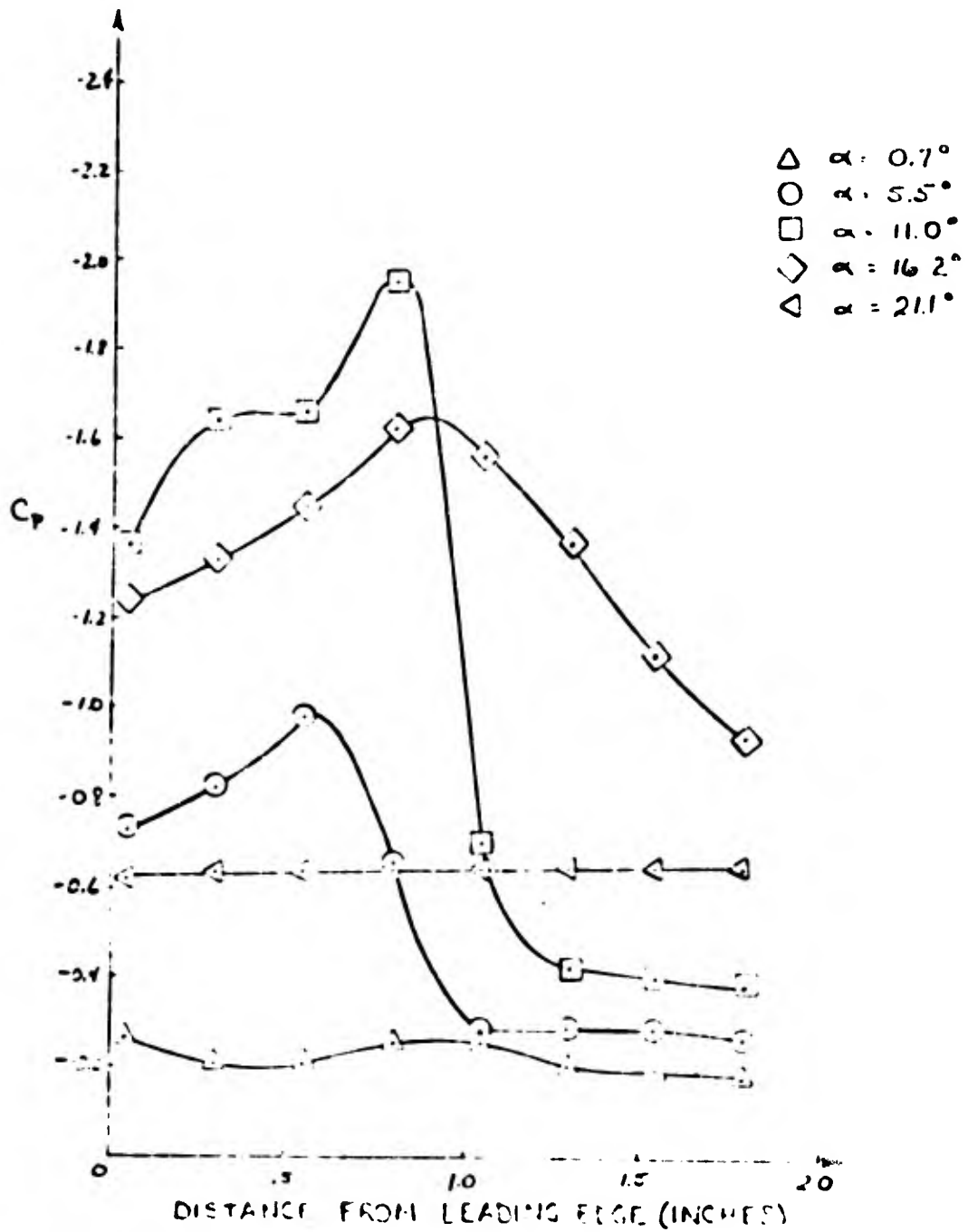


FIGURE 34
PRESSURE DISTRIBUTION: TWELVE INCH TRAPEZOIDAL

R3



FIGURE 35

SMOKE FLOW AROUND DELTA WING NEAR EDGE OF VORTEX FLOW



FIGURE 36

SMOKE FLOW AROUND DELTA WING: NEAR CORE OF VORTEX



FIGURE 37

SMOKE FLOW NEAR CORE: FRONT VIEW

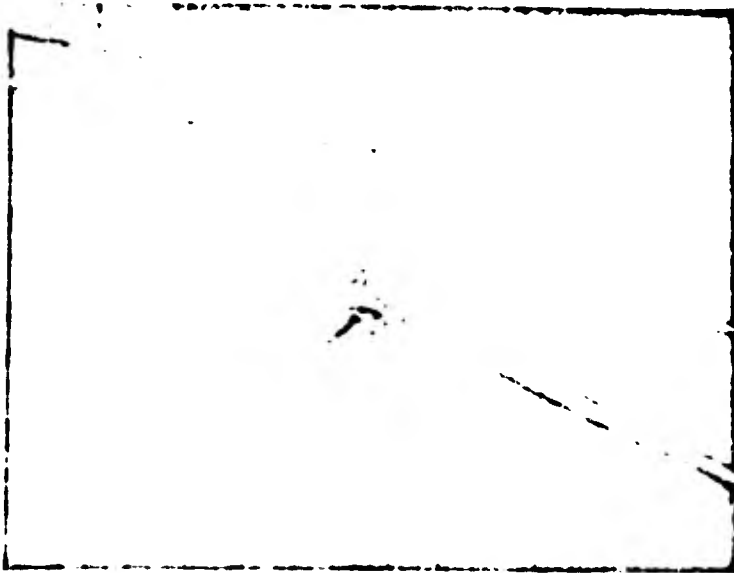


FIGURE 38

SMOKE FLOW NEAR CORE: CLOSE UP

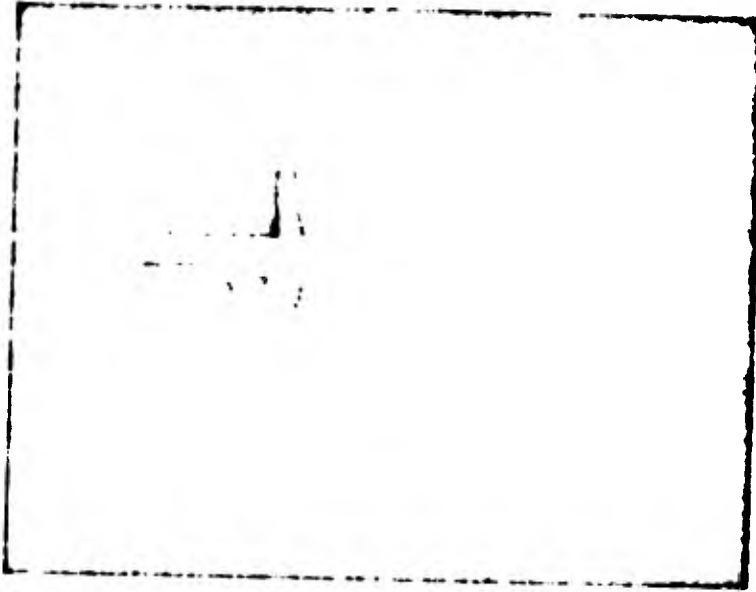
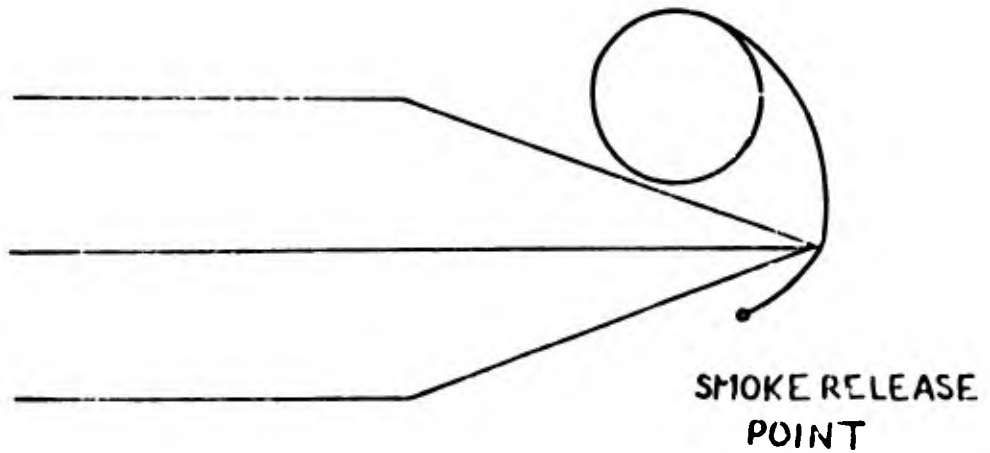


FIGURE 39
SMOKE FLOW AROUND TWELVE INCH TRAPEZOIDAL WING



VIEW ALONG LEADING EDGE OF DELTA
WING FROM UPSTREAM SMOKE
RELEASED AT ABOUT $\frac{1}{3}$ CHORD.
SHOWN TWICE ACTUAL SIZE.

FIGURE 40
SKETCH OF FLOW NEAR LEADING EDGE

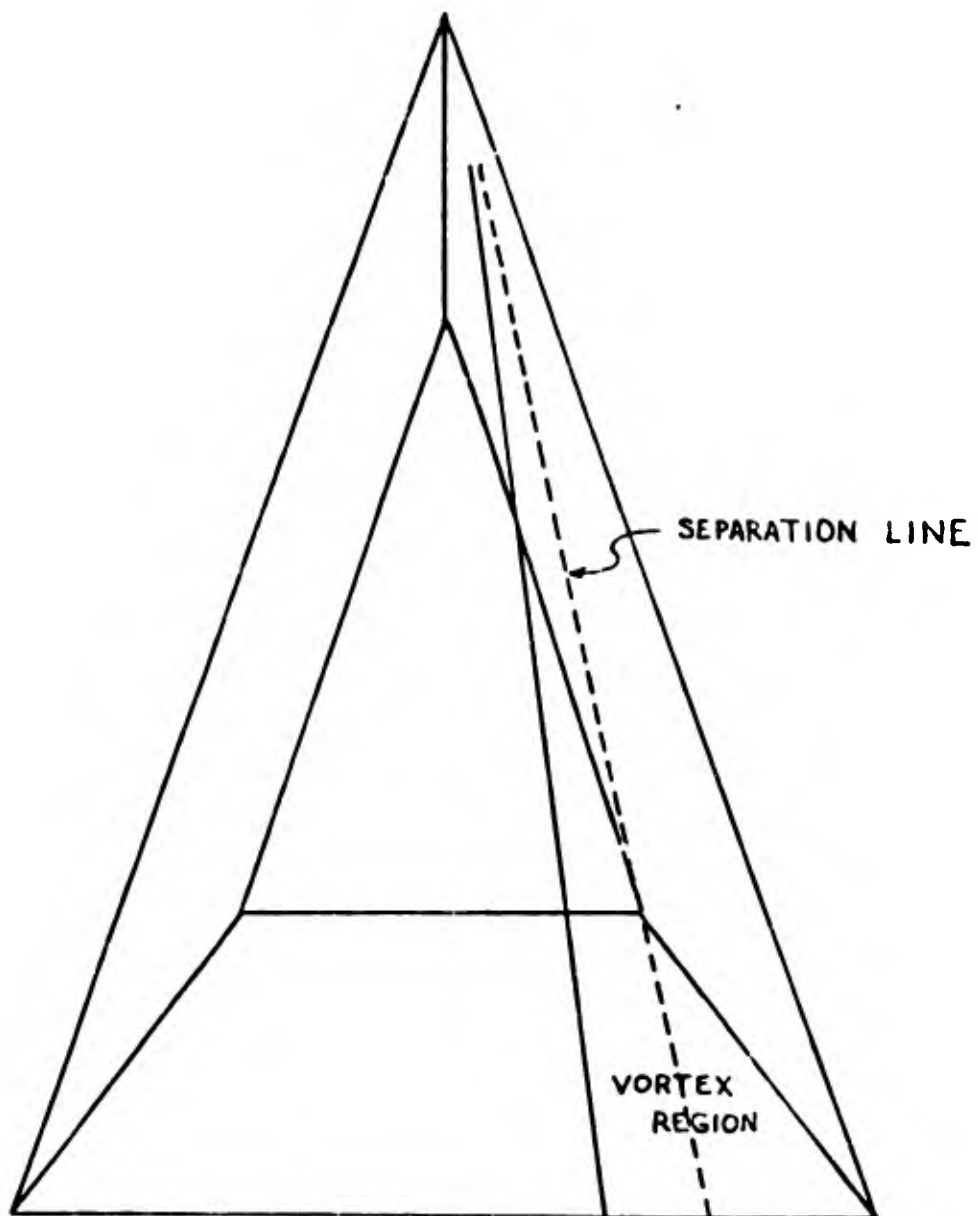
 $\alpha = 20^\circ$

FIGURE 41
SKETCH OF FLOW OVER DELTA WING

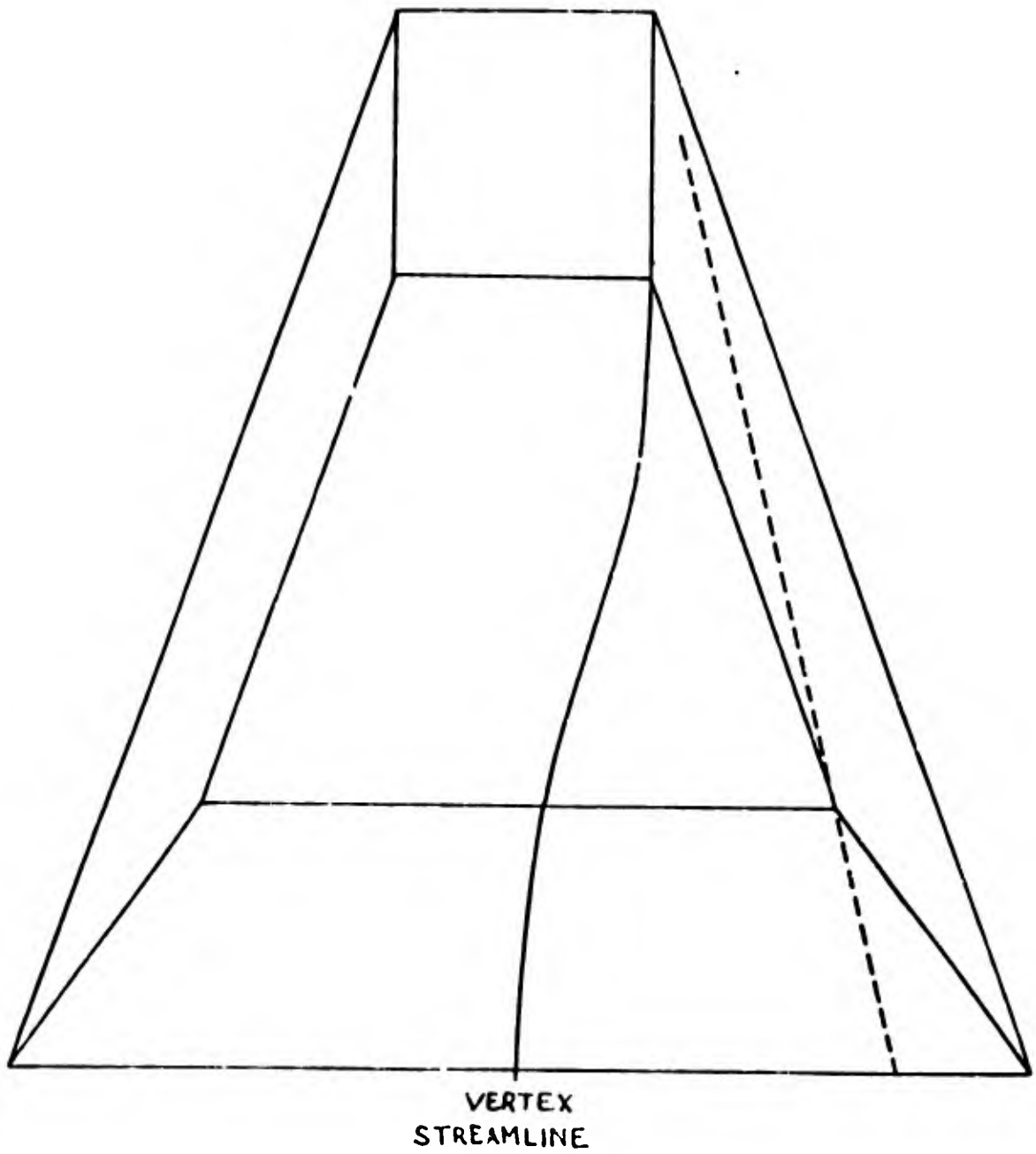
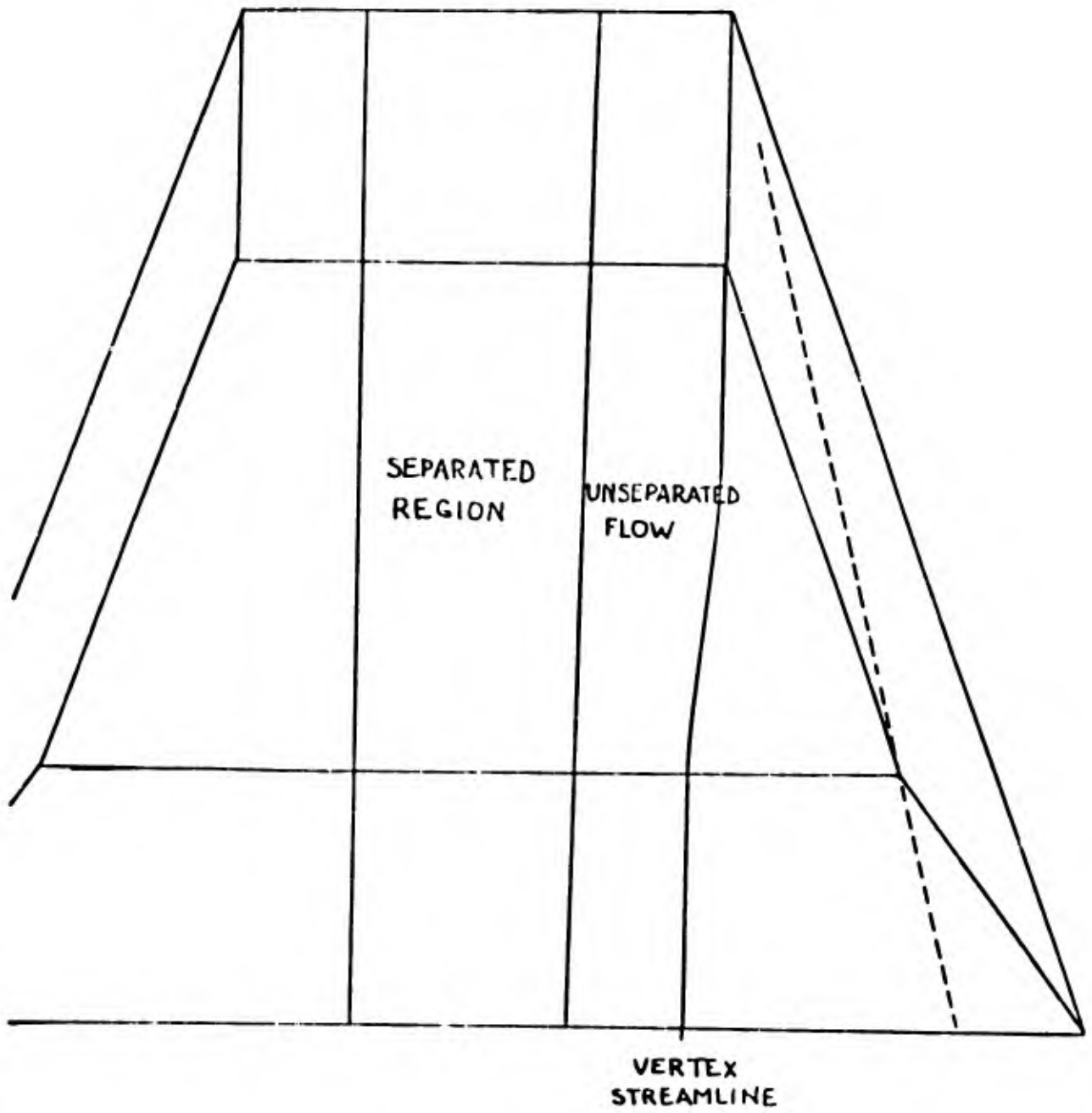
 $\alpha = 122^\circ$

FIGURE 42
SKETCH OF FLOW OVER THREE INCH TRAPEZOIDAL WING



$$\alpha = 8.8^\circ$$

FIGURE 43

SKETCH OF FLOW OVER SIX INCH TRAPEZOIDAL WING

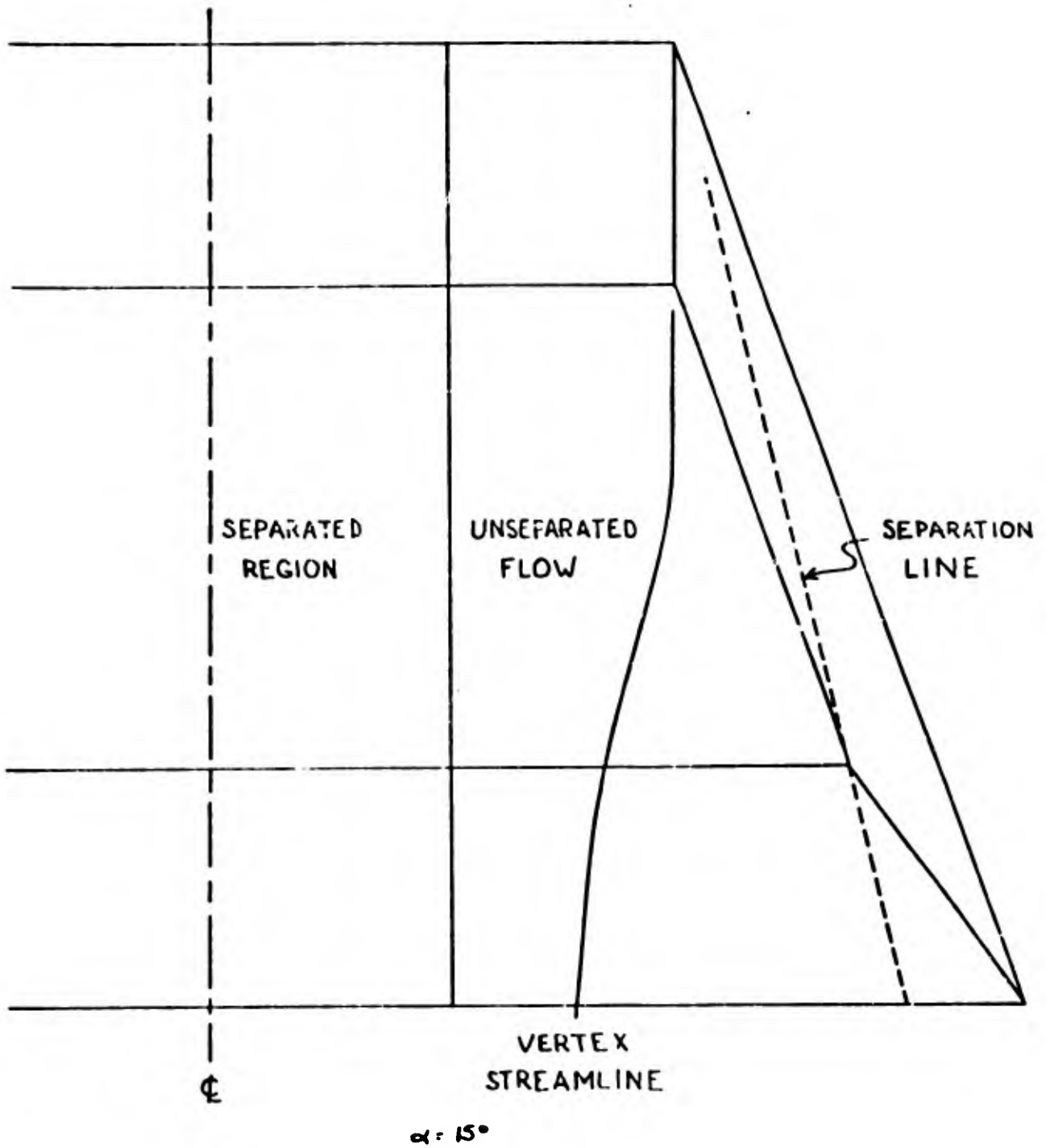


FIGURE 44

SKETCH OF FLOW OVER TWELVE INCH TRAPEZOIDAL WING

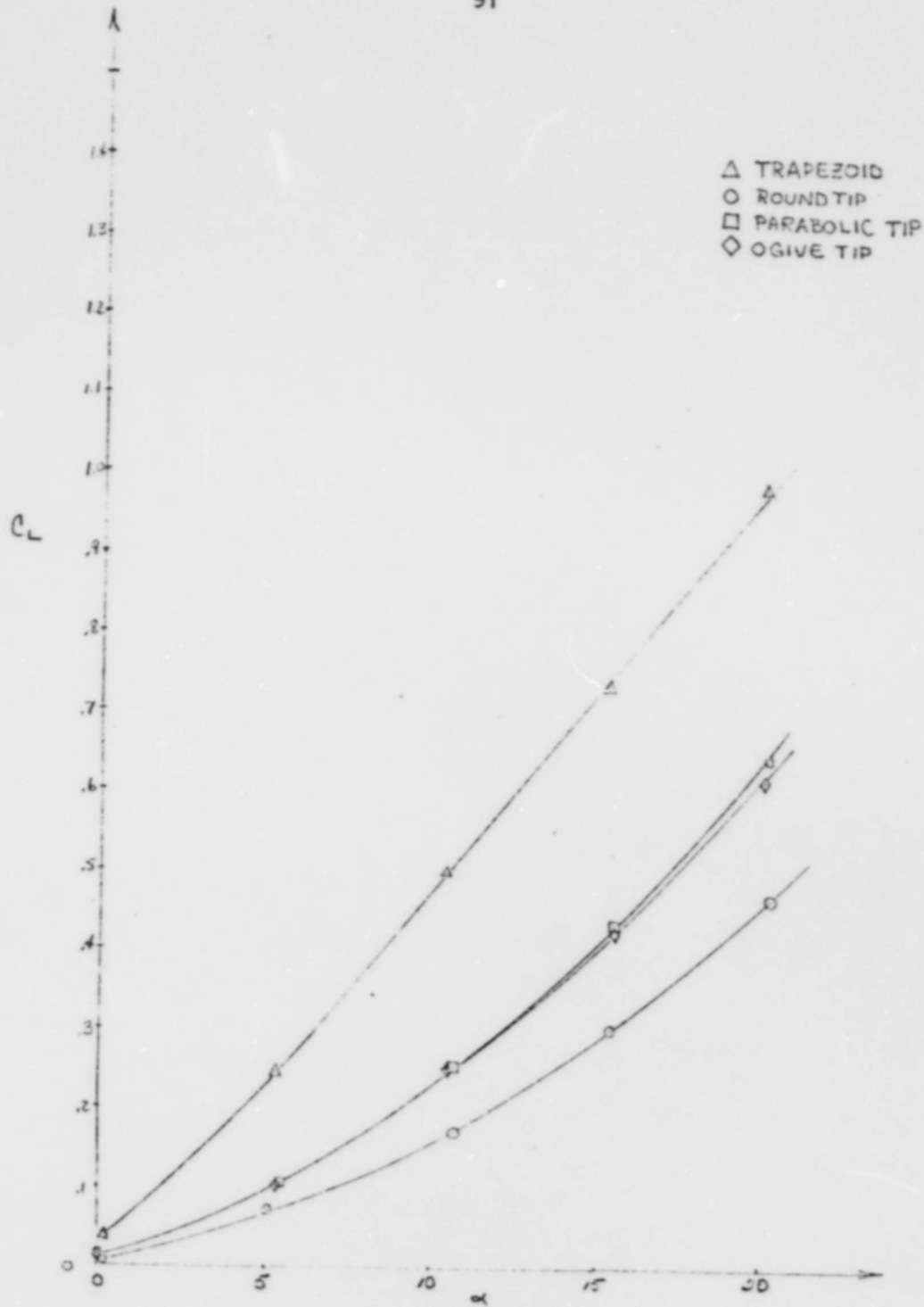


FIGURE 45
COEFFICIENT OF LIFT VS ANGLE OF ATTACK: THREE INCH RECTANGULAR WING

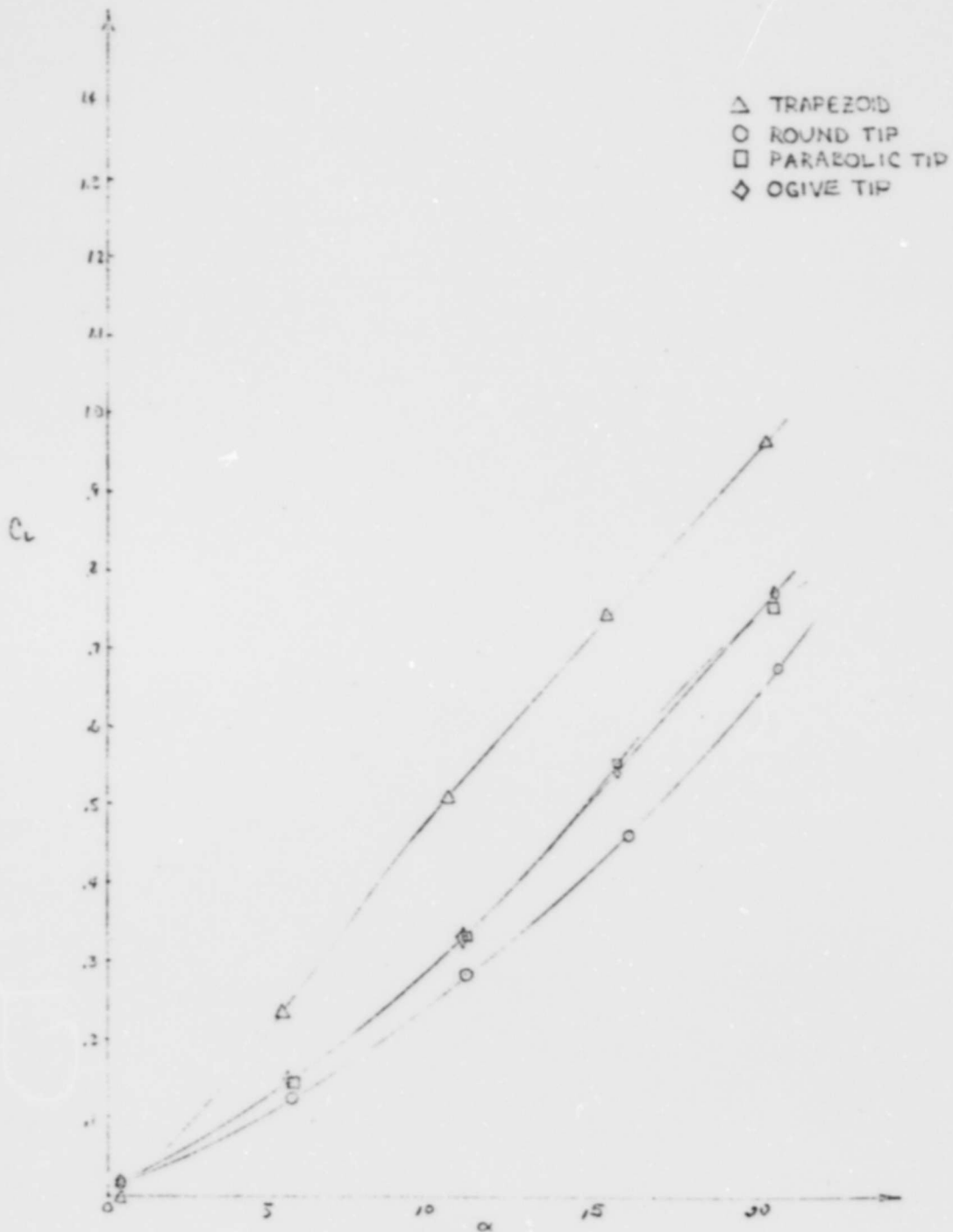


FIGURE 46
COEFFICIENT OF LIFT VS ANGLE OF ATTACK: SIX INCH RECTANGULAR WING

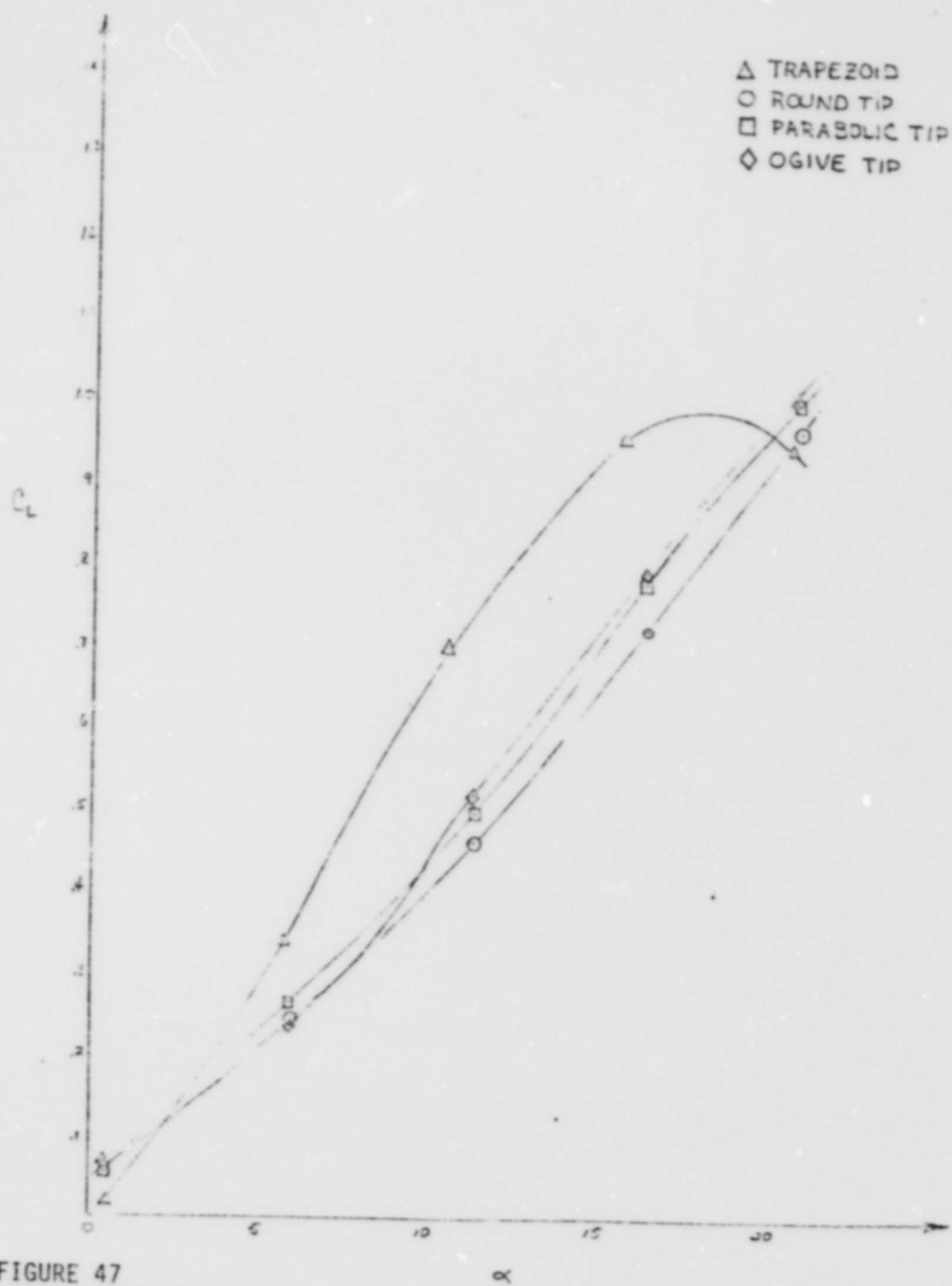


FIGURE 47
COEFFICIENT OF LIFT VS ANGLE OF ATTACK: TWELVE INCH RECTANGULAR WING

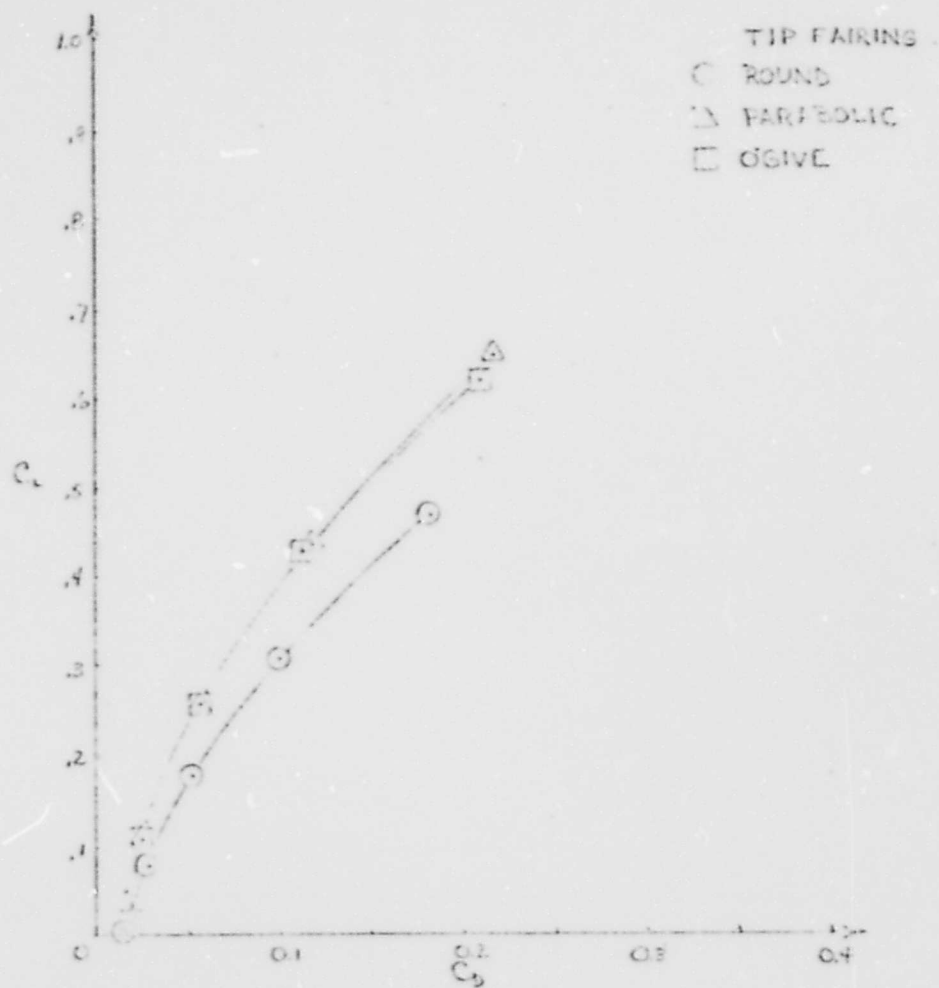


FIGURE 48

COEFFICIENT OF LIFT VS COEFFICIENT OF DRAG:
3 INCH RECTANGULAR WING

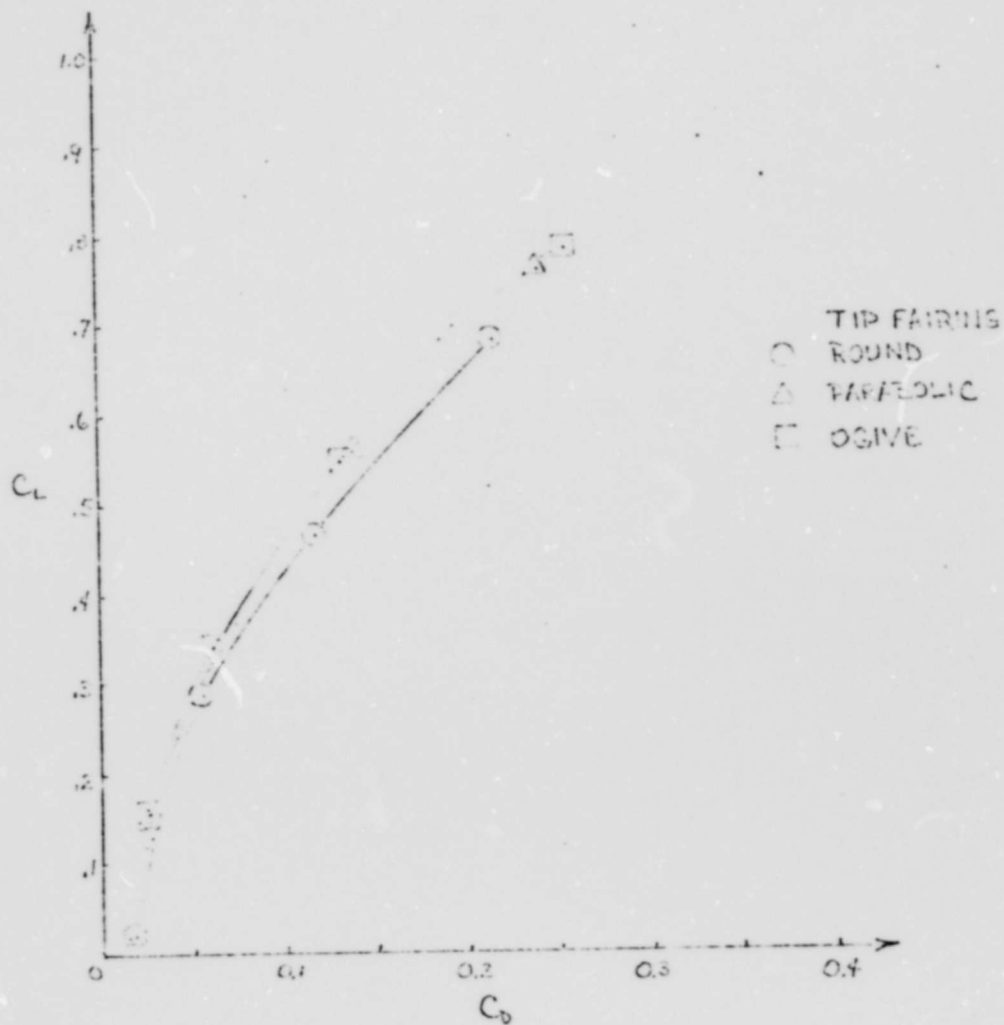


FIGURE 49

COEFFICIENT OF LIFT VS COEFFICIENT OF DRAG:
6 INCH RECTANGULAR WING

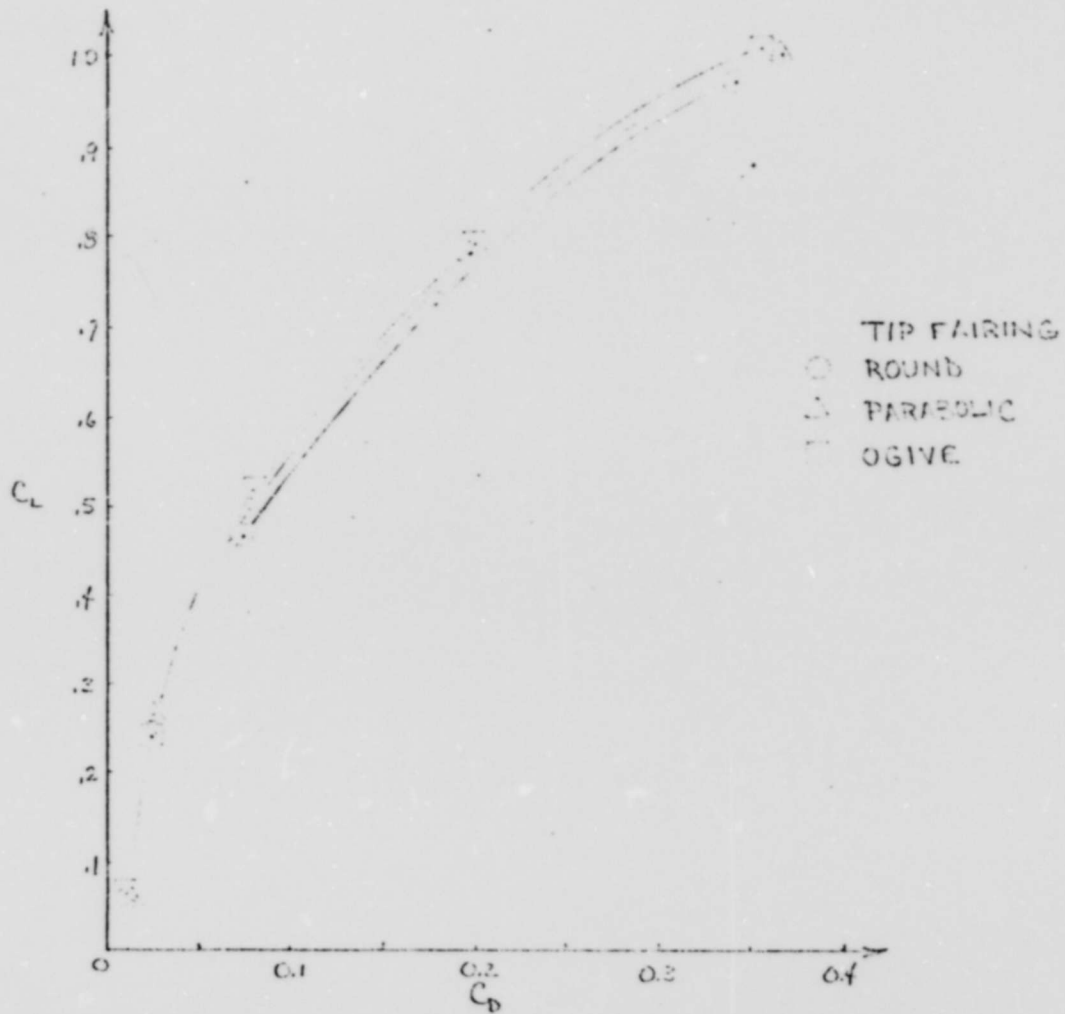


FIGURE 50

COEFFICIENT OF LIFT VS COEFFICIENT OF DRAG:
TWELVE INCH RECTANGULAR WING

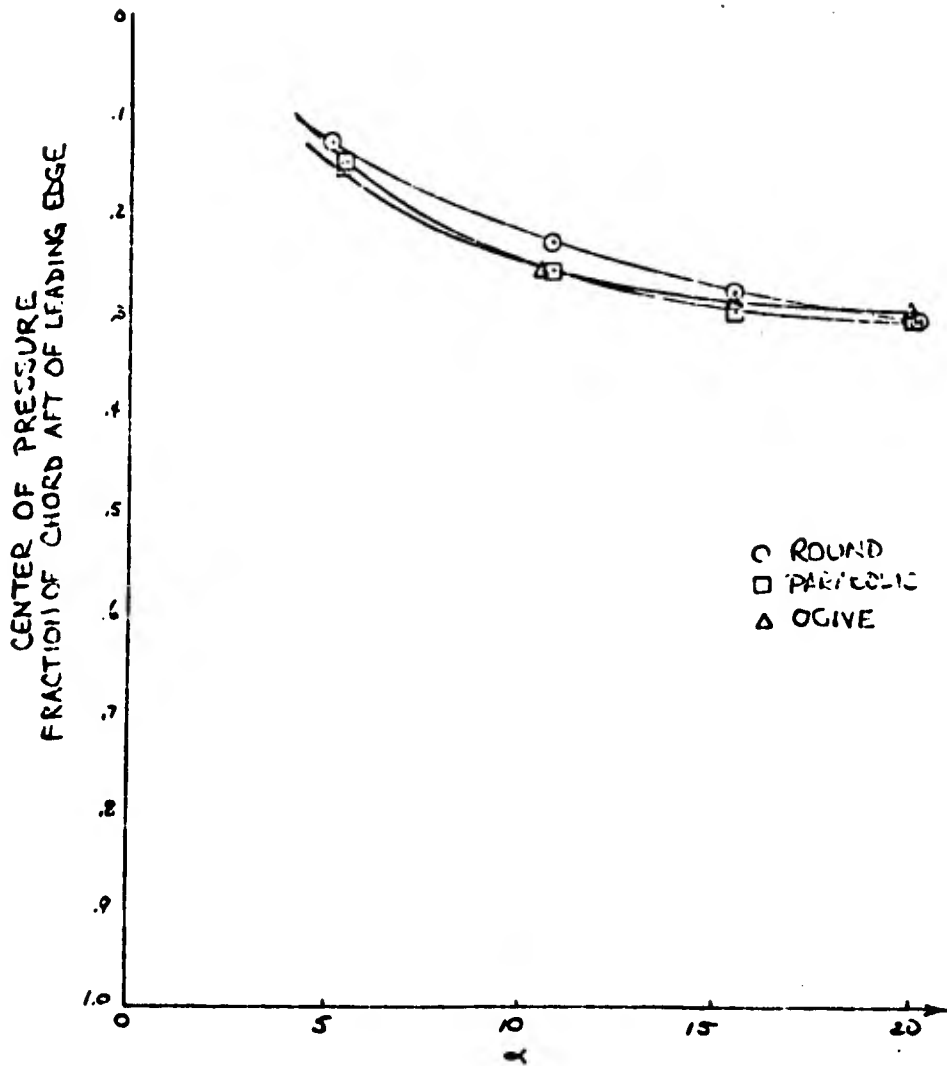


FIGURE 51

CENTER OF PRESSURE LOCATION: THREE INCH RECTANGULAR WING

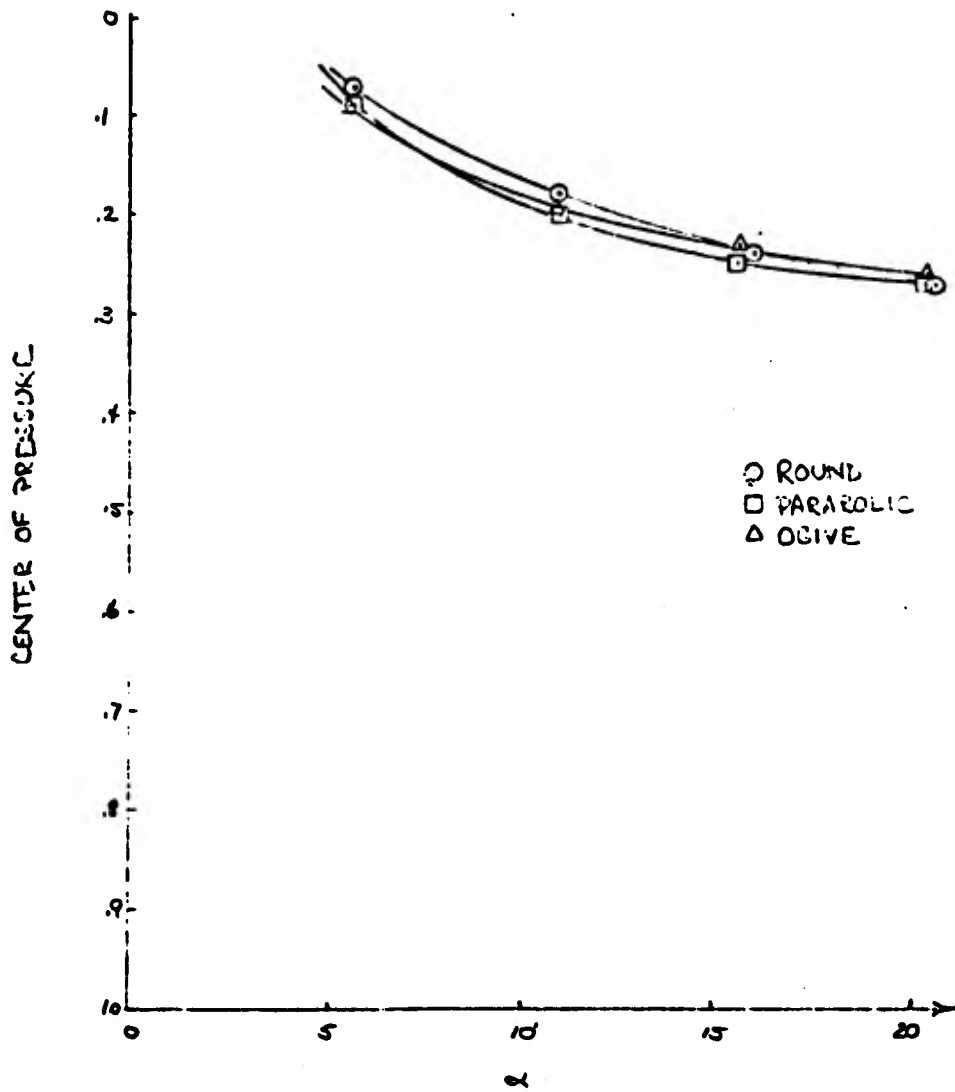


FIGURE 52

CENTER OF PRESSURE LOCATION: SIX INCH RECTANGULAR WING

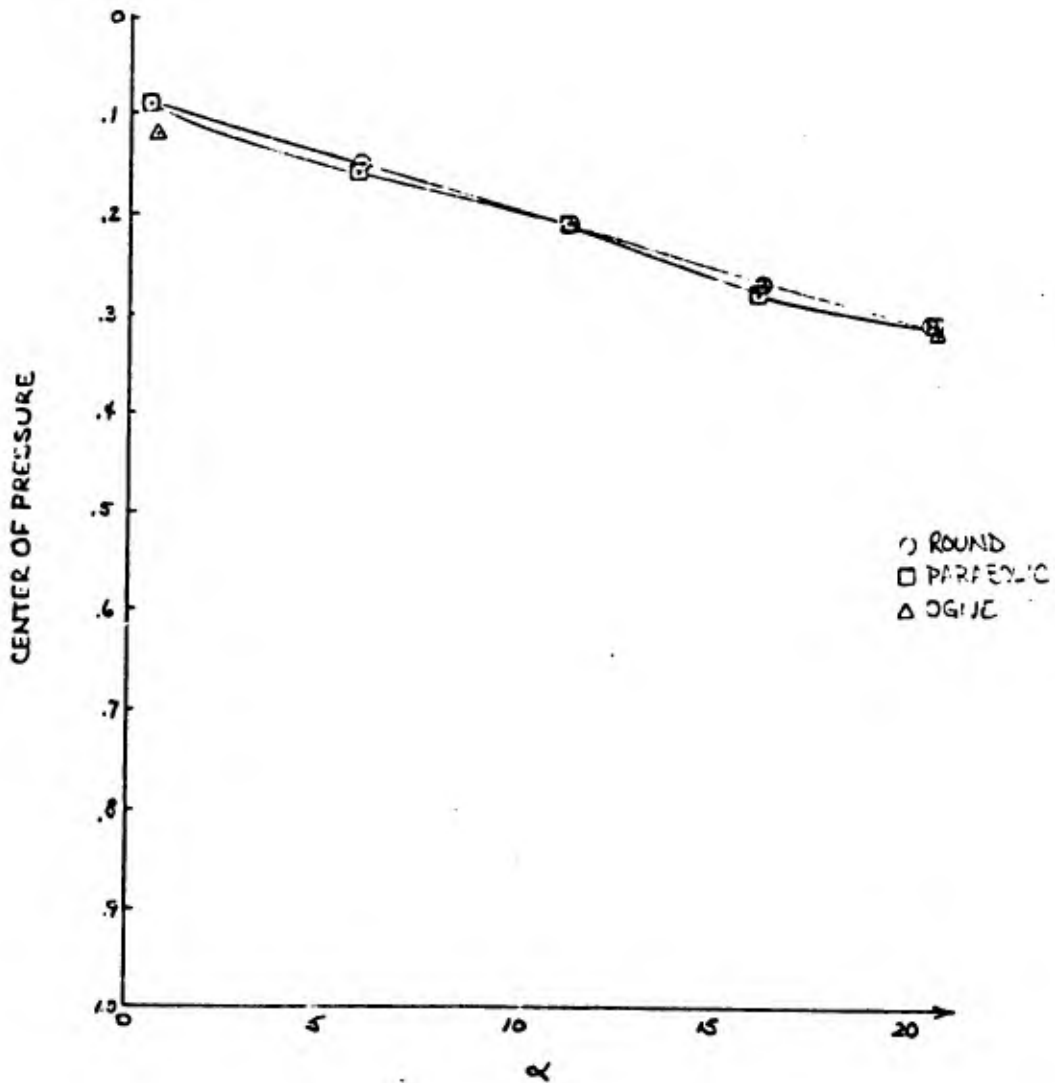


FIGURE 53

CENTER OF PRESSURE LOCATION: TWELVE INCH RECTANGULAR WING

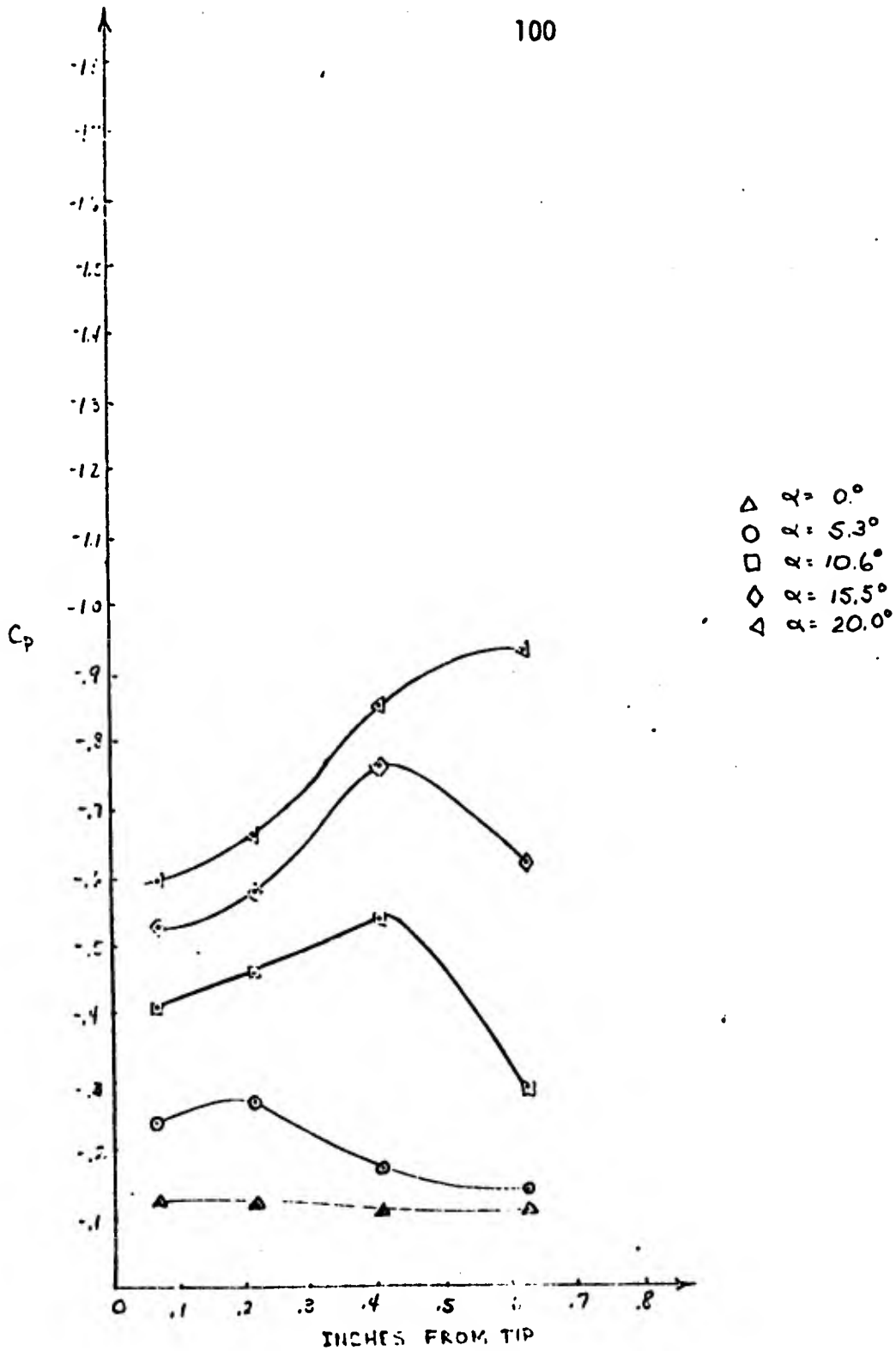


FIGURE 54

PRESSURE DISTRIBUTION: THREE INCH RECTANGULAR WING

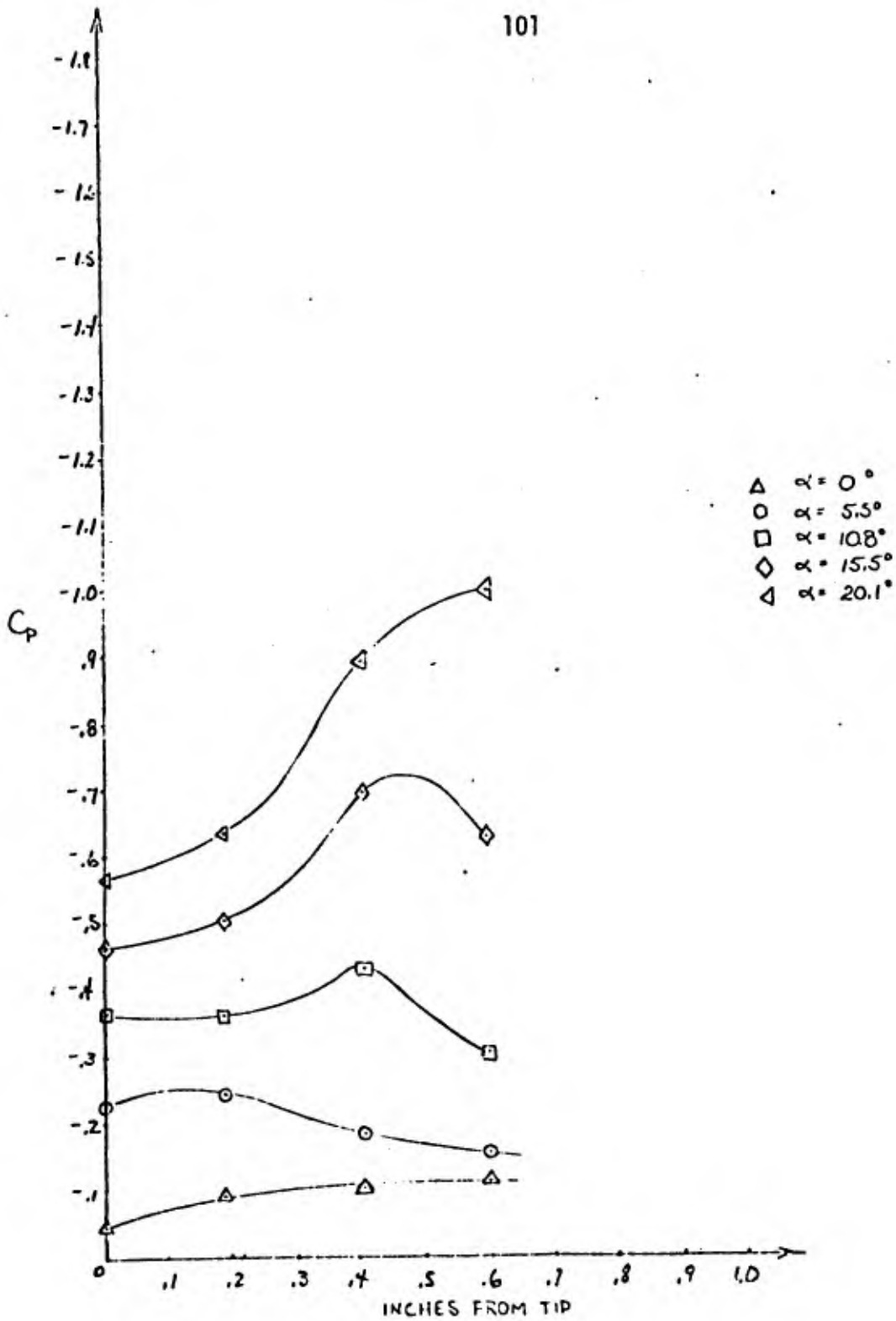


FIGURE 55

PRESSURE DISTRIBUTION: THREE INCH RECTANGULAR WING

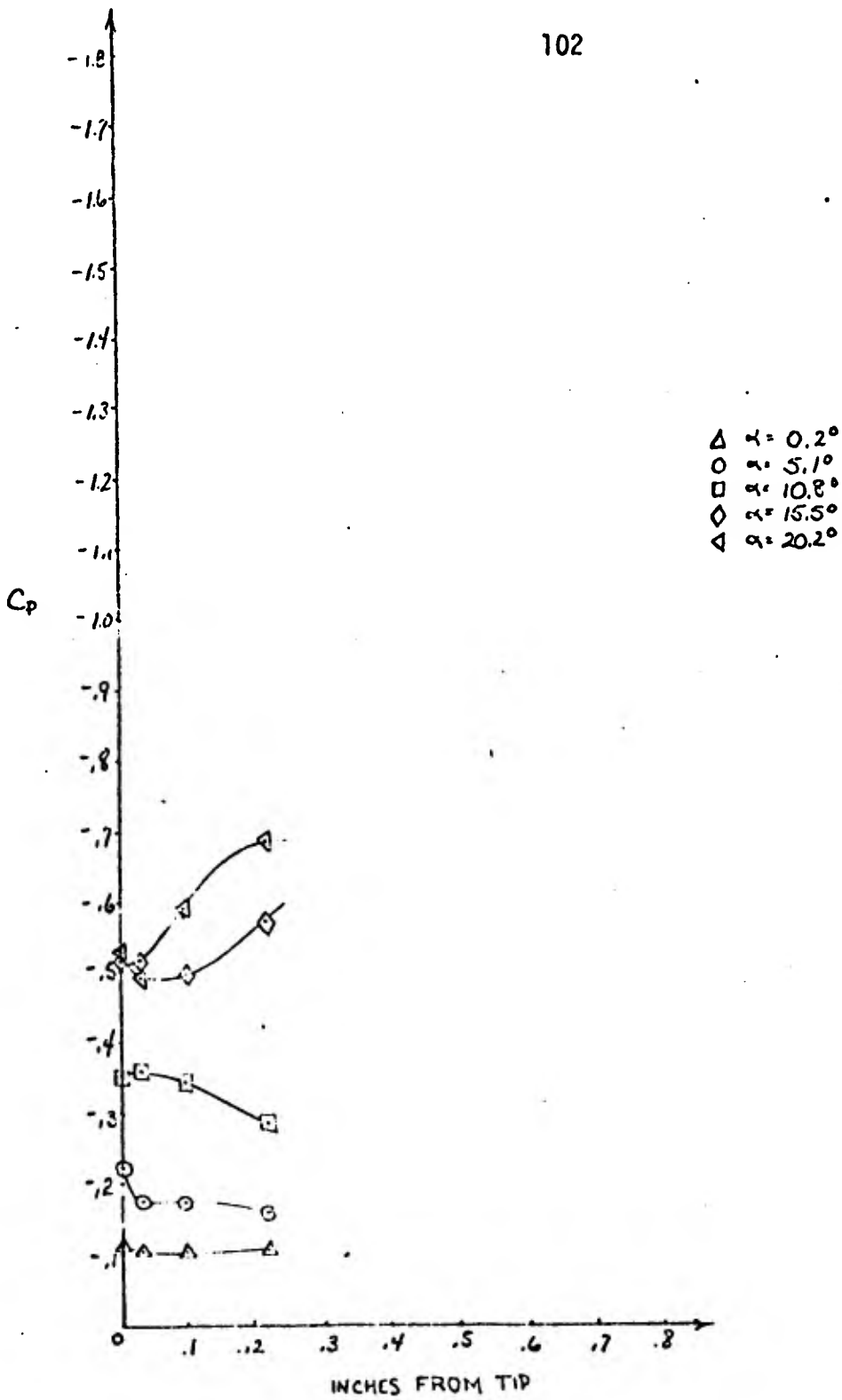


FIGURE 56

PRESSURE DISTRIBUTION: THREE INCH RECTANGULAR WING

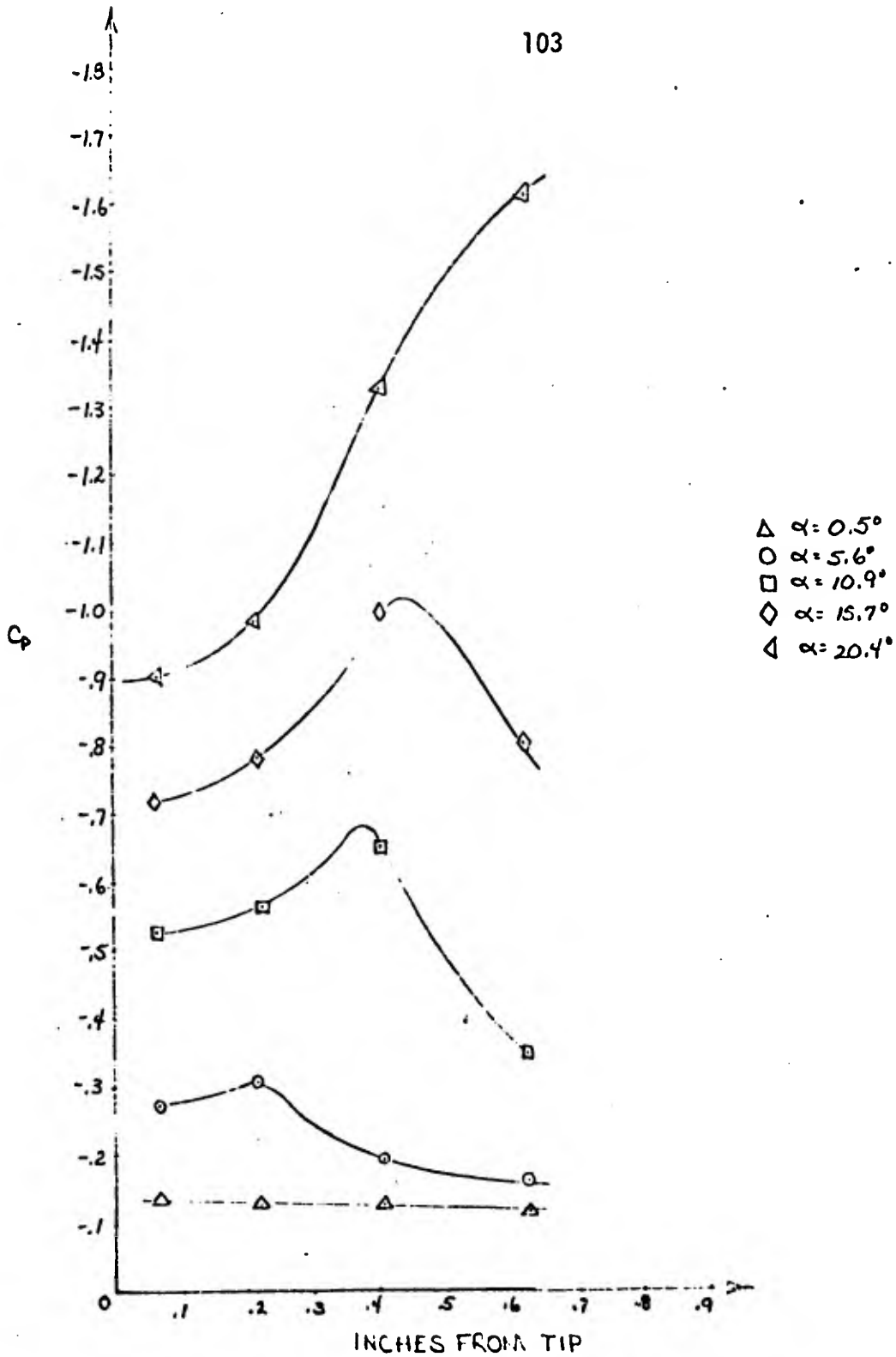


FIGURE 57

PRESSURE DISTRIBUTION: SIX INCH RECTANGULAR WING

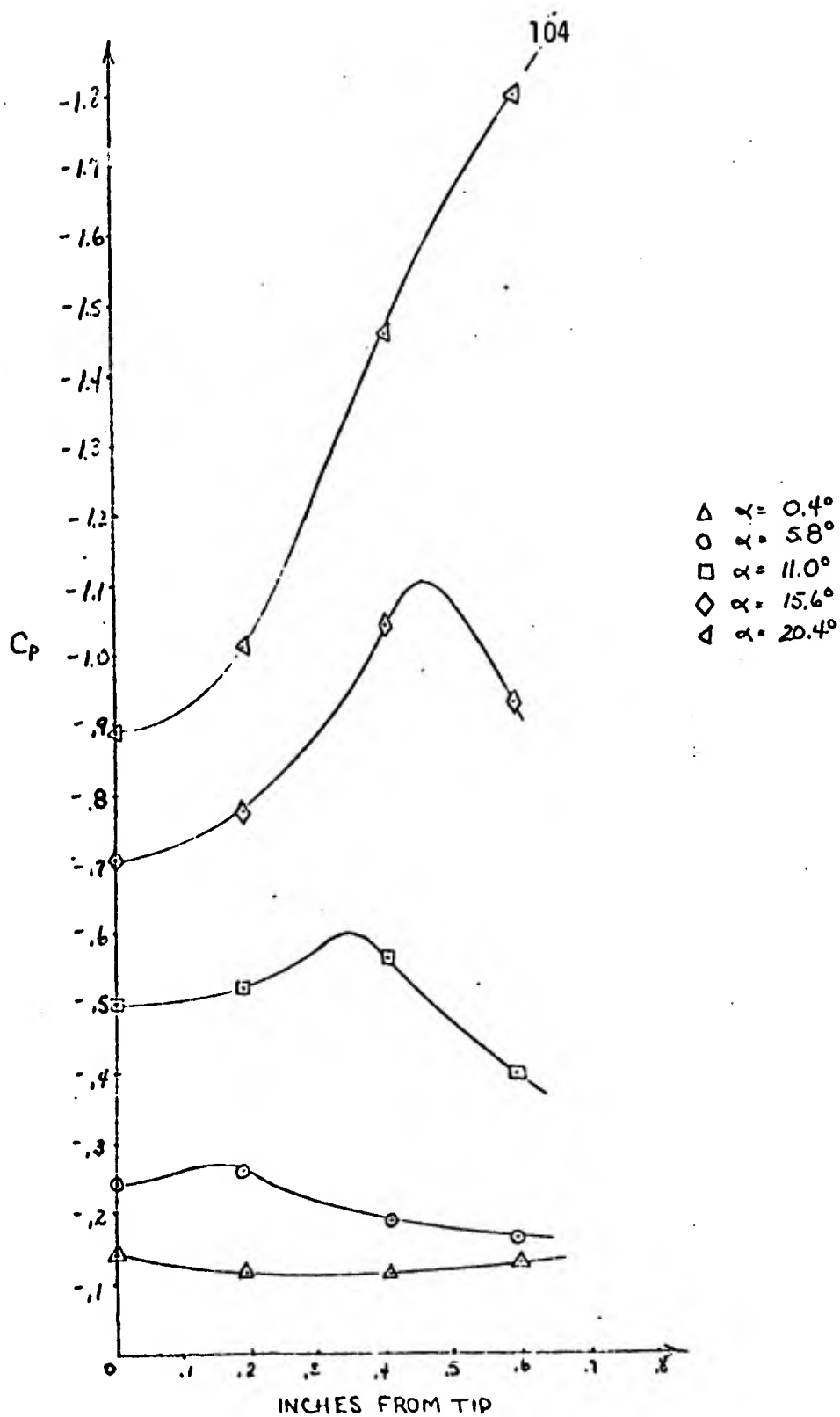


FIGURE 58

PRESSURE DISTRIBUTION: SIX INCH RECTANGULAR WING

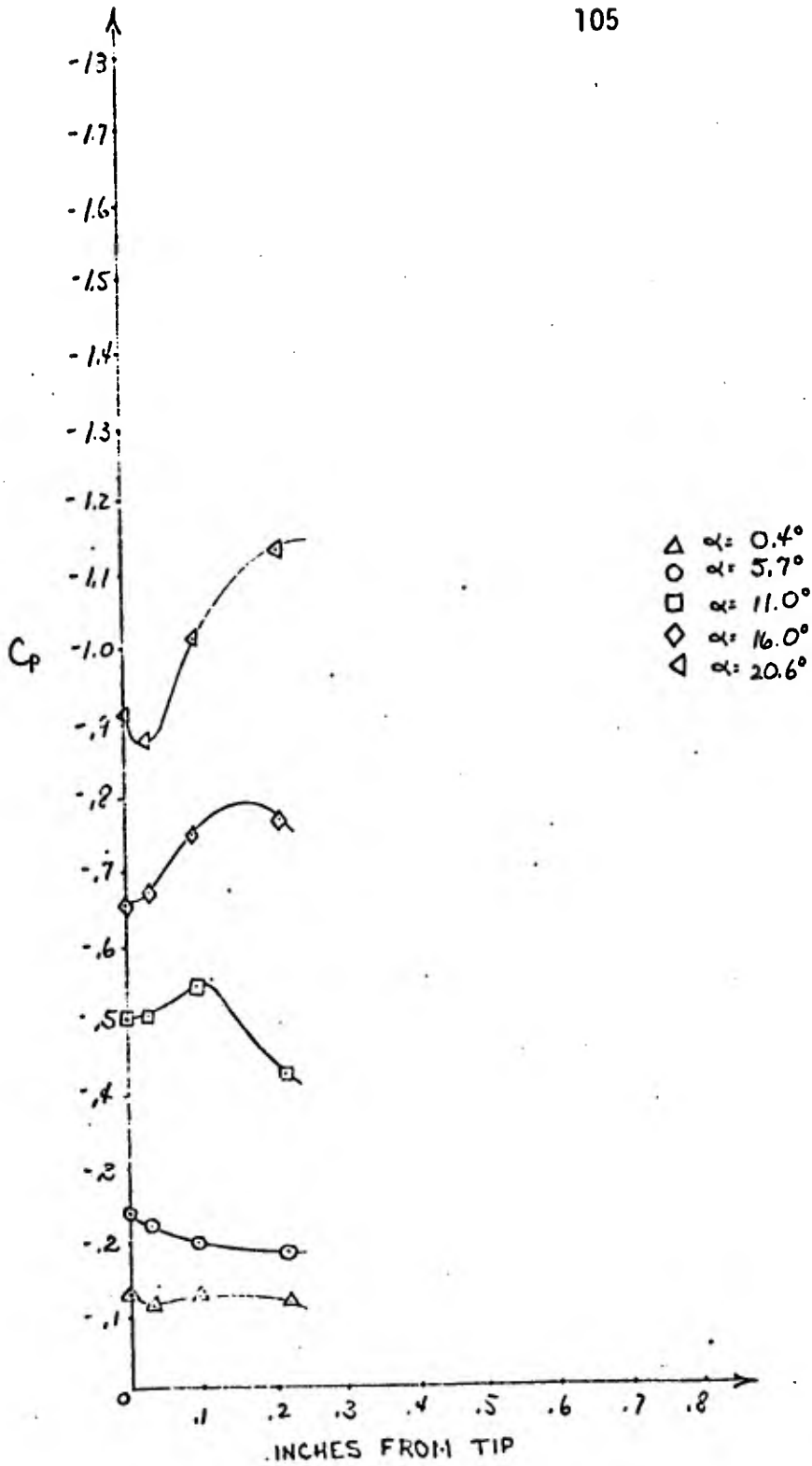


FIGURE 59

PRESSURE DISTRIBUTION: SIX INCH RECTANGULAR WING

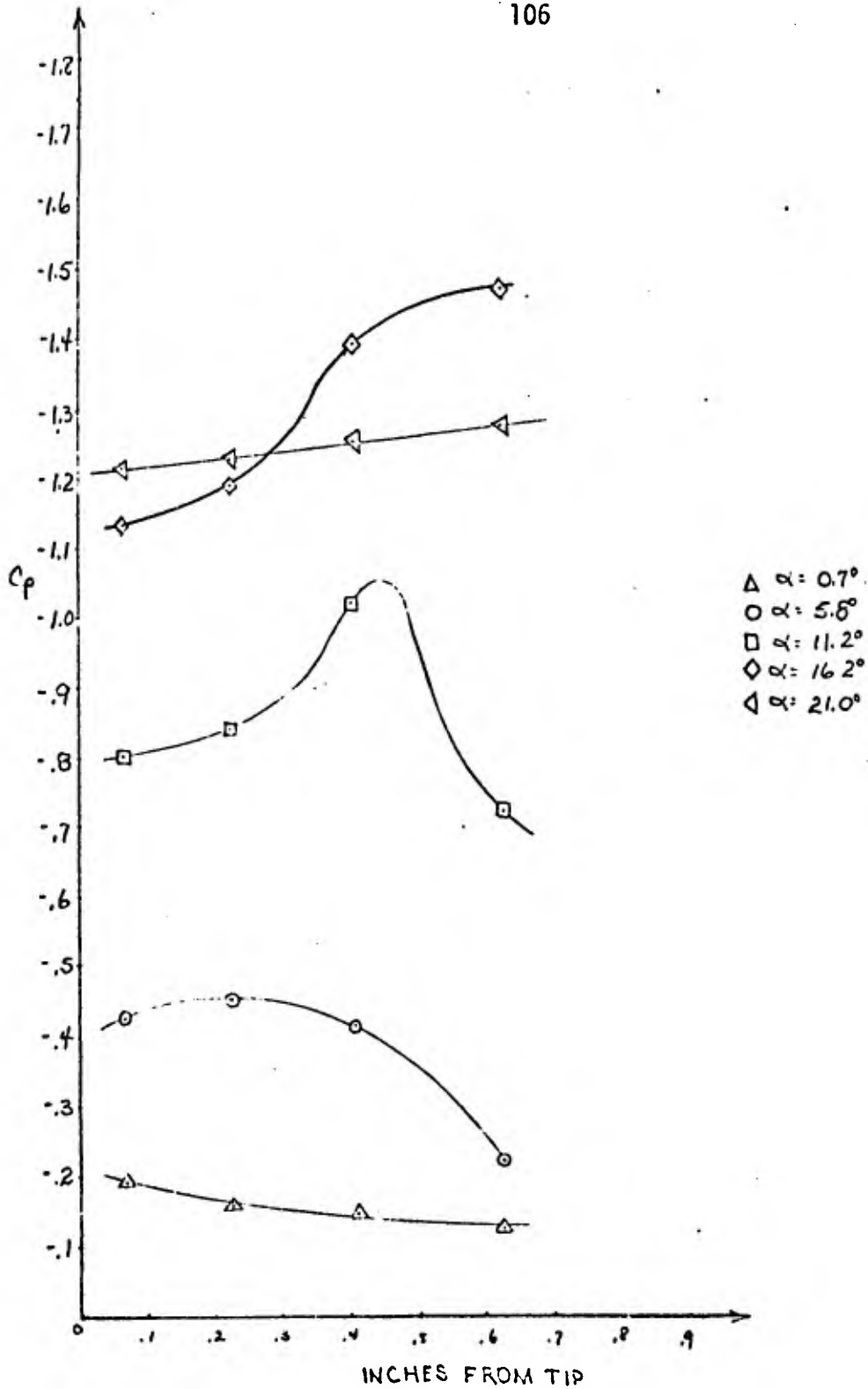


FIGURE 60

PRESSURE DISTRIBUTION: TWELVE INCH RECTANGULAR WING

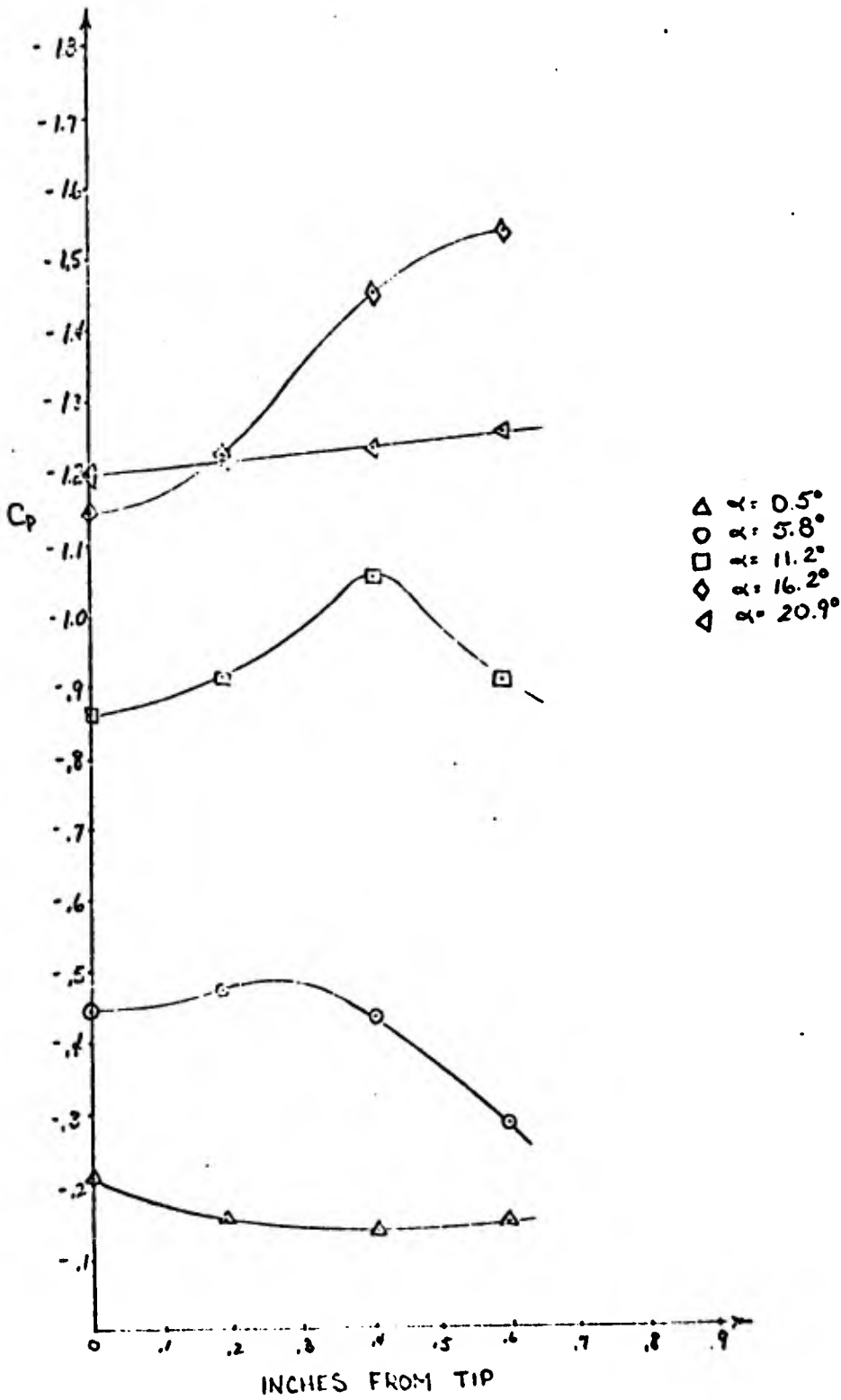


FIGURE 61

PRESSURE DISTRIBUTION: TWELVE INCH RECTANGULAR WING

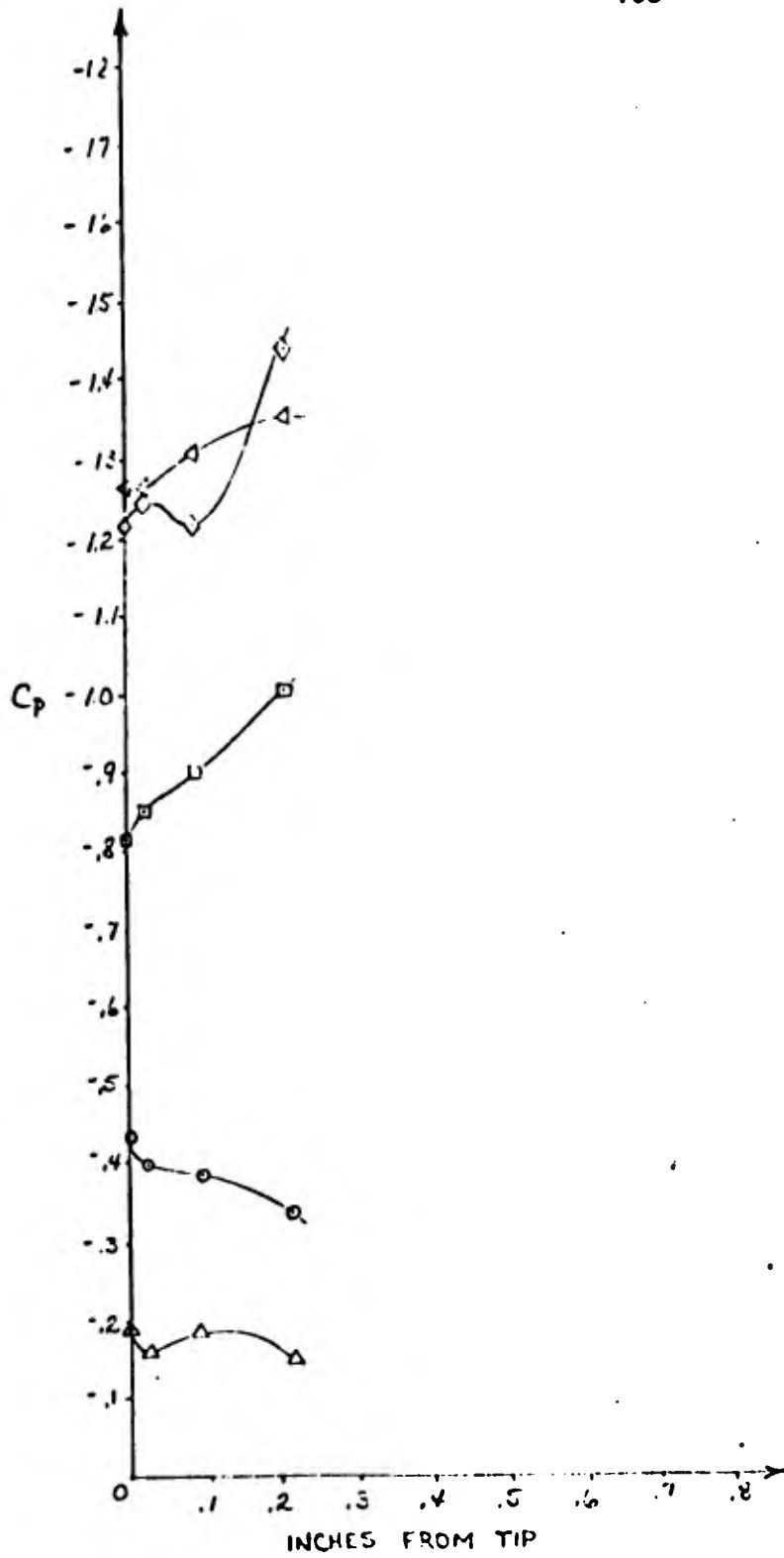


FIGURE 62

PRESSURE DISTRIBUTION: TWELVE INCH RECTANGULAR WING

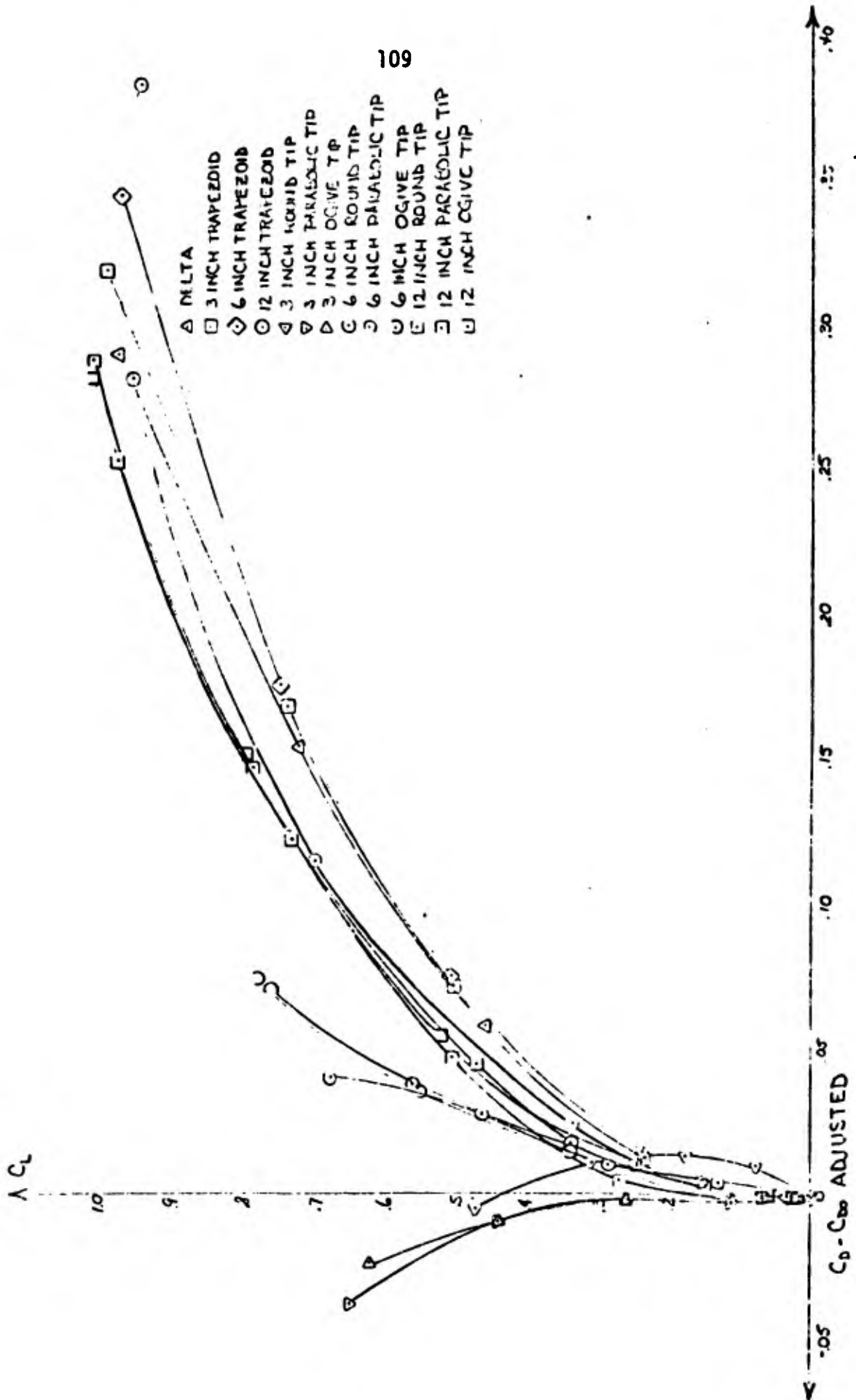


FIGURE 63
ADJUSTED DRAG COEFFICIENT FOR ALL MODELS

TABLE 1

| CONFIGURATION | AREA (ft^2) | ASPECT RATIO | $C_{L_{\alpha_0}}$ (per degree) |
|---------------------------|-----------------|--------------|---------------------------------|
| Delta Wing | .375 | 1.50 | .034 |
| Three Inch Trapezoid | .625 | 1.60 | .034 |
| Six Inch Trapezoid | .875 | 1.79 | .044 |
| Twelve Inch Trapezoid | 1.375 | 2.23 | .058 |
| Three Inch Round Tip | .297 | .329 | .011 |
| Three Inch Parabolic Tip | .344 | .409 | .011 |
| Three Inch Ogive Tip | .344 | .409 | .011 |
| Six Inch Round Tip | .547 | .579 | .015 |
| Six Inch Parabolic Tip | .594 | .658 | .021 |
| Six Inch Ogive Tip | .594 | .658 | .021 |
| Twelve Inch Round Tip | 1.047 | 1.078 | .030 |
| Twelve Inch Parabolic Tip | 1.094 | 1.157 | .038 |
| Twelve Inch Ogive Tip | 1.094 | 1.157 | .028 |

REFERENCES

1. Earnshaw, P. B., "An Experimental Investigation of the Structure of a Leading Edge Vortex," "ARC Reports and Memoranda 3281, 1961.
2. Fink, P. T., and Taylor, J., "Some Early Experiments on Vortex Separation," ARC Reports and Memoranda 3489, 1967.
3. Earnshaw, P. B., and Lawford, J. A., "Low Speed Wind Tunnel Experiments on a Series of Sharp Edged Delta Wings," ARC Reports and Memoranda 3424, 1966.
4. Thwaites, B., Incompressible Aerodynamics, Oxford University Press, New York, 1960.
5. Spreiter, J. R., and Sacks, A. H., "The Rolling Up of the Trailing Vortex Sheet and Its Effect on the Downwash Behind Wings," JAS, Vol. 18, Jan. 1951, p. 21-32.
6. Jones, R. T., and Cohen, D., High Speed Wing Theory, Princeton University Press, Princeton, New Jersey, 1960.
7. Edwards, R. H., "Leading Edge Separation from Delta Wings," JAS, Vol. 21, Feb. 1954, p. 134-135.
8. Mangler, K. W. and Smith, J. H. B., "A Theory of the Flow Past a Slender Delta Wing with Leading Edge Separation," Proc. Roy. Soc. (London), Ser. A, Vol. 251, 1959, pp. 200-217.
9. Coe, P. L., "A Vortex Entrainment Model Applied to Slender Delta Wings," AIAA Journal, Vol. 12, No. 1, January, 1974, pp. 110-112.
10. Pohlhamus, E. C., "A Concept of the Vortex Lift of Sharp-Edge Delta Wings Based on a Leading-Edge-Suction Analogy," NASA TN D-3767, August 1966.
11. Pohlhamus, E. C., "Prediction of Vortex-Lift Characteristics Based on a Leading-Edge Suction Analogy," AIAA Paper No. 69-1133.
12. Schlichting, H., Boundary Layer Theory, McGraw-Hill Book Company, New York, 1968, p. 17.
13. Pope, A., and Harper, J. J., Low Speed Wind Tunnel Testing, John Wiley and Sons, Inc., 1966, p. 331.
14. Prandtl, L., "Applications of Modern Hydrodynamics to Aeronautics," NACA Report 116, 1921, p. 38-40.